Physical Layer Techniques for OFDM-Based Cognitive Radios

by

Ehsan Haj Mirza Alian Aminabadi

A thesis
presented to the University of Waterloo
in fulfillment of the
thesis requirement for the degree of
Doctor of Philosophy
in
Electrical and Computer Engineering

Waterloo, Ontario, Canada, 2014

I hereby declare that I am the sole author of this thesis. This is a true copy of the thesis, including any required final revisions, as accepted by my examiners.

I understand that my thesis may be made electronically available to the public.

Abstract

Cognitive radio has recently been proposed as a promising approach for efficient utilization of radio spectrum. However, there are several challenges to be addressed across all layers of a cognitive radio system design, from application to hardware implementation. From the physical layer point-of-view, two key challenges are spectrum sensing and an appropriate signaling scheme for data transmission. The modulation techniques used in cognitive radio not only should be efficient and flexible but also must not cause (harmful) interference to the primary (licensed) users.

Among all the proposed signaling schemes for cognitive radio, orthogonal frequency division multiplexing (OFDM) has emerged as a promising one due to its robustness against multipath fading, high spectral efficiency, and capacity for dynamic spectrum use. However, OFDM suffers from high out-of-band radiation which is due to high sidelobes of subcarriers. In this thesis, we consider spectral shaping in OFDM-based cognitive radio systems with focus on reducing interference to primary users created by by out-of-band radiation of secondary users' OFDM signal.

In the first part of this research, we first study the trade-off between time-based and frequency-based methods proposed for sidelobe suppression in OFDM. To this end, two recently proposed techniques, active interference cancellation (AIC) and adaptive symbol transition (AST), are considered and a new joint time-frequency scheme is developed for both single-antenna and multi-antenna systems. Furthermore, knowledge of wireless channel is used in the setting of the proposed joint scheme to better minimize interference to the primary user. This scheme enables us to evaluate the trade-off between the degrees of freedom provided by each of the two aforementioned methods.

In the second part of this research, a novel low-complexity technique for reducing out-of-band radiation power of OFDM subcarriers for both single-antenna and multi-antenna systems is proposed. In the new technique, referred to as a *phase adjustment* technique, each OFDM symbol is rotated in the complex plane by an optimal phase such that the interference to primary users is minimized. It is shown that the phase adjustment technique neither reduces the system throughput, nor does increase the bit-error-rate of the system. Moreover, the performance of the technique in interference reduction is evaluated analytically in some special cases and is verified using numerical simulations.

Due to high sensitivity of OFDM systems to time and frequency synchronization errors, performance of spectral shaping techniques in OFDM is significantly affected by timing jitter in practical systems. In the last part of this research, we investigate the impact of timing jitter on sidelobe suppression techniques. Considering AIC as the base method

of sidelobe suppression, we first propose a mathematical model for OFDM spectrum in presence of timing jitter and evaluate the performance degradation to AIC due to timing jitter. Then, a precautionary scheme based on a *minimax* approach is proposed to make the technique robust against random timing jitter.

Acknowledgements

I would like to thank all the people who made this possible, particularly my supervisor, Prof. Patrick Mitran.

Dedication

To my parents, my wife, my brothers, and my sister.

Table of Contents

List of Tables x

List of Figures xi

1 Introduction 1

1.1 Background and motivation 1

1.2 Related works 3

1.2.1 Single-antenna cognitive transmitter 3

1.2.2 Multiple-antenna cognitive transmitter 4

1.3 Contributions 6

1.3.1 Interference reduction trade-offs 6

1.3.2 A phase adjustment approach for interference reduction 7

1.3.3 Jitter-robust spectral shaping in OFDM 8

2 Interference Reduction Trade-offs 10

2.1 Introduction 10

2.1.1 Single-antenna Cognitive Transmitter 10

2.1.2 Multiple-antenna Cognitive Transmitter 12

2.2 Cognitive OFDM System Model 12

2.3 Single-antenna Cognitive transmitter: joint time-frequency optimization . . 15

2.3.1 The joint time/frequency method 15

2.3.2 Simulation results and discussion . . . 19
2.4 Multiple-antenna cognitive transmitter: joint antenna optimization . . . 24
2.4.1 The joint antenna method . . . 25
2.4.2 Simulation results and discussion . . . 27
2.5 Conclusion . . . 29

3 A Phase Adjustment Approach for Interference Reduction 31
3.1 Introduction . . . 31
3.2 Single-antenna OFDM Cognitive Transmitter . . . 32
3.2.1 System and Signal Model . . . 32
3.2.2 The Phase Adjustment Technique for Single-antenna OFDM Transmitter . . . 34
3.2.3 Performance Analysis . . . 38
3.3 Multi-antenna OFDM Cognitive Transmitter . . . 40
3.3.1 System and Signal Model . . . 40
3.3.2 The Phase Adjustment Technique for Multi-antenna OFDM Transmitter . . . 41
3.3.3 Performance Analysis . . . 44
3.4 Simulation Results . . . 48
3.4.1 Single-antenna OFDM Cognitive Transmitter . . . 48
3.4.2 Multi-antenna OFDM Cognitive Transmitter . . . 49
3.5 Conclusion . . . 51
3.A Appendices . . . 52
3.A.1 Proof of Theorem 1 . . . 52
3.A.2 Proof of Theorem 2 . . . 52
3.A.3 Proof of Theorem 3 . . . 53
3.A.4 Proof of Theorem 4 . . . 54

4 Jitter-Robust Spectral Shaping in OFDM **59**

4.1 Introduction . . . 59

4.2 System Model . . . 60

4.3 Effect of Timing Jitter on Spectral Shaping Techniques . . . 64

4.3.1 The AIC technique and jitter effect . . . 64

4.3.2 Numerical results . . . 65

4.4 Jitter-robust AIC . . . 67

4.4.1 Problem formulation . . . 67

4.4.2 Problem solution . . . 68

4.5 Numerical Results . . . 72

4.5.1 Power spectral density . . . 72

4.5.2 Performance gain . . . 74

4.6 Conclusion . . . 75

5 Conclusion and Future Work **76**

5.1 Summary of achievements and conclusion . . . 76

5.1.1 Time-frequency trade-off study . . . 76

5.1.2 Phase adjustment technique . . . 77

5.1.3 Jitter-robust AIC . . . 78

5.2 Future work . . . 79

5.2.1 Timing jitter effect . . . 79

5.2.2 Other synchronization errors . . . 79

5.2.3 Other modulation techniques . . . 80

References **81**

List of Tables

1.1 Comparison of different proposed techniques for sidelobe suppression in OFDM 5

3.1 The improvement factor and upper bound for 1-sided and 2-sided OFDM signals 49

3.2 Improvement of the proposed technique for different channel models. . . . 50

List of Figures

2.1 Using cancellation carriers to reduce the interference power in the primary band. . . . 11

2.2 Cognitive OFDM transmitter block diagram. . . . 13

2.3 A pair of OFDM symbols in the time domain in which the first symbol has been optimized. . . . 16

2.4 Single wideband interference, power spectrum of the output OFDM signal; $N = 256$, number of primary bands=1, $B = 32$. . . . 20

2.5 Effect of adding extension samples on the amount of interference reduction in single wideband interference case. . . . 21

2.6 Multiple narrowband interference: Power spectrum of the output OFDM signal; $N = 256$, number of primary bands $= 6$, $B = 4$. . . . 23

2.7 The effect of adding extension samples on the amount of interference reduction in multiple narrowband interference. . . . 24

2.8 Multiple-antenna cognitive system. . . . 25

2.9 Comparison of the spectra of MISO-OFDM signal at the primary receiver in the frequency selective fading channel; 4 cancellation carriers on each side of the primary band and a time extension of length 4 are used. . . . 29

2.10 Effect of adding extension samples on the amount of interference reduction. 30

3.1 Block diagram of the single-antenna phase adjusted OFDM cognitive transmitter. . . . 33

3.2 Considering $m + 1$ successive symbols in each step in the phase adjustment technique for single-antenna transmitter. . . . 34

3.3 System model of a multiple-antenna cognitive system. 41
3.4 The eigenvalue ratio (ER). 46
3.5 Comparison of the proposed techniques for finding the optimal adjustment phases in the single-antenna case where $m = 3$. 48
3.6 Power spectrum of the phase adjusted OFDM signal transmitted from a single-antenna cognitive transmitter where $m = 3$; (a): optimal phases are found using the BCD algorithm, (b): optimal phases are found using the greedy technique. 56
3.7 Improvement of the proposed technique in interference reduction for different channel gains ratios $\frac{|h_1|}{|h_0|}$ for the multi-antenna case with two transmitter antennas. 57
3.8 Power spectrum of the phase adjusted OFDM signal transmitted from a 4-antenna cognitive transmitter using the BCD and the greedy technique. . 57
3.9 Comparison of the proposed techniques for finding the optimal adjustment phases in the multiple-antenna case with four transmit antennas. 58
3.10 Spectrum of the received OFDM signals transmitted from three antennas with frequency selective fading channels. Adjustment phases are calculated using the BCD algorithm. 58

4.1 Simplified block diagram of a typical OFDM transmitter. 61
4.2 Impact of the timing jitter on the performance of the AIC technique. . . . 66
4.3 Performance degradation to the AIC technique due to timing jitter for different jitter levels. 67
4.4 Power spectral density of the OFDM signal in presence of timing jitter using the jitter-robust technique compared to the case when the jitter is ignored in the AIC technique; $N = 256$, primary user bandwidth = 64 subcarriers, $\sigma_\varepsilon = 0.1T_s$. 73
4.5 Median performance improvement achieved by the proposed jitter-robust technique compared to the traditional AIC technique in presence of random timing jitter. 74

Chapter 1

Introduction

1.1 Background and motivation

The extensive growth of wireless applications over the past decade has caused an increasing demand for radio spectrum resources. Within the current spectrum regulatory framework, almost all of the available frequency bands have been allocated to existing applications [1], which has resulted in spectrum shortage for new ones. However, actual measurements have shown an inefficient spectrum usage as most of the licensed spectrum goes unused in a specific location or period of time [2]. In 2000, J. Mitola [3] introduced cognitive radio as a promising solution to the spectrum shortage problem and suggested using spectrum in an opportunistic manner.

Cognitive radio, refers to a new class of radios that are able to reliably sense the spectral environment over a wide bandwidth, detect unused spectrum bands, and communicate without causing harmful interference to the primary licensed users. Although the notion of cognitive radio opened new horizons in radio spectrum usage, there are several challenges to be addressed across all layers of a cognitive radio system design, from applications to hardware implementation. Since functionality of a cognitive radio mainly depends on the observations from the geographical environment, the physical layer is an important layer to be studied in order to understand the capabilities and limitations which affect the design of upper layers [4].

From a physical layer perspective, key issues of a cognitive radio are:

- *Reliable spectrum sensing:* First and foremost, a cognitive radio should be able to sense the spectrum and detect unoccupied bands reliably. The key challenges in

spectrum sensing include detecting weak signals in noisy environments while retaining a very small probability of detection miss, and sensing over a wide range of spectrum.

- *Appropriate transmission scheme:* According to the detected unoccupied bands, a cognitive radio must use a flexible signaling scheme in order to be able to change the signal bandwidth and frequency to fit into the detected unused band. Also, the signaling scheme used for transmission must not cause interference to the existing primary users using either the same spectrum band or adjacent bands.

Some techniques have been proposed as candidates for cognitive radio modulation technique in the literature such as filter bank multi-tone modulation [5], single carrier frequency division multiple access (SC-FDMA) [6], and multicarrier modulation [7–9]. Orthogonal frequency division multiplexing (OFDM) is the most well-known multicarrier modulation that uses sines/cosines as basis functions. Recently, it has been suggested to replace the sines/cosines basis functions in OFDM with wavelet bases such as Daubchies and Haar [8].

Among the abovementioned modulation techniques, OFDM has become very popular and is widely used in high data rate wireless systems. This is due to its robustness against multipath fading, high spectral efficiency, and its capacity for dynamic spectrum use. It also has the ability to allocate different power and data rates to distinct subchannels. On the other hand, the FFT/IFFT module that exists in each OFDM system also enables some form of spectral analysis, which is an important task in cognitive radios. Thus, OFDM appears to be a good candidate signaling technique for cognitive radios, as it is easy to turn on/off subcarriers in accordance to available sensed spectrum. A more detailed scheme called *spectrum pooling* is introduced in [7].

Besides all the abovementioned advantages, OFDM suffers from a few shortcomings such as high peak-to-average power ratio (PAPR), sensitivity to time and frequency synchronization errors, and high out-of-band emission power. As mentioned, it is necessary in cognitive radio applications that the secondary user's signal spectrum fits into the detected spectrum opportunities and meets the corresponding standard requirements. However, due to the signal truncation in the time-domain, OFDM subcarriers have significant sidelobes in the frequency-domain creating high out-of-band radiation power. This is particularly a critical issue in cognitive radio applications where the secondary users must avoid causing interference to the primary licensed users. Hence, in OFDM-based cognitive systems, turning off the subcarriers that correspond to primary spectrum activity is not enough to mitigate interference to the primary user and other mechanisms should also be taken into consideration. To overcome this impairment, several methods have been investigated.

In the next section, we review the related work on spectral shaping with focus on

sidelobe suppression in OFDM. We address the works done in both single-antenna and multiple-antenna OFDM systems.

1.2 Related works

1.2.1 Single-antenna cognitive transmitter

The simplest methods for suppressing OFDM sidelobes are windowing in the time-domain and using guard bands in the frequency-domain [10]. The former expands the OFDM symbol in the time-domain using a smooth shaping windowing scheme such as a raised-cosine [11], a better than raised-cosine (BTRC) [12], a flipped inverse hyperbolic secant (farch-sech) [13], or a Bartlett [14] window. The latter, however, deactivates a few subcarriers that reside in the vicinity of primary band to create a guard band [11]. Due to the diminishing tail of OFDM subcarriers, a frequency-domain guard band is successful in reducing the out-of-band radiation power. Although these methods have low complexity, their main drawbacks are low efficiency and loss in system throughput.

Another work is [15], in which subcarrier weighting (SW) is introduced to suppress the sidelobes. In SW, all data subcarriers are weighted with an optimal set of coefficients such that the residual interference in the primary band is minimized. The optimal weights on the data subcarriers are computed via solving a minimization problem for each OFDM symbol where the cost function is the interference to the primary user. Although SW does not sacrifice throughput, it suppresses the sidelobes at the cost of increased bit-error-rate (BER) and high complexity. The increase in BER is because data subcarriers are perturbed in this technique. In other words, the SW technique is applicable only to the systems using constant envelope modulation schemes such as phase shift keying (PSK). Another interference cancellation method in OFDM is multiple choice sequences (MCS), introduced in [16]. There, the original data sequence is mapped into a set of sequences and the sequence in the set with the lowest sidelobe levels is chosen to be transmitted. MCS, however, suffers from high complexity as well as loss in data throughput as it needs side information to be sent along with the data.

In [17], the authors proposed a new method based on carrier-by-carrier partial response signaling to shape the spectrum. In this scheme, a controlled amount of correlation is introduced among modulated symbols on each subcarrier in consecutive blocks. This method does not decrease data throughput, however, it increases the frame-error-rate (FER).

Two other novel and efficient techniques addressed in the literature are active interference cancellation (AIC) [18] and adaptive symbol transition (AST) [19]. Both of these

methods use least squares (LS) optimization to minimize the power in the primary band. In the AIC method, a few subcarriers at the border of the primary band, called cancellation subcarriers, are modulated by intentional complex-valued data such that their sidelobes cancel those of the data subcarriers. This technique was later developed in [20] where a power constraint in the cancellation subcarriers is considered in order to keep the power of those subcarriers to a reasonable level. The AIC technique, although more complex, outperforms the guard band method since it uses optimized data instead of just deactivating subcarriers at the border. In [21], an improvement to the AIC techinque is presented where the authors reduce the complexity of the technique using statistical relation among data carried by the subcarriers and control the amount of spectral overshoot on cancellation subcarriers.

The AST technique uses the same approach as of the AIC, yet in the time-domain. It lengthens the OFDM symbol with a data-dependent extension which is computed to minimize the power level in the primary band. The resulting extension in fact appears to be a smooth transition between consecutive time-domain OFDM symbols. This technique performs better than time-domain windowing at the cost of higher complexity. Although both AIC and AST offer better performance in terms of interference cancellation compared to the mentioned methods, they both suffer from high complexity and data throughput reduction.

Finally, in [22], the authors propose a novel technique that reserves a few subcarriers and modulates them in an attempt to match a first few derivatives at the OFDM symbols endpoints. Similar to the AST technique, this results in a smooth transition between consecutive symbols in the time-domain and accordingly reduces subcarrier sidelobes. This technique, however, has the same shortcomings as the AIC technique as a part of subcarriers are reserved for sidelobe reduction purpose and do not carry data.

1.2.2 Multiple-antenna cognitive transmitter

OFDM can also be employed in multiple-antenna cognitive systems in order to increase system capacity [23] and exploit diversity in fading channels [24]. However, only a few techniques in the literature have been proposed for sidelobe suppression in multiple-antenna OFDM transmitters and most are extensions of the AIC technique to multiple antennas. In [25], the authors apply the AIC technique to all transmitter antenna symbols and compute the optimum value of cancellation subcarriers jointly over multiple antennas. A more efficient extension of AIC for multi-antenna non-contiguous OFDM systems is presented in [26], where it is suggested to insert cancellation subcarriers in the OFDM symbols of

Table 1.1: Comparison of different proposed techniques for sidelobe suppression in OFDM

Research work	Advantage(s)	Disadvantage(s)
Time domain windowing [11–13]	Low complexity, No BER increase	Throughput reduction, Low efficiency
Subcarrier weighting (SW) [15]	No throughput reduction	High complexity, BER increase
Multiple choice sequences (MCS) [16]	No BER increase	High complexity, Throughput reduction
Active interference cancellation (AIC) [18, 25, 26]	No BER increase	High complexity, Throughput reduction
Adaptive symbol transition (AST) [19]	No BER increase	High complexity, Throughput reduction
N-continuous OFDM [27, 28]	No BER increase	Throughput reduction

only one of the transmitter antennas in an attempt to cancel the interference produced by other antennas.

In another work [27], the authors apply the N-continuous OFDM technique [28] to a multi-antenna transmitter OFDM cognitive system. However, this inevitably increases the BER due to the precoder used at the transmitter to suppress the OFDM sidelobes.

Although the AIC technique shows acceptable performance in creating deep spectrum notches, it has somewhat high computational complexity as it needs to solve a constrained convex optimization problem for each symbol. The problem is acute in multi-antenna OFDM cognitive transmitters as the number of cancellation subcarriers grows with the number of transmitter antennas. Moreover, in the aforementioned techniques, channel state information is not considered, while it is necessary in multiple-antenna systems to involve the effect of the channel since the received signal spectrum is the superposition of transmitted signals from each antenna passed through different fading channels. Therefore, reducing the spectrum before the channel (at the transmitter) does not necessarily result in reducing the spectrum after the channel (at the receiver). Whereas, in cognitive radio applications, we are interested in reducing interference at the location of the primary user.

In Table 1.1 the advantages and disadvantages of the proposed techniques for sidelobe suppression in OFDM for both single-antenna and multiple-antenna systems are presented.

1.3 Contributions

1.3.1 Interference reduction trade-offs

In Chapter 2, we consider the problem of cross-band interference reduction in both single-antenna and multiple-antenna OFDM-based cognitive systems and study the time/frequency trade-offs. As mentioned in Section 1.2.1, both AIC and AST techniques have analogous complexity –as they both use LS optimization– and effect on data throughput. The main difference is that the AIC is performed in the frequency-domain while the AST is performed in the time-domain. Therefore, in order to study the time/frequency trade-offs, the AIC and AST techniques are considered in Chapter 2.

In the first part of Chapter 2, we propose a joint time-frequency scheme in which the interference to the primary user is jointly minimized over the time-domain extension and frequency-domain cancellation carriers using *channel state information (CSI)*. The objective is to study the *trade-off* between these two methods to find the best trade-off point, that is the best combination of cancellation carriers and symbol extension for a given amount of interference reduction. In other words, using the trade-off study results, the data rate can be maximized for a desired level of interference reduction.

The contributions of this part are as follows:

- A new joint time/frequency scheme considering knowledge of the channel is proposed to study the time/frequency trade-off in LS based sidelobe suppression methods.
- We show that the time/frequency trade-off between the AIC and AST methods depends on the configuration of spectral opportunities and specifically, whether there is one large primary band, or multiple smaller primary bands.
- Based on the trade-off study results, we show that at the best trade-off point, significant system complexity reduction is possible by an approximation to the least squares optimization.

In the second part of Chapter 2, we consider the problem of interference minimization in multiple-antenna OFDM cognitive systems. Using channel state information, we propose a novel technique, referred to as the *joint antenna* method, to reduce the interference at the location of the primary receiver. Our system consists of a secondary transmitter with multiple antennas sending data to its own receiver, while trying to minimize interference to a primary user. In the joint antenna technique, the streams of OFDM symbols transmitted from the secondary antennas are designed such that the resultant interference *at the*

primary receiver is minimized, assuming full channel state information at the secondary. Simulation results show significant improvement of the proposed method of more than 10 dB compared to optimizing over each antenna separately, and/or optimizing without considering effect of the channel.

The contributions of this part are the following:

- A novel interference reduction technique in multiple-antenna OFDM cognitive systems is proposed.
- We study the time/frequency trade-off in the multiple-antenna case as well.
- Again, based on the trade-off study results, we propose an approximation at the best trade-off point which significantly reduces the system complexity.

The results presented in this chapter have been published in [29].

1.3.2 A phase adjustment approach for interference reduction

As noted in Section 1.2, the proposed interference reduction techniques in OFDM suffer from one or more of these shortcomings: high computational complexity, reduction in useful data throughput, and increase in BER. Therefore, in Chapter 3, we propose a novel low complexity technique referred to as a *phase adjustment* technique, to reduce the interference power coming from the out-of-band radiation of the secondary OFDM system to the primary user. It is shown in Chapter 3 that the proposed technique has none of the above shortcomings. We also evaluate the performance of the proposed technique in interference reduction analytically in some special cases for both single-antenna and multi-antenna secondary transmitters.

In the phase adjustment technique, the phase of each OFDM symbol is adjusted in an attempt to minimize the interference caused by the secondary user to the primary. Unlike prior methods, this technique does not decrease data throughput and has no impact on the bit-error-rate and peak-to-average power ratio of the OFDM symbols. Furthermore, to calculate the adjustment phases, three heuristics, one of which is very low complexity and achieves near optimal performance in numerical simulations, are also proposed.

The contributions of this chapter are as follows:

- A new phase adjustment technique is proposed for sidelobe suppression in single-antenna and multi-antenna OFDM systems.

- The performance of the proposed technique is evaluated analytically in some special cases in single and multi-antenna cognitive transmitters, and is verified by numerical simulations.

The results of this chapter have been published in our paper [30].

1.3.3 Jitter-robust spectral shaping in OFDM

In practical systems, the sampling clock times of the digital-to-analog converter (DAC) –at the transmitter– and the analog-to-digital converter (ADC) –at the receiver– have deviations from the ideal sampling times. This is usually referred to as *timing jitter* and can lead to a performance degradation in OFDM systems by introducing inter-carrier interference (ICI). Timing jitter has impact not only on the error-rate performance of the OFDM systems, but also on the performance of spectral shaping techniques in OFDM. Spectral shaping techniques usually refer to techniques where the aim is to achieve a desired spectral shape for the transmitted signal. This includes creating spectrum notches at particular designated frequencies, fitting the spectrum into a predefined spectral mask, or –more commonly– reducing the out-of-band radiation created by high sidelobes of OFDM subcarriers.

In Chapter 4, we consider the effect of timing jitter on the performance of sidelobe suppression techniques in OFDM. In particular, the AIC technique is chosen as the base method of sidelobe suppression as it is known to be one of the most effective out-of-band radiation reduction techniques in OFDM. However, the analysis throughout this chapter is general and can be applied to many other techniques in this area.

In the first part of this chapter, we analyze and investigate the impact of the timing jitter on the performance of the AIC technique in out-of-band radiation reduction. In particular, exact mathematical expressions will be derived for the excessive interference due to timing jitter. Then, using a first order Maclaurin series expansion, the jittery OFDM signal spectrum is analyzed. Finally, through numerical simulations, we will show how jitter can degrade the technique's performance.

In the second part of this chapter, a precautionary solution is proposed as a modification to the AIC technique in order to make the technique robust against the timing jitter. In the proposed scheme, which is based on a *minimax* approach, the effect of white random jitter is considered in solving an optimization problem in the setting of the AIC technique. To this end, the problem of sidelobe reduction using the AIC technique is reformulated

considering the jitter effect, forming a minimax optimization. Then, a new mathematical framework is proposed for solving the problem.

The contributions of this chapter are as follows:

- A mathematical model for timing jitter is presented and the effect of timing jitter on the spectrum of OFDM signal is analyzed.
- A novel jitter-robust scheme is proposed for interference reduction in OFDM systems in presence of timing jitter.

The results of this chapter have been submitted to *IEEE Transactions on Wireless Communications* in December 2013.

Chapter 2

Interference Reduction Trade-offs

2.1 Introduction

In this chapter, the problem of cross-band interference reduction in OFDM-based cognitive radio systems is considered. As noted in Chapter 1, cross-band interference, which is a major challenge in OFDM-based cognitive systems, is mainly caused by high OFDM sidelobes. We study this problem in two different cases.

2.1.1 Single-antenna Cognitive Transmitter

In the first part of this chapter, we consider the problem of interference minimization in single-antenna transmitter cognitive systems. In this case, high sidelobes of data subcarriers of a single-antenna secondary transmitter cause interference to the primary users. To suppress the sidelobes, several methods have been proposed among which some are performed in the time-domain and some in the frequency-domain. In this chapter, the objective is to propose a framework to study the trade-off between time and frequency in sidelobe suppression techniques. To this end, we consider the two recently proposed techniques, i.e. active interference cancellation (AIC) and adaptive symbol transition (AST).

In the AIC method, which is performed in the frequency-domain, a few subcarriers are inserted at the border of the primary bandwidth. These subcarriers, referred to as *cancellation carriers*, do not carry data, but are modulated by data-dependent complex

The results presented in this chapter have already been published in [29].

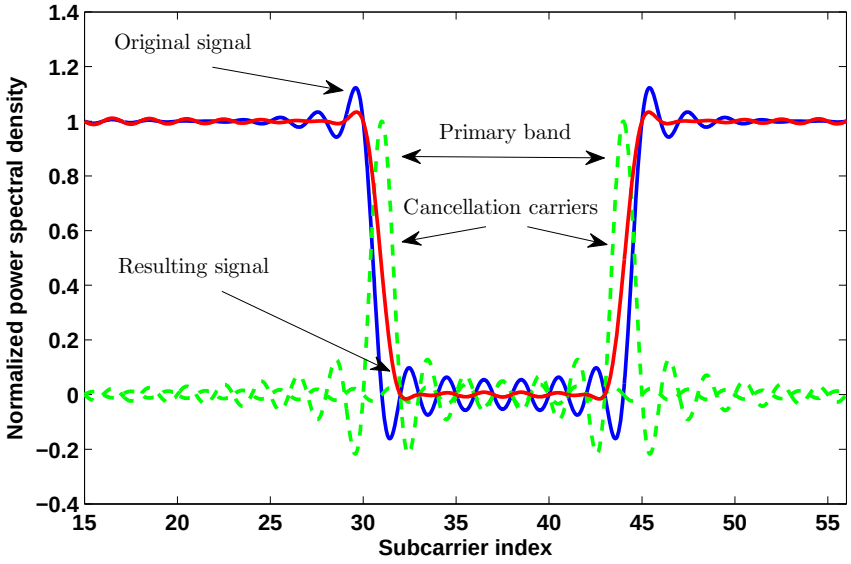

Figure 2.1: Using cancellation carriers to reduce the interference power in the primary band.

values such that their sidelobes cancel those of the original transmission signal. The idea is depicted in Fig. 2.1 [20], where two cancellation carriers are shown to reside at the edge of the primary band. To calculate the complex values of the cancellation carriers, least squares (LS) optimization is used. The main drawback of this method is the loss in throughput since some of the subcarriers no longer convey useful data.

The AST method uses the same approach as the AIC yet in the time-domain. In the AST method, instead of windowing the signal, each OFDM symbol is extended in the time-domain with a complex valued data-dependent extension which is calculated to minimize the power level in the primary band. The idea relies on the fact that the smoother the transition between successive OFDM symbols, the lower the sidelobe levels. The objective is to find the extension vector such that the total interference of the two OFDM symbols and the spectrum of the extension in the primary band cancel each other as much as possible. Similar to the AIC, LS optimization is used to find the extension vector in AST. This technique reduces interference at the cost of throughput degradation as a portion of time is not used to send useful information.

AST and AIC techniques are similar in the sense that they both use a part of available

system resources in an optimal way as to minimize the interference at the desired part of frequency spectrum. Accordingly, in order to study the time/frequency trade-off, we propose a joint time-frequency scheme in which the interference to the primary user is jointly minimized over the time-domain extension and frequency-domain cancellation carriers. The proposed scheme helps us to find the best combination of cancellation carriers and symbol extension for a desired amount of interference reduction.

It is worth mentioning that in all the proposed techniques for interference cancellation in OFDM-based cognitive radios –including AST and AIC–, the effect of the channel is not taken into account. However, it is important to note that this only works well for low scattering environments, where the channel does not have a serious effect on the spectrum of the transmitted signal. If an OFDM signal is to be transmitted over a frequency-selective fading channel, one can expect that the interference will be better minimized using knowledge of the channel.

The use of channel state information to minimize interference has been studied in a different context for flat fading channels [31–33]. There, channel state information is used to perform dynamic power control to optimize the transmission rate to secondary user(s), subject to primary interference constraints. In this chapter, however, we consider the channel state information in the proposed joint time/frequency method to better minimize the interference to the primary user.

2.1.2 Multiple-antenna Cognitive Transmitter

In multiple-antenna cognitive systems, the total interference to the primary user results from the interference power caused by each antenna separately. To minimize the total interference power, in the second part of this chapter, we extend the proposed joint time/frequency technique proposed in Section 2.3, to multiple antennas. In the new technique, called the joint antenna technique, by using the channel state information, interference at the location of the primary user is minimized jointly over multiple antennas.

2.2 Cognitive OFDM System Model

We consider a cognitive radio system in which primary users are detected by a cognitive controller engine. The secondary user should avoid causing interference to the primary user. It is assumed that the cognitive system employs OFDM modulation with N subcarriers.

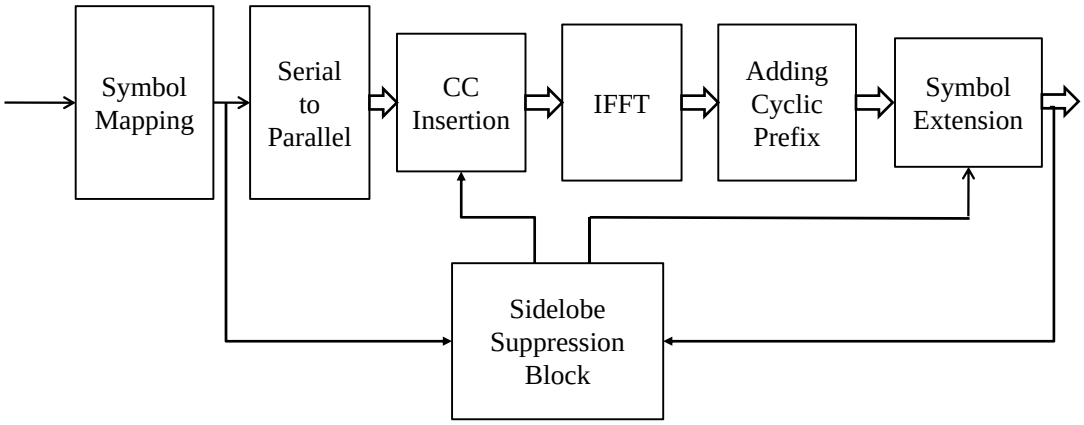

Figure 2.2: Cognitive OFDM transmitter block diagram.

The block diagram of the transmitter is depicted in Fig. 2.2. The input bits are symbol-mapped using a linear modulation scheme such as PSK or QAM. The symbols are then serial to parallel converted resulting in a complex vector to modulate the active subcarriers according to the bandwidth of detected primary user(s). The output of the serial to parallel block is fed into the cancellation carriers (CC) insertion block which inserts a few cancellation tones whose amplitudes are calculated by the sidelobe suppression unit to suppress the interference to the primary user. The resulting vector $\mathbf{X} = [X_0, X_1, ..., X_{N-1}]^T$ then passes through the inverse fast Fourier transform (IFFT) module and produces the time-domain vector $\hat{\mathbf{x}} = [x_0, x_1, ..., x_{N-1}]^T$ where

$$x_n = \frac{1}{\sqrt{N}} \sum_{k=0}^{N-1} X_k e^{j2\pi kn/N}. \tag{2.1}$$

We can rewrite (2.1) in matrix form as $\hat{\mathbf{x}} = \frac{1}{\sqrt{N}} W_{N,N}^{\dagger} \mathbf{X}$, where $W_{N,N}^{\dagger}$ denotes the conjugate transpose of matrix $W_{N,N}$, which is the $N \times N$ discrete Fourier transform (DFT)

matrix defined as

$$W_{N,N} = \begin{bmatrix} 1 & 1 & 1 & \dots & 1 \\ 1 & w & w^2 & \dots & w^{N-1} \\ 1 & w^2 & w^4 & \dots & w^{2(N-1)} \\ \vdots & \vdots & \vdots & \ddots & \vdots \\ 1 & w^{N-1} & w^{2(N-1)} & \dots & w^{(N-1)(N-1)} \end{bmatrix},$$

and w is the primitive Nth root of unity $e^{-j2\pi/N}$. To avoid intersymbol interference, the cyclic prefix of the OFDM modulated sequence, i.e., the last G samples of the IFFT output, is appended at the beginning of the symbol, where G is assumed to be larger than the maximum delay spread of the channel. To include the cyclic prefix, we define the modified DFT matrix as $W_{N,N+G} = [A \quad W_{N,N}]$, where A is the submatrix of $W_{N,N}$ consisting of the last G columns of $W_{N,N}$. Hence, the time-domain OFDM symbol including the cyclic prefix is expressed as

$$\mathbf{x} = \frac{1}{\sqrt{N}} W_{N,N+G}^{\dagger} \mathbf{X}. \tag{2.2}$$

The extension insertion unit then extends each symbol by optimal extension samples calculated by the sidelobe suppression unit to further mitigate interference to the primary user. Finally, each OFDM symbol in the time-domain is pulse shaped using a pulse shaping filter and sent by the antenna.

Remark: In order to investigate the spectrum of OFDM symbols in-between the subcarrier frequencies, we use an upsampled (by L) discrete Fourier transform defined by the $NL \times N$ matrix

$$W_{N,N}^{(L)} = \begin{bmatrix} 1 & 1 & \dots & 1 \\ 1 & w^{1/L} & \dots & w^{(N-1)/L} \\ 1 & w^{2/L} & \dots & w^{2(N-1)/L} \\ \vdots & \vdots & \ddots & \vdots \\ 1 & w^{(NL-1)/L} & \dots & w^{(NL-1)(N-1)/L} \end{bmatrix}.$$

Hence, the upsampled spectrum of $\mathbf{X}$ is calculated as

$$\mathbf{X}_L = \frac{1}{N} W_{N,N+G}^{(L)} W_{N,N+G}^{\dagger} \mathbf{X}, \tag{2.3}$$

where $W_{N,N+G}^{(L)} = [A^{(L)} \quad W_{N,N}^{(L)}]$ is the modified upsampled DFT matrix in which $A^{(L)}$ is the submatrix of $W_{N,N}^{(L)}$ consisting of the last G columns of $W_{N,N}^{(L)}$.

2.3 Single-antenna Cognitive transmitter: joint time-frequency optimization

In this section, the joint time/frequency method for the single-antenna cognitive transmitter is presented. First, we describe the details of the joint method that uses least squares optimization in attempt to minimize interference to the primary user jointly over time and frequency. Using this fact, we employ the joint method to study the trade-off between time and frequency interference reduction. Simulation results and discussion are given afterwards.

2.3.1 The joint time/frequency method

As mentioned, both the AIC and AST techniques have approximately the same complexity. Also, they both result in the same approximate decrease in system data throughput, i.e., sacrificing two subcarriers has almost the same impact as extending each OFDM symbol by two samples. By applying the joint optimization, there are two degrees of freedom: the number of subcarriers used as cancellation carriers, and the size of time domain extension. Thus, for a fixed level of interference suppression, there is a tradeoff between the number of tones to be allocated as cancellation carriers and the size of the symbol extension. In other words, for an acceptable loss in data throughput, using the joint technique enables us to minimize the interference, or, for a desired level of interference reduction, data throughput is maximized by allocating the optimal number of cancellation subcarriers in the frequency domain and extension samples in the time domain.

The method is based on jointly minimizing the interference over time and frequency *at the location of primary receiver*, using knowledge of the channel between the secondary transmitter and primary receiver. Namely, in the frequency domain, a number of cancellation carriers on each side of the primary band are used, and in the time domain, a symbol extension is added to each OFDM symbol. Considering the effect of the wireless channel, the weights of the cancellation carriers and the values of the extension are jointly optimized such that the interference to the primary user is minimized.

The secondary user employs the cognitive engine to sense the spectrum. It can also use the received signals from the primary user to accurately estimate the channel between the primary and secondary users. Alternatively, the primary user may be employing coexistence features which provide the secondary users with channel state information as this reduces impact to the primary network. The beacon in IEEE 802.22.1 is an example of

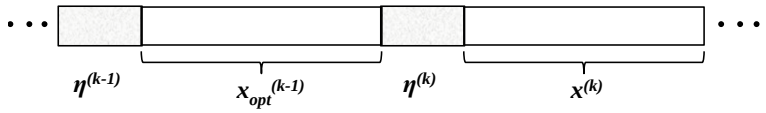

Figure 2.3: A pair of OFDM symbols in the time domain in which the first symbol has been optimized.

coexistence features. Accordingly, here we assume that the secondary transmitter has full knowledge of the channel which is a reasonable assumption (see e.g. [34]).

According to [18], to find the optimum weights for the cancellation carriers of each OFDM symbol, only the spectrum of that symbol is considered during the calculations, while the optimum values of the time domain extensions are found by considering the spectrum of two successive OFDM symbols [19]. To resolve this, we consider a pair of OFDM symbols and their extensions as shown in Fig. 2.3, assuming that the first symbol has already been well-optimized over time (extension) and frequency (cancellation carriers) to have the least interference to the primary user. The objective is to compute the complex values of the cancellation carriers (denoted by the vector $\boldsymbol{\mu}$) and extension (denoted by the vector $\boldsymbol{\eta}$) of the second symbol.

First, we find the interference to the primary user caused by the OFDM symbol pair, before performing any optimization on the second symbol in the symbol pair. Without loss of generality, we assume that there is a single primary user whose bandwidth is spread over B consecutive subcarriers $[X_{t+1}, X_{t+2}, \ldots, X_{t+B}]$, which are located in the middle of the total available bandwidth of the cognitive radio system, where $B < N$. Depending on the primary bandwidth, a number of subcarriers of the OFDM system are deactivated, or equivalently, corresponding elements in $\mathbf{X}$ are forced to zero. Let $\mathbf{X}_d^{(k)}$ denote the kth OFDM symbol in which tones within the primary band and the cancellation carriers are set to zero, i.e.,

$$\mathbf{X}_d^{(k)} = [X_0^{(k)}, \ldots, X_{t-g}^{(k)}, 0, \ldots, 0, X_{t+B+g+1}^{(k)}, \ldots, X_{N-1}^{(k)}]^T, \tag{2.4}$$

where g is the number of subcarriers used as cancellation carriers on each side of the primary band and $\mathbf{X}_{opt}^{(k)}$ denotes the kth OFDM symbol in which the optimum cancellation carries are inserted from the previous round. Also, let $\mathbf{x}_d^{(k)}$ and $\mathbf{x}_{opt}^{(k)}$ be the corresponding time domain symbols, respectively. We denote the upsampled frequency response of the channel

between the secondary transmitter and the primary receiver by $\mathbf{h} = [h_0, h_1, \ldots, h_{NL-1}]^T$. Thus, the upsampled spectrum of the non-optimized symbol pair is

$$\mathbf{S} = HW^{(L)}_{N,2(N+G+a)}\boldsymbol{\chi}_d = [S_0, S_1, \ldots, S_{NL-1}]^T, \tag{2.5}$$

where

$$H = \begin{bmatrix} h_0 & 0 & \ldots & 0 \\ 0 & h_1 & \ldots & 0 \\ \vdots & \vdots & \ddots & \vdots \\ 0 & 0 & \ldots & h_{NL-1} \end{bmatrix},$$

and

$$\boldsymbol{\chi}_d = \begin{bmatrix} \boldsymbol{\eta}^{(k-1)} \\ \mathbf{x}^{(k-1)}_{opt} \\ \mathbf{0}_a \\ \mathbf{x}^{(k)}_d \end{bmatrix}$$

in which a is the length of the extension and $\mathbf{0}_a$ is the zero vector of length a. $\boldsymbol{\eta}^{(k-1)}$ denotes the optimal extension vector of the $(k-1)$th symbol calculated in the previous iteration. Hence, the interference vector is

$$\mathbf{d} = \mathbf{S}^{(t+1)L,(t+B)L}, \tag{2.6}$$

which is a subvector of $\mathbf{S}$ containing indexed elements $(t+1)L$ through $(t+B)L$. $\|\mathbf{d}\|^2$ represents the amount of interference power to the primary user and is to be minimized. To this end, the next step is to calculate the contribution of the cancellation carriers and the extension of the second symbol in the primary band.

The upsampled spectrum of the jth unit-weight cancellation carrier is computed as

$$\mathbf{c}_j = \frac{1}{\sqrt{N}} W^{(L)}_{N,2(N+G+a)}\hat{\mathbf{c}}_j, \tag{2.7}$$

in which

$$\hat{\mathbf{c}}_j = \begin{cases} \begin{bmatrix} \mathbf{0}_{N+G+2a} \\ \frac{1}{\sqrt{N}} W^{\dagger}_{N,N+G}\mathbf{e}^{(t-g+j)}_N \end{bmatrix}, & j = 1, \ldots, g, \\ \begin{bmatrix} \mathbf{0}_{N+G+2a} \\ \frac{1}{\sqrt{N}} W^{\dagger}_{N,N+G}\mathbf{e}^{(t+B-g+j)}_N \end{bmatrix}, & j = g+1, \ldots, 2g, \end{cases}$$

where $\mathbf{e}_N^{(k)}$ is an $N \times 1$ zero vector except the kth entry which is 1. Thus, the spectrum of the jth unit-weight cancellation carrier in the primary band is

$$\widetilde{\mathbf{c}}_j = \mathbf{c}_j^{(t+1)L,(t+B)L}. \tag{2.8}$$

Similarly, setting the data symbols to zero, the upsampled spectrum of the jth unit-weight sample of the extension is

$$\mathbf{z}_j = \frac{1}{\sqrt{N}} W_{N,2(N+G+a)}^{(L)} \mathbf{e}_{2(N+G+a)}^{(N+G+a-1+j)}, \ j = 1, 2, \ldots, a. \tag{2.9}$$

Therefore, the contribution of the extension's jth unit-weight sample in the primary band is

$$\widetilde{\mathbf{z}}_j = \mathbf{z}_j^{(t+1)L,(t+B)L}. \tag{2.10}$$

The cancellation carriers and the extension samples are then weighted by some complex values. These values are jointly optimized such that the interference to the primary user is minimized at the primary receiver location. Letting $C = [\widetilde{\mathbf{c}}_1 \ \ \widetilde{\mathbf{c}}_2 \ \ \ldots \ \ \widetilde{\mathbf{c}}_{2g}]$ and $Z = [\widetilde{\mathbf{z}}_1 \ \ \widetilde{\mathbf{z}}_2 \ \ \ldots \ \ \widetilde{\mathbf{z}}_a]$, we have

$$\begin{aligned} (\boldsymbol{\mu}_{\mathsf{opt}}^{(k)}, \boldsymbol{\eta}_{\mathsf{opt}}^{(k)}) = & \arg\min_{(\boldsymbol{\mu},\boldsymbol{\eta})} \|\mathbf{d} + \widetilde{H} C \boldsymbol{\mu} + \widetilde{H} Z \boldsymbol{\eta}\|^2, \\ \text{s.t.} \quad & |\mu_i|^2 \leq \alpha, \quad i = 1, \ldots, 2g, \\ \text{and} \quad & \|\boldsymbol{\eta}\|^2 \leq p, \end{aligned} \tag{2.11}$$

where

$$\widetilde{H} = \begin{bmatrix} h_{(t+1)L} & 0 & \ldots & 0 \\ 0 & h_{(t+1)L+1} & \ldots & 0 \\ \vdots & \vdots & \ddots & \vdots \\ 0 & 0 & \ldots & h_{(t+B)L} \end{bmatrix},$$

and $\boldsymbol{\eta} = [\eta_1, \eta_2, \ldots, \eta_a]^T$ and $\boldsymbol{\mu} = [\mu_1, \mu_2, \ldots, \mu_{2g}]^T$ are the complex weight vectors of the extension samples and the cancellation carriers respectively. $\alpha = \mathbb{E}\{|X_i|^2\}, i = 1, \ldots, N$, is the power constraint on the cancellation subcarriers where $\mathbb{E}$ represents the expectation operation. This type of power constraint avoids creating overshoot in the resulting signal spectrum. Furthermore, according to [19], by choosing the power constraint on the symbol extension properly, the peak-to-average power ratio (PAPR) of the OFDM signals is not increased. A proper choice for the power constraint is

$$p = a \cdot \frac{E_s}{N+G}, \tag{2.12}$$

where E_s is the OFDM symbol energy before applying the joint method.

Now, by defining $\mathbf{r} \triangleq [\boldsymbol{\mu}^T \quad \boldsymbol{\eta}^T]^T$ and $D \triangleq [\widetilde{H}C \quad \widetilde{H}Z]$, (2.11) is simplified to

$$\begin{aligned} \mathbf{r}_{\mathsf{opt}} &= \arg\min_{\mathbf{r}} \|\mathbf{d} + D\mathbf{r}\|^2, \\ \text{s.t.} \quad & |r_i|^2 \leq \alpha, \quad i = 1, \ldots, 2g, \\ \text{and} \quad & \|\tilde{\mathbf{r}}\|^2 \leq p, \end{aligned} \tag{2.13}$$

where $\tilde{\mathbf{r}} = \mathbf{r}^{2g+1,2g+a}$.

The optimization problem defined in (2.13) is called a "linear least squares optimization problem with multiple quadratic inequality constraints" which is a well-studied optimization problem. To solve this problem, we first calculate the pseudo inverse of the argument on the right hand side of equation (2.13) as

$$\mathbf{r} = -(D^\dagger D)^{-1} D^\dagger \, \mathbf{d}. \tag{2.14}$$

If $\mathbf{r}$, which is computed from (2.14), satisfies the power constraints, then $\mathbf{r}_{\mathsf{opt}} = \mathbf{r}$, the optimum solution. If it violates any one of the power constraints, then at least one constraint is tight. In this case, to the best of our knowledge, no analytical solution for solving (2.13) is known that gives a closed form expression. However, there are efficient solvers that solve the problem iteratively employing numerical algorithms [35]. In this work, to solve (2.13), we used `cvx`, a package for specifying and solving convex programs [36, 37].

2.3.2 Simulation results and discussion

Simulations are run to investigate the performance of the proposed joint method. An OFDM-based cognitive radio using $N = 256$ subcarriers is considered where a cyclic prefix of length 64 is added to each symbol. Data subcarriers are modulated with BPSK symbols and the upsampling factor is $L = 16$. The channel between the secondary transmitter and the primary receiver is assumed to be a frequency selective fading channel. The model that we use for the channel is the SUI-4 channel model [38] which is a tapped-delay-line model with 4 taps. In the following simulations, interference power is calculated as the normalized norm of the interference vector in the primary band. We examine the performance of the joint method in two different scenarios.

Single wideband interference

In this case, the detected primary user has a rather wide bandwidth which is spread over 32 subcarriers from subcarrier 112 to subcarrier 143. Fig. 2.4 shows the power spectral

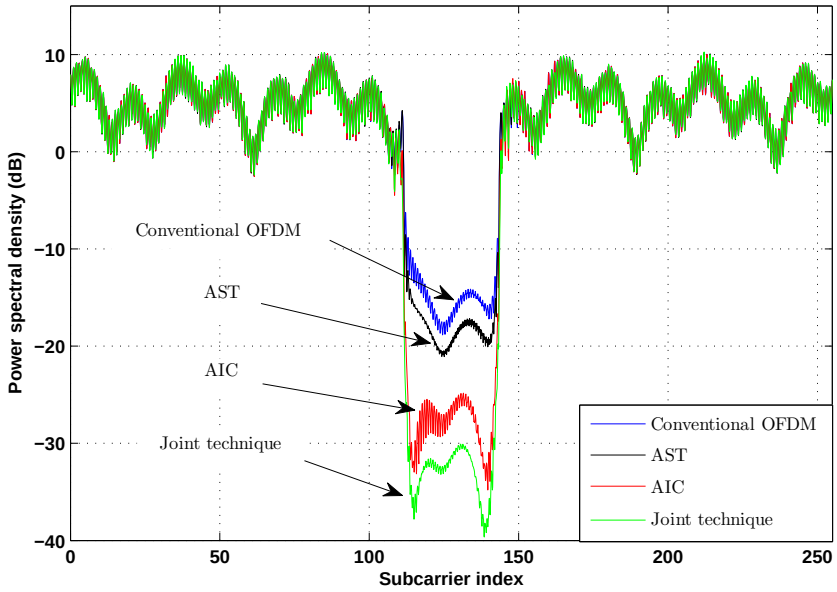

Figure 2.4: Single wideband interference, power spectrum of the output OFDM signal; $N = 256$, number of primary bands=1, $B = 32$.

density of the output OFDM signal at the location of primary receiver in four different cases. The first case is the conventional OFDM signal spectrum where only the subcarriers in the primary bandwidth are deactivated. The second one is the OFDM signal spectrum using the AST method where the length of symbol extension is 4. In the third case, OFDM signal spectrum using the AIC method with 4 cancellation subcarriers on each side of the primary bandwidth is depicted. Finally, the fourth one is the signal spectrum using the proposed joint technique with 4 cancellation carriers at each side of the primary bandwidth and an extension of length 4. Note that Fig. 2.4 is not a fair comparison of the performance of the different techniques. Therefore, in order to study the time/frequency trade-off, the amount of interference power for different numbers of cancellation carriers and extension lengths is computed. The results are as follows.

Trade-off study: We study the tradeoff between the number of cancellation carriers and the extension size in terms of interference reduction, and design the system to maximize the rate for a fixed interference level. Indeed, we find the best combination of time extensions and cancellation subcarriers to better improve the performance. Fig. 2.5 depicts

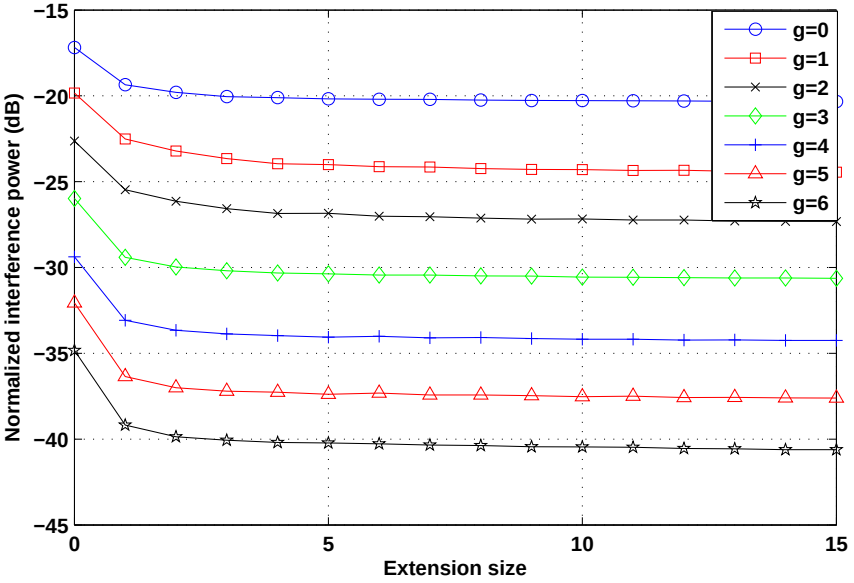

Figure 2.5: Effect of adding extension samples on the amount of interference reduction in single wideband interference case.

the change of interference level for different numbers of cancellation carriers g on each side of the primary band and the number of time extensions. It can be seen from Fig. 2.5 that there is a dominant break point on each curve in the first extension sample, which implies that while keeping the number of cancellation carriers fixed, the most significant gain is achieved by adding the first extension sample. Furthermore, beyond a single extension, the marginal interference reduction of adding 2 more extension samples is less than that achieved by adding a pair of cancellation carriers. Also, unlike adding extensions, the interference reduction obtained by adding cancellation carriers does not appear to have diminishing returns as each pair of cancellation subcarriers generally reduces the interference by about 4 dB. Because adding 2 extension samples or a pair of cancellation carriers degrades complexity and throughput features approximately equally, the best trade-off is achieved by using only one sample extension and several cancellation carriers for a desired interference reduction level.

Extension approximation: Since the extension is calculated to suppress the sidelobes by smoothing the transition between successive OFDM symbols, instead of solving (2.13) to find the optimal extension sample, one can compute the average of the two consecutive

OFDM symbols endpoints. If the transition between the symbols is approximated by a linear curve fitting, i.e.,

$$\eta_1^{(k)} = \frac{x_{N-1}^{(k-1)} + x_{N-G}^{(k)}}{2}, \tag{2.15}$$

where $\eta_1^{(k)}$ is the extension sample between the $(k-1)$th and the kth OFDM symbols, then this approximation significantly reduces the complexity as there is now no need to compute (2.9) and find the extension via solving (2.13), i.e., the size of matrices will be reduced and the cancellation carriers can be found separately. The cost of this approximation has been observed in simulations to be small.

Multiple narrowband interference

In the second scenario, there are multiple primary bands which are relatively narrow compared to the total available bandwidth of the cognitive system and are used by the same primary receiver. An example of narrow primary bands is IEEE 802.22 (WRAN) standard which is a standard for license-exempt devices to work on a non-interfering basis in the TV Broadcast Service spectrum. A cognitive radio in this band can use up to three consecutive TV channels (18 MHz). Police dispatch devices and wireless microphones which require approximately 200 KHz of bandwidth are considered as narrowband primary users in this band.

In simulations, we assume that the primary bands are spread over six narrow bands whose width are equivalent to 4 subcarriers. Two cancellation subcarriers are inserted on each side of each primary band and the length of the extension is 10. The rest of the parameters are the same as the single wideband case.

Fig. 2.6 shows the performance of the joint method compared to the conventional OFDM system, the AST method that uses an extension of length 10, and the AIC method where two cancellation subcarriers are inserted on each side of each primary band.

Trade-off study: Similar to the wideband interference case, Fig. 2.7 depicts the tradeoff between the number of subcarriers g on each side of each primary band and the size of the extension in interference reduction. It can be observed from Fig. 2.7 that in this case, unlike the single wideband interference case, increasing the size of the symbol extension provides more consistent interference suppression, i.e., the marginal return is not negligible after one extension sample. We attribute the better performance of symbol extension to the fact that by sharpening the subcarrier sidelobes, each additional extension sample reduces the interference in all of the narrow primary bands.

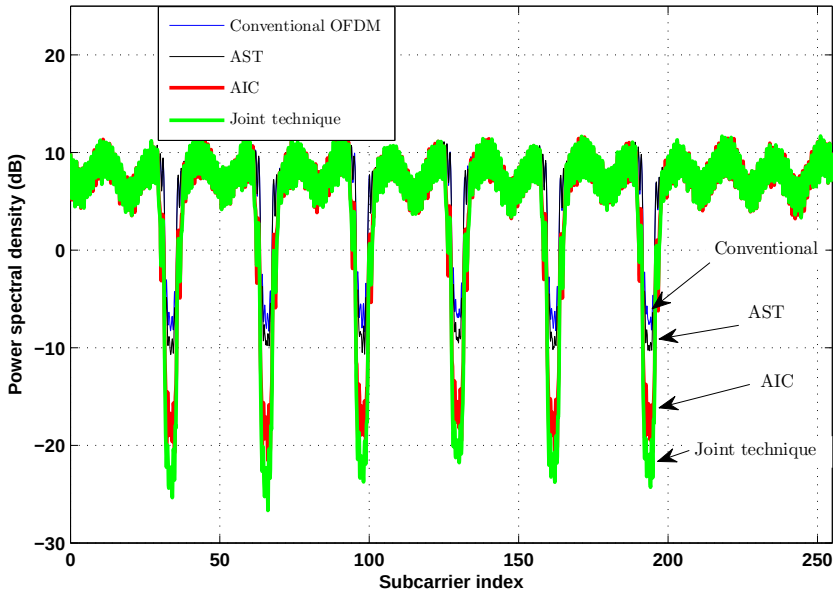

Figure 2.6: Multiple narrowband interference: Power spectrum of the output OFDM signal; $N = 256$, number of primary bands $= 6$, $B = 4$.

Also, note that in this case, each of the narrow primary bands needs cancellation subcarriers at its edge, resulting in $2g \times m_b$ subcarriers where m_b is the number of primary bands. Hence, adding a pair of cancellation carriers decreases the throughput $2m_b$ times more than adding an extension sample. Therefore, in terms of data throughput, it can be better to increase the length of symbol extension than to add cancellation subcarriers. For example, in Fig. 7, subcarriers reduce the interference by at most 0.83 dB/subcarrier (10 dB for each addition of 12 subcarriers), whereas the extensions can reduce interference by 1 to 2 dB/extension sample for $g \geq 3$.

As a result, we conclude that the best time/frequency trade-off depends on the configuration of the detected spectral opportunities, whether there is a single large primary band or there are multiple narrow primary bands. In either cases, at the best trade-off point, the joint method achieves a higher interference reduction compared to the pure AIC or AST techniques using the same amount of resources.

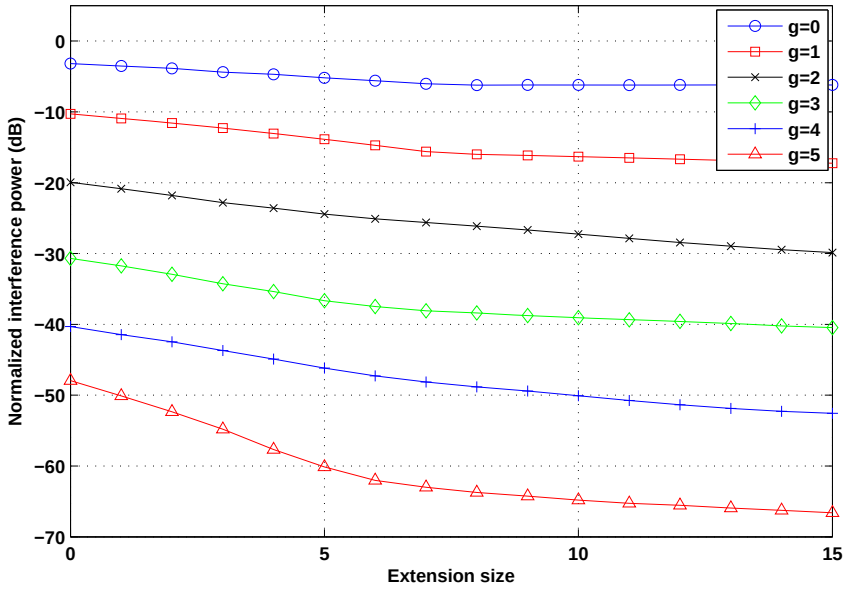

Figure 2.7: The effect of adding extension samples on the amount of interference reduction in multiple narrowband interference.

2.4 Multiple-antenna cognitive transmitter: joint antenna optimization

In this section, we present a new method, called the joint antenna method, for suppressing the interference to the primary user in multiple-antenna OFDM-based cognitive systems based on the idea introduced in Section 2.3. Our proposed method minimizes the interference to the primary user *at the location of the primary receiver*, requiring knowledge of the channel state information. Moreover, interference minimization is jointly performed over all transmitter antennas. In this case, we will show that a good improvement in interference reduction can be achieved. We use the simulation results to study the time/frequency trade-off as well.

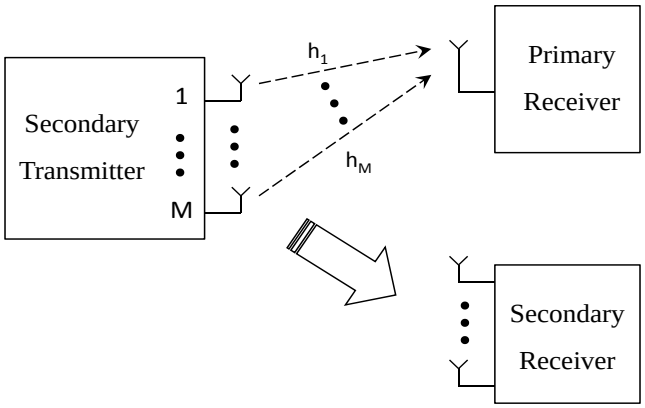

Figure 2.8: Multiple-antenna cognitive system.

2.4.1 The joint antenna method

We assume that the secondary transmitter uses M antennas with sufficient spatial separation, that send streams of OFDM symbols and try to avoid causing interference to a single primary receiver, as shown in Fig. 2.8. The set of the secondary transmitter antennas and primary receiver antenna forms a multiple-input single-output (MISO) system. Let $\mathbf{h}_i = [h_{i,0}, h_{i,1}, \ldots, h_{i,NL-1}]^T$ denote the upsampled frequency response of the channels between the ith secondary transmitter antenna and the primary receiver antenna. Therefore, the upsampled spectrum of the received signal at the primary receiver is

$$\mathbf{Y} = \sum_{i=1}^{M} H_i \mathbf{S}_i, \tag{2.16}$$

where

$$H_i = \begin{bmatrix} h_{i,0} & 0 & \ldots & 0 \\ 0 & h_{i,1} & \ldots & 0 \\ \vdots & \vdots & \ddots & \vdots \\ 0 & 0 & \ldots & h_{i,NL-1} \end{bmatrix}$$

and $\mathbf{S}_i$ is the upsampled signal transmitted by the ith secondary transmitter antenna, $i = 1, 2, \ldots, M$.

In the multiple-antenna case, to avoid secondary signals interfering with the primary user, the secondary transmitter forms the transmission OFDM symbols on each antenna in

such a way that, after passing through the channels, their effect at the primary band cancel each other as much as possible and the power in the primary band is minimized. To this end, we extend the joint time/frequency optimization technique introduced in Section 2.3 for the single-antenna case to multiple antennas where the optimization is done jointly, using the channel state information, over multiple antennas. We refer to the proposed method as the *joint antenna* method.

In the joint antenna method, cancellation carriers are inserted in every transmission OFDM symbol of each transmitter antenna in the frequency-domain. Each symbol is also extended in the time-domain by a symbol extension. The optimal values of the extensions and the cancellation carriers of the M OFDM symbols of the M transmitter antennas are jointly computed considering the effect of the channel, in order to minimize the interference to the primary receiver. Therefore, similar to Section 2.3, an OFDM symbol pair is considered for each transmitter antenna where the first symbol is already optimized.

Let $\mathbf{d}_i$ denote the upsampled interference vector of the non-optimized symbol pairs of the ith secondary antenna, which is calculated in the same way as in Section 2.3. Thus, the total interference vector at the primary receiver is

$$\mathbf{d} = \sum_{i=1}^{M} \widetilde{H}_i \, \mathbf{d}_i, \tag{2.17}$$

where

$$\widetilde{H}_i = \begin{bmatrix} h_{i,(t+1)L} & 0 & \dots & 0 \\ 0 & h_{i,(t+1)L+1} & \dots & 0 \\ \vdots & \vdots & \ddots & \vdots \\ 0 & 0 & \dots & h_{i,(t+B)L} \end{bmatrix}.$$

We denote the complex values of the second symbol's extension samples and cancellation carriers in the OFDM symbol pair of the ith transmitter antenna by the complex vectors $\boldsymbol{\eta}_i$ and $\boldsymbol{\mu}_i$, respectively. Therefore, the interference contribution of the extension samples of the ith antenna in the primary band at the location of the primary receiver is determined as $\widetilde{H}_i Z \boldsymbol{\eta}_i, i = 1, 2, \dots, M$. Similarly, the interference contribution of the cancellation carriers of the ith antenna in the primary band at the location of the primary receiver is $\widetilde{H}_i C \boldsymbol{\mu}_i, i = 1, 2, \dots, M$, where matrices C and Z are defined in Section 2.3. Thus, the

interference minimization problem is expressed as

$$
\begin{aligned}
&(\boldsymbol{\mu}_{1_{opt}}, \ldots, \boldsymbol{\mu}_{M_{opt}}, \boldsymbol{\eta}_{1_{opt}}, \ldots, \boldsymbol{\eta}_{M_{opt}}) \\
&= \underset{(\boldsymbol{\mu}_1, \ldots, \boldsymbol{\mu}_M, \boldsymbol{\eta}_1, \ldots, \boldsymbol{\eta}_M)}{\arg\min} \|\mathbf{d} + \sum_{i=1}^{M} \widetilde{H}_i (C\boldsymbol{\mu}_i + Z\boldsymbol{\eta}_i)\|^2, \\
&\text{s.t.} \quad |\mu_{ij}|^2 \leq \alpha, \quad i = 1, \ldots, M, \ j = 1, \ldots, 2g, \\
&\text{and} \quad \|\boldsymbol{\eta}_i\|^2 \leq p, \quad i = 1, \ldots, M,
\end{aligned}
\tag{2.18}
$$

where $\alpha = \mathbb{E}\{|X_i|^2\}, i = 1, \ldots, N$, is the power constraint on each cancellation carrier and p is the power constraint on the symbol extension of each antenna and is chosen according to Section 2.3. By introducing

$$
J \triangleq [\widetilde{H}_1 C \ \ldots \ \widetilde{H}_M C \ \ \widetilde{H}_1 Z \ \ldots \ \widetilde{H}_M Z] \tag{2.19}
$$

and

$$
\mathbf{t} \triangleq [\boldsymbol{\mu}_1^T \ \ldots \ \boldsymbol{\mu}_M^T \ \ \boldsymbol{\eta}_1^T \ \ldots \ \boldsymbol{\eta}_M^T]^T, \tag{2.20}
$$

equation (2.18) can be expressed as

$$
\begin{aligned}
&\mathbf{t}_{\mathsf{opt}} = \underset{\mathbf{t}}{\arg\min} \|\mathbf{d} + J\mathbf{t}\|^2, \\
&\text{s.t.} \quad |t_j|^2 \leq \alpha, \quad j = 1, \ldots, 2gM, \\
&\text{and} \quad \|\tilde{\mathbf{t}}_i\|^2 \leq p, \quad i = 1, \ldots, M,
\end{aligned}
\tag{2.21}
$$

where $\tilde{\mathbf{t}}_i = \mathbf{t}^{2gM+(i-1)a+1, 2gM+ia}$. Equation (2.21) is a "linear least squares problem with multiple quadratic inequality constraints". The same procedure as in Section 2.3 is used to solve this problem.

2.4.2 Simulation results and discussion

The MISO case is also examined using numerical simulations. We consider a secondary transmitter with two spatially separate antennas. The model we use for the channel between each secondary transmitter and the primary receiver is the SUI-4 channel model, the same as in Section 2.3. The two channels are assumed to be independent of each other. The OFDM communication system uses $N = 256$ subcarriers per antenna. The detected primary user bandwidth is assumed to occupy 32 subcarriers between subcarrier 112 and subcarrier 143. BPSK modulation is employed to modulate the data subcarriers. A cyclic prefix of length 64 is used and the upsampling factor is $L = 16$.

Fig. 2.9 shows the spectrum of the OFDM signal at the receiver in four cases. First, the conventional MISO-OFDM spectrum where only the subcarriers at the primary band are deactivated in each transmitted OFDM signal. In the second case, separate antenna optimization, the MISO system is considered as two separate single-input single-output (SISO) systems, where each of the transmitted sequences are separately designed using the optimization method described in Section 2.3, considering the channel state information. The sequences are then passed through the channels and the spectrum of the received signal is computed. The third case is similar to the second case except that it is assumed that the transmitter antennas do not have channel state information, or equivalently, assuming $H_i = I,\ i = 1, \cdots, M$, where I is the identity matrix. Finally, in the fourth scenario, joint antenna optimization is performed where the two transmitted sequences are jointly optimized over time, frequency and space (antennas) using the channel information. As Fig. 2.9 shows, the joint antenna optimization method suppresses the interference by almost 10 dB more than the separate antenna optimization method, and thus, channel state information at the transmitter can provide significant improvement for interference reduction in multiple-antenna systems.

Trade-off study: In Fig. 2.10, the trade-off between the number of cancellation carriers and the extension size with respect to the amount of interference reduction is depicted. Similar to the single-antenna case, it can be seen from Fig. 2.10 that adding the first extension sample gives the most significant gain in interference suppression.

Extension approximation: We can conclude from Fig. 2.10 the same result of the single-antenna case that at the best trade-off, instead of calculating the extension sample using the optimization problem stated in (2.18), we can solve the optimization problem only for the cancellation carriers and use a single sample for the extension. The extension sample can be easily approximated as the average of the two endpoints of the two consecutive OFDM symbols, i.e.,

$$\eta_{i1}^{(k)} = \frac{x_{i,N-1}^{(k-1)} + x_{i,N-G}^{(k)}}{2}, \quad i = 1, 2, \ldots, M, \tag{2.22}$$

where $\eta_{i1}^{(k)}$ is the extension sample between the $(k-1)$th and the kth OFDM symbols of the ith antenna.

Finally, simulation results for the multiple narrowband primary user case also demonstrate that, similar to the single-antenna case, interference reduction per extension sample in dB/sample for the first few extensions is greater than the reduction per subcarrier in dB/subcarrier. Therefore, the trade-off study in the multiple-antenna secondary transmitter case has the same result as the single-antenna case.

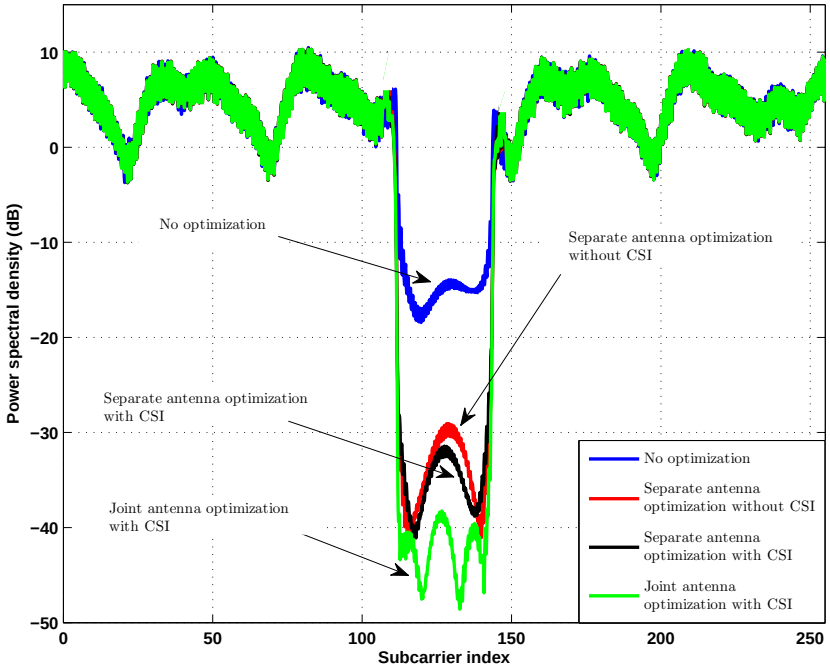

Figure 2.9: Comparison of the spectra of MISO-OFDM signal at the primary receiver in the frequency selective fading channel; 4 cancellation carriers on each side of the primary band and a time extension of length 4 are used.

2.5 Conclusion

In this chapter, the problem of interference reduction in OFDM-based cognitive radios in single-antenna and multiple-antenna secondary transmitter for single primary user band and multiple primary user bands is considered. In the single-antenna case, we propose a new joint time/frequency scheme to investigate the trade-off between active interference cancellation and adaptive symbol transition techniques. The new method optimizes jointly over the symbol extension and cancellation subcarriers to minimize the interference to the primary user. In view of symbol extension, it is shown that for a single wideband primary, most of the gain in interference cancellation is achieved by adding the first extension sample. Hence, the complexity can be significantly reduced by using one extension sample whose value is easily calculated as the average of the two endpoint of two successive OFDM

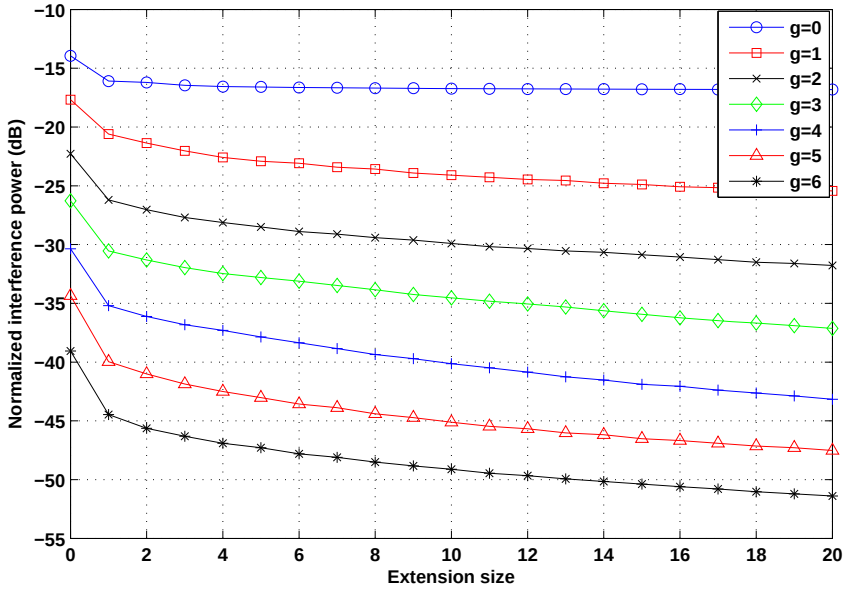

Figure 2.10: Effect of adding extension samples on the amount of interference reduction.

symbols. Furthermore, we show that the effect of the channel on the transmitted secondary signals can be used to improve interference cancellation. Using this fact, in the multiple-antenna case, we propose a new method, called the joint antenna method, in which the transmitted sequences from the secondary transmitter antennas are designed such that the interference at the primary receiver antenna is minimized. Simulation results also demonstrate significant improvement in jointly optimizing over two antennas compared to two separate antenna interference minimization.

Chapter 3

A Phase Adjustment Approach for Interference Reduction

3.1 Introduction

In this chapter, in order to reduce the interference power from out-of-band radiation of the secondary OFDM system to the primary user, we propose a novel low complexity technique, referred to as the *phase adjustment* technique. In the phase adjustment technique, each OFDM symbol is rotated by a common phase in such a way as to minimize the interference to the primary user. The technique is proposed for both single-antenna and multiple-antenna secondary systems. Furthermore, the performance is analytically investigated in both scenarios for some special cases and is verified by numerical simulations.

For the multi-antenna cognitive transmitter case, the proposed technique rotates symbols transmitted from each antenna in the complex plane based on the symbols transmitted from other antennas at the same time. The optimal rotation phase of each antenna is computed such that, after passing through the channel, the total interference spectrum at the primary receiver due to all secondary antennas is minimized.

Since in the multi-antenna case the interference minimization is performed across the transmitter antennas, there should exist at least two secondary transmitter antennas for this approach to work. Thus, for the single-antenna cognitive transmitter case, we propose a phase rotation technique that considers multiple consecutive OFDM symbols. In the proposed single-antenna technique, subcarriers of each OFDM symbol are rotated by an

The results presented in this chapter have already been published in [30].

optimal phase, based on the previous OFDM symbols, such that the resulting interference due to the considered consecutive OFDM symbols is minimized, i.e., Welch's spectrum estimate of the transmitted OFDM symbol stream is minimized at the primary band. The approach of reducing the interference due to multiple consecutive symbols has been taken in some of prior works, e.g. [19, 28].

In some special cases, the optimal phase rotation can be calculated using a simple inner product. For the other cases, three different novel and low complexity heuristics are presented for approximating the required rotation phases of the OFDM symbols. One of the heuristics, i.e., the block coordinate descent method, is found to achieve near optimal performance obtained by exhaustive search, at very low complexity.

Moreover, in the proposed techniques, all subcarriers of an OFDM symbol are rotated by the same phase. This phase can be regarded as part of a common phase (CP) which can be considered as a part of the channel effect known as common phase error (CPE), and is compensated for in any practical OFDM system. Therefore, the receiver can compensate for the phase rotation using one of the several methods that have been proposed for mitigating the CPE in the literature [39, 40]. As a result, the proposed phase adjustment method does not need explicit side information to be sent to the receiver for data recovery and data throughput is not decreased.

Finally, the phase adjustment method does not introduce any increase in bit-error-rate (BER) since it rotates all of the subcarriers by the same phase and thus, the location of the constellation points with respect to each other remain unchanged.

As noted above, in the single-antenna case, in contrast to the multi-antenna case, interference is minimized over different symbols which belong to consecutive transmission times. Therefore, as explained in Section 3.2.3, the performance analysis for the single-antenna case is not a special case of the multi-antenna case with one transmitter antenna, and requires its own separate analysis.

3.2 Single-antenna OFDM Cognitive Transmitter

3.2.1 System and Signal Model

A cognitive system with one transmit antenna employing non-contiguous OFDM signaling is considered. The cognitive receiver may have one or more antennas. The OFDM system is assumed to use a total of N subcarriers where some of them are switched off according to the detected primary user(s) activity. The transmitter block diagram is shown in Fig. 3.1.

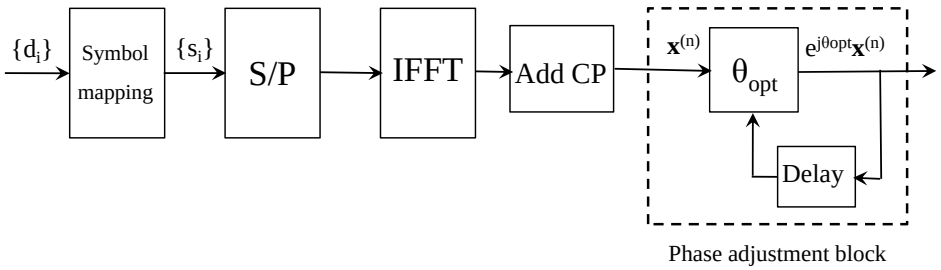

Figure 3.1: Block diagram of the single-antenna phase adjusted OFDM cognitive transmitter.

The input data bit stream is symbol-mapped resulting in a series of complex constellation points $\{s_i\}$ which are to modulate the active subcarriers.

The serial-to-parallel block converts the stream of $\{s_i\}$ into the complex-valued vector $\mathbf{X}^{(n)}$ where n is the symbol index. The cognitive engine deactivates the subcarriers that coincide with the primary user band according to the detected spectrum opportunity. $\mathbf{X}^{(n)}$ is then passed through the IFFT block generating the time-domain symbol as

$$\hat{\mathbf{x}}^{(n)} = \frac{1}{\sqrt{N}} W_{N,N}^{\dagger} \mathbf{X}^{(n)}, \tag{3.1}$$

where $W_{N,N} = [\omega^{kl}],\ k, l = 0, \ldots, N-1$, is the $N \times N$ discrete Fourier transform (DFT) matrix defined in Section 2.2. To avoid intersymbol interference (ISI), a cyclic prefix of length G is added to $\hat{\mathbf{x}}^{(n)}$, resulting in

$$\mathbf{x}^{(n)} = \frac{1}{\sqrt{N}} W_{N,N+G}^{\dagger} \mathbf{X}^{(n)}. \tag{3.2}$$

In order to further decrease interference to the primary user, $\mathbf{x}^{(n)}$ is passed through the phase adjustment block that rotates each OFDM symbol by an appropriate phase.

To evaluate the spectrum in the primary band in-between the subcarrier frequencies, we use the upsampled FFT matrix $W_{N,N}^{(L)}$ as defined in Section 2.2. Hence, the upsampled spectrum of the nth OFDM symbol $\mathbf{X}^{(n)}$ is calculated as

$$\mathbf{X}_L^{(n)} = \frac{1}{N} W_{N,N+G}^{(L)} W_{N,N+G}^{\dagger} \mathbf{X}^{(n)}. \tag{3.3}$$

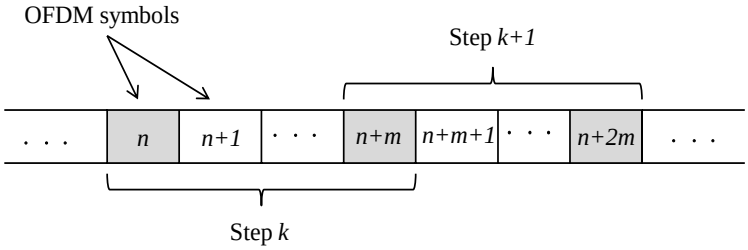

Figure 3.2: Considering $m+1$ successive symbols in each step in the phase adjustment technique for single-antenna transmitter.

3.2.2 The Phase Adjustment Technique for Single-antenna OFDM Transmitter

The objective of the phase adjustment technique is to reduce the interference at the primary band by adjusting the phase of the transmitted OFDM symbols. In the phase adjustment technique for the single-antenna transmitter, all subcarriers of each OFDM symbol are rotated in complex space by the same optimal phase to minimize the interference to the primary user.

Considering $m+1$ successive OFDM symbols in each step, the optimal rotation phase of the last m symbols are computed in such a way that the entire interference of the $m+1$ symbols is minimized. The spectrum of the resulting symbols is computed using Welch's method [41], where a window length equal to $m+1$ OFDM symbols is considered for each spectrum estimation segment and the amount of overlap of the segments is one OFDM symbol, as shown in Fig. 3.2. Therefore, in each step, the first symbol's phase shift is assumed to be obtained by optimization from the previous step and thus, m optimal phases are to be calculated. Consequently, the $(m+1)$th symbol in the current step will be considered as the first symbol in the next step.

Let $\mathbf{x}^{(n)}, \mathbf{x}^{(n+1)} \cdots \mathbf{x}^{(n+m)}$ denote the $m+1$ consecutive OFDM symbols in the current

step. The upsampled spectrum of the $m+1$ symbols is then calculated as

$$\mathbf{S}^{(n)} = W^{(L)}_{N,(m+1)(N+G)} \begin{bmatrix} \mathbf{x}^{(n)} \\ \vdots \\ \mathbf{x}^{(n+m)} \end{bmatrix} \tag{3.4}$$

$$= \sum_{i=0}^{m} D_i W^{(L)}_{N,N+G} \mathbf{x}^{(n+i)}, \tag{3.5}$$

where $D_i = \text{diag}\{e^{-2\pi jki(N+G)/NL}\},\ k = 0, \ldots, NL-1$.

Without loss of generality, we assume that the primary user occupies a bandwidth equivalent to B successive subcarriers $[X_{t+1}, X_{t+2}, \ldots, X_{t+B}]$, where $B < N$. Thus, the interference vectors due to $\mathbf{x}^{(n)}, \cdots, \mathbf{x}^{(n+m)}$ are expressed as

$$\mathbf{d}^{(n+i)} = \widetilde{D}_i \widetilde{W}^{(L)}_{N,N+G} \mathbf{x}^{(n+i)},\ i = 0, 1, \cdots, m, \tag{3.6}$$

where $\widetilde{W}^{(L)}_{N,N+G}$ is a submatrix of $W^{(L)}_{N,N+G}$ containing only the rows that correspond to the primary band, i.e., rows $(t+1)L+1$ through $(t+B)L$, and $\widetilde{D}_i$ is a submatrix of D_i defined as

$$\widetilde{D}_i = \text{diag}\{e^{-2\pi jki(N+G)/NL}\},\ k = (t+1)L+1, \ldots, (t+B)L. \tag{3.7}$$

In the proposed phase adjustment technique, the objective is to find the optimal rotation phase of the symbols $\mathbf{x}^{(n)}, \cdots, \mathbf{x}^{(n+m)}$ to minimize the total interference of

$$\begin{bmatrix} \mathbf{x}^{(n)} \\ \mathbf{x}^{(n+1)} \\ \vdots \\ \mathbf{x}^{(n+m)} \end{bmatrix} \tag{3.8}$$

to the primary user. Therefore, using a least square minimization criterion, the optimal rotation phase is calculated as

$$\boldsymbol{\theta}_{\mathsf{opt}} = \arg\min_{\boldsymbol{\theta}} \|\mathbf{d}^{(n)} + e^{j\theta_1}\mathbf{d}^{(n+1)} + \cdots + e^{j\theta_m}\mathbf{d}^{(n+m)}\|^2, \tag{3.9}$$

which is a least squares (LS) optimization problem in which $\boldsymbol{\theta}_{\mathsf{opt}} = [\theta_{1_{\mathsf{opt}}} \cdots \theta_{m_{\mathsf{opt}}}]^T$ is the set of optimal rotation phases of the considered symbols. The LS problem expressed in (3.9) can be reformulated as

$$\boldsymbol{\rho}_{\mathsf{opt}} = \arg\min_{\boldsymbol{\rho}} \|\mathbf{d}^{(n)} + P\ \boldsymbol{\rho}\|^2, \tag{3.10}$$

$$\text{s.t.} \quad |\rho_i|^2 = 1, \quad i = 1, \cdots, m,$$

where $\boldsymbol{\rho} = [e^{j\theta_1}, \cdots e^{j\theta_m}]^T$ and $P = [\mathbf{d}^{(n+1)} \cdots \mathbf{d}^{(n+m)}]$. Therefore, $\theta_i = \arg(\rho_i)$. The optimization problem defined in (3.10) is a least squares problem with multiple equality constraints.

For the special case of $m = 1$, the problem specializes as

$$\theta_{\mathsf{opt}} = \arg\min_{\theta_1} \|\mathbf{d}^{(n)} + e^{j\theta_1}\mathbf{d}^{(n+1)}\|^2, \tag{3.11}$$

which is a single constraint LS minimization. Theorem 1 gives the solution to this problem.

***Theorem* 1** *Given two arbitrary complex vectors $\boldsymbol{d}^{(n)}$ and $\boldsymbol{d}^{(n+1)}$ of the same length,*

$$\theta = \pi - \arg\langle \boldsymbol{d}^{(n)}, \boldsymbol{d}^{(n+1)} \rangle \tag{3.12}$$

minimizes $\|\boldsymbol{d}^{(n)} + e^{j\theta}\boldsymbol{d}^{(n+1)}\|^2$, where $\langle \cdot, \cdot \rangle$ denotes the complex inner product. ■

Proof: See Appendix 3.A.1. □

According to Theorem 1, in the case of $m = 1$, the optimal rotation phase in the phase adjustment technique is simply found by calculating the inner product of the interference vectors, which implies that the complexity is very low.

In order to solve the problem for the general case of $m > 1$, we propose three algorithms, namely, a block coordinate descent (BCD) method, a greedy technique, and an opportunistic co-phase technique. The performance of these methods are evaluated in Section 3.4.1.

Block coordinate descent (BCD) method

The block coordinate descent or nonlinear Gauss-Seidel method is a suitable and efficient method for solving optimization problems where the cost function is continuously differentiable over the constraint set [42], which is true for the optimization problem defined in (3.10).

In the block coordinate descent method, the next iterate $\boldsymbol{\theta}^{k+1} = [\theta_1^{k+1}, \cdots, \theta_m^{k+1}]^T$ is calculated according to the iteration

$$\begin{aligned}\theta_i^{k+1} = \arg\min_{\theta_i} \|\mathbf{d}^{(n)} &+ e^{j\theta_1^{k+1}}\mathbf{d}^{(n+1)} + \cdots + e^{j\theta_{i-1}^{k+1}}\mathbf{d}^{(n+i-1)} \\ &+ e^{j\theta_i}\mathbf{d}^{(n+i)} + e^{j\theta_{i+1}^{k}}\mathbf{d}^{(n+i+1)} + \cdots + e^{j\theta_m^{k}}\mathbf{d}^{(n+m)}\|^2,\end{aligned} \tag{3.13}$$

Algorithm 1: The Block Coordinate Descent Method for the Single-antenna Case

Result: Heuristic approximation $\boldsymbol{\theta}^\star$ to the solution of (3.9).
Compute $\mathbf{d}^{(n)}, \mathbf{d}^{(n+1)}, \cdots, \mathbf{d}^{(n+m)}$ from (3.6);
Initialize $\boldsymbol{\theta}^0 = \mathbf{0}$
for $k = 1$ to Num-Iterations **do**
  for $i = 1$ to m **do**
    $\hat{\mathbf{d}}^{(n,\bar{i})} = \mathbf{d}^{(n)} + e^{j\theta_1^k}\mathbf{d}^{(n+1)} + \cdots + e^{j\theta_{i-1}^k}\mathbf{d}^{(n+i-1)} + e^{j\theta_{i+1}^{k-1}}\mathbf{d}^{(n+i+1)} + \cdots + e^{j\theta_m^{k-1}}\mathbf{d}^{(n+m)}$,
    $\theta_i^k = \pi - \arg\langle \hat{\mathbf{d}}^{(n,\bar{i})}, \mathbf{d}^{(n+i)} \rangle$.
$\boldsymbol{\theta}^\star = \boldsymbol{\theta}^{\text{Num-Iterations}}$.

which can be simplified as

$$\theta_i^{k+1} = \arg\min_{\theta_i} \|\hat{\mathbf{d}}^{(n)} + e^{j\theta_i}\mathbf{d}^{(n+i)}\| \tag{3.14}$$

where

$$\hat{\mathbf{d}}^{(n)} = \mathbf{d}^{(n)} + e^{j\theta_1^{k+1}}\mathbf{d}^{(n+1)} + \cdots + e^{j\theta_{i-1}^{k+1}}\mathbf{d}^{(n+i-1)} + e^{j\theta_{i+1}^{k}}\mathbf{d}^{(n+i+1)} + \cdots + e^{j\theta_m^{k}}\mathbf{d}^{(n+m)}.$$

Equation (3.14) is then a single constraint LS minimization and has a *unique* solution which is calculated using Theorem 1 as

$$\theta_i^{k+1} = \pi - \arg\langle \hat{\mathbf{d}}^{(n)}, \mathbf{d}^{(n+i)} \rangle. \tag{3.15}$$

Furthermore, according to [42, proposition 2.7.1], every limit point of the sequence $\{\boldsymbol{\theta}^k\}$ generated by the BCD method is a stationary point of the objective function in (3.9). Finding a solution to (3.9) using the block coordinate descent method is summarized in Algorithm 1.

Greedy technique

This technique is a simple and fast technique for finding a suboptimal solution to (3.9). In the greedy technique, elements of the suboptimal solution $\boldsymbol{\theta}^\star$ are calculated via solving

$$\begin{aligned}\theta_i^\star &= \arg\min_{\theta_i} \|\mathbf{d}^{(n)} + e^{j\theta_1^\star}\mathbf{d}^{(n+1)} + \cdots + e^{j\theta_{i-1}^\star}\mathbf{d}^{(n+i-1)} \\ &\quad + e^{j\theta_i}\mathbf{d}^{(n+i)} + \mathbf{d}^{(n+i+1)} + \cdots + \mathbf{d}^{(n+m)}\|^2 \\ &= \arg\min_{\theta_i} \|\hat{\mathbf{d}}^{(n)} + e^{j\theta_i}\mathbf{d}^{(n+i)}\|\end{aligned} \tag{3.16}$$

where

$$\hat{\mathbf{d}}^{(n)} = \mathbf{d}^{(n)} + e^{j\theta_1^\star}\mathbf{d}^{(n+1)} + \cdots + e^{j\theta_{i-1}^\star}\mathbf{d}^{(n+i-1)} + \mathbf{d}^{(n+i+1)} + \cdots + \mathbf{d}^{(n+m)},$$

and thus,

$$\theta_i^\star = \pi - \arg\langle \hat{\mathbf{d}}^{(n)}, \mathbf{d}^{(n+i)} \rangle. \tag{3.17}$$

The greedy technique is in fact one iteration of the BCD method when initial phases are zero, and therefore, cannot outperform the BCD technique. However, it is faster and has less computational complexity.

Opportunistic co-phase technique

The technique is initially proposed in [43] to solve a problem of signal to interference and noise ratio (SINR) maximization in a multiple-input single-output (MISO) system. We exploit this technique here to find a suboptimal rotation phase vector of OFDM symbols to minimize the interference to the primary user.

Let $\{\boldsymbol{\theta}^i\},\ i = 1, \cdots, P$, be sets of candidate phase vectors to be employed in (3.9), where $\boldsymbol{\theta}^i = [\theta_1^i, \cdots, \theta_m^i]^T$ and θ_j^i are random phases each chosen independently and uniformly over $[0, 2\pi)$. By defining $\mathbf{d}^i = \mathbf{d}^{(n)} + e^{j\theta_1^i}\mathbf{d}^{(n+1)} + \cdots + e^{j\theta_m^i}\mathbf{d}^{(n+m)}$, then,

$$\hat{i} = \underset{i=1,\cdots,P}{\arg\min} \|\mathbf{d}^i\|^2, \tag{3.18}$$

is the index of the phase vector that has the least interference to the primary user, i.e., $\boldsymbol{\theta}^{\hat{i}}$ is the algorithm's approximation of $\boldsymbol{\theta}_{\mathsf{opt}}$. It is clear that by increasing the size of the phase set P, better approximations to $\boldsymbol{\theta}_{\mathsf{opt}}$ are expected. Quantitative evaluation of the technique is presented in Section 3.4.1.

It is also worth noting that in the phase adjustment technique presented in this section, the phase rotation is the same for all subcarriers within one OFDM symbol. This allows the receiver to consider the rotation as a part of the CPE. There are several methods in the literature for estimating the CPE (see e.g. [39, 40]). Hence, the transmitter does not need to send explicit side information along with data.

3.2.3 Performance Analysis

Based on the solutions provided in the previous section, only for the case of $m = 1$, an analytical solution to (3.9) is known. Therefore, in this section, the performance of the phase adjustment technique for $m = 1$ is analyzed.

For the analysis, we first define the *improvement factor* as

$$\xi \triangleq \frac{\mathbb{E}\{\|\mathbf{d}^{(n)} + \mathbf{d}^{(n+1)}\|^2\}}{\mathbb{E}\{\min_\theta \|\mathbf{d}^{(n)} + e^{j\theta}\mathbf{d}^{(n+1)}\|^2\}}, \tag{3.19}$$

where $\mathbb{E}\{\cdot\}$ represents the expectation operator.

Entries of the interference vectors are the superposition of a relatively large number of sampled sidelobes of active subcarriers in the OFDM symbol with different weights. Thus, due to the central limit theorem, the interference vectors are approximated as *Gaussian* vectors. Assuming now that $\mathbf{d}^{(n)}$ and $\mathbf{d}^{(n+1)}$ are Gaussian, let R_n and R_{n+1} denote covariance matrices of $\mathbf{d}^{(n)}$ and $\mathbf{d}^{(n+1)}$, respectively, i.e.,

$$\begin{aligned} R_n &= \mathbb{E}\{\mathbf{d}^{(n)}\mathbf{d}^{(n)\dagger}\} \\ &= \widetilde{W}^{(L)}_{N,N+G}\mathbb{E}\{\mathbf{x}^{(n)}\mathbf{x}^{(n)\dagger}\}\widetilde{W}^{(L)\dagger}_{N,N+G}, \end{aligned} \tag{3.20}$$

and

$$\begin{aligned} R_{n+1} &= \mathbb{E}\{\mathbf{d}^{(n+1)}\mathbf{d}^{(n+1)\dagger}\} \\ &= \widetilde{D}_1\widetilde{W}^{(L)}_{N,N+G}\mathbb{E}\{\mathbf{x}^{(n+1)}\mathbf{x}^{(n+1)\dagger}\}\widetilde{W}^{(L)\dagger}_{N,N+G}\widetilde{D}_1^\dagger \qquad (3.21) \\ &= \widetilde{D}_1 R_n \widetilde{D}_1^\dagger, \qquad (3.22) \end{aligned}$$

where (3.20) and (3.21) follow from (3.6). Using matrix diagonalization, we have

$$R_n = U\Sigma U^\dagger, \tag{3.23}$$

$$R_{n+1} = \widetilde{D}_1 U\Sigma U^\dagger \widetilde{D}_1^\dagger, \tag{3.24}$$

where $\Sigma = \mathrm{diag}(\lambda_i),\ i = 1, \ldots, K$, is the matrix of eigenvalues, K is the length of interference vectors, and $U = [\mathbf{u}_1\ \mathbf{u}_2\ \ldots\ \mathbf{u}_K]$ is the eigenvectors matrix of R_n which is unitary since R_n is Hermitian. Thus, $\mathbf{d}^{(n)}$ and $\mathbf{d}^{(n+1)}$ can be expressed as

$$\mathbf{d}^{(n)} = U\mathbf{a}, \tag{3.25}$$

$$\mathbf{d}^{(n+1)} = \widetilde{D}_1 U\mathbf{b}, \tag{3.26}$$

where a_i and b_i are i.i.d Gaussian random variables with $a_i, b_i \sim \mathcal{CN}(0, \lambda_i)$, $i = 1, \ldots, K$. The following theorem gives an upper bound on the improvement factor ξ.

***Theorem* 2** *The improvement factor ξ, defined in (3.19), is upperbounded as*

$$\xi \leq \frac{\mathbb{T}r(R_n)}{\mathbb{T}r(R_n) - [\mathbb{T}r(R_n R_{n+1})]^{\frac{1}{2}}}, \tag{3.27}$$

where $\mathbb{T}r(\cdot)$ denotes the matrix trace. ■

Proof: See Appendix 3.A.2. □

As Theorem 2 states, the upper bound depends only on the covariance matrices of the interference vectors. Each interference vector can be written as

$$\mathbf{d}^{(n)} = \sum_{i=1}^{N_a} X_i^{(n)} \mathbf{S}'_i, \tag{3.28}$$

in which N_a is the number of active subcarriers, $X_i^{(n)}$ is the complex weight of the ith subcarrier which we assume to be a zero-mean random variable with variance $\sigma_X^2 = 1$, and $\mathbf{S}'_i$ is the sampled tail of the ith subcarrier in the primary band. Therefore,

$$R_n = \sum_{i=1}^{N_a} \sum_{j=1}^{N_a} (\mathbb{E}\{X_i^{(n)} X_j^{*(n)}\} \mathbf{S}'_i \mathbf{S}'^{\dagger}_j) = \sum_{i=1}^{N_a} \mathbf{S}'_i \mathbf{S}'^{\dagger}_i, \tag{3.29}$$

where (3.29) follows from the fact that $X_i^{(n)}$s are i.i.d. and zero-mean with $\sigma_X^2 = 1$. Therefore, the covariance matrix does not depend on the data symbols and can be calculated separately. It depends only on the location of active subcarriers or, in other words, on the configuration of the primary user activity. In Section 3.4, we numerically calculate the improvement factor as well as the upper bound for different configurations of primary activity and show that the derived upper bound is relatively tight.

3.3 Multi-antenna OFDM Cognitive Transmitter

3.3.1 System and Signal Model

In this section, we consider a multi-antenna OFDM cognitive transmitter. More specifically, it is assumed that the cognitive transmitter employs $M + 1$ antennas to send information to the secondary receiver, and the secondary receiver has one or more antennas. A primary user is also assumed to receive the secondary signals and therefore is to be protected from the secondary user's interference, as shown in Fig. 3.3.

For the signals transmitted from each antenna, we assume the same model as in Section 3.2.1, except the index used to denote the antenna from which the signal is being transmitted, i.e.,

$$\mathbf{x}_i^{(n)} = \frac{1}{\sqrt{N}} W_{N,N+G}^{\dagger} \mathbf{X}_i^{(n)}, \quad i = 0, 1, \cdots, M, \tag{3.30}$$

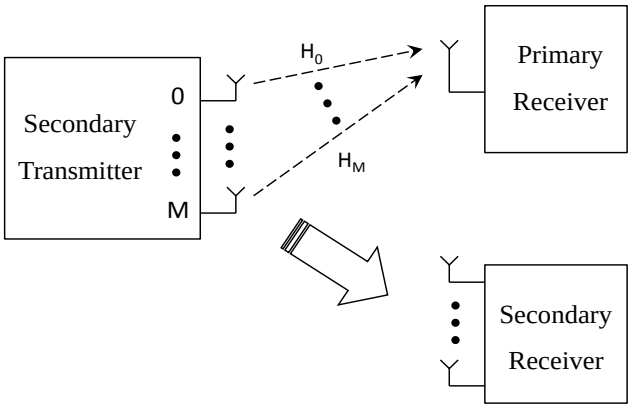

Figure 3.3: System model of a multiple-antenna cognitive system.

and

$$\mathbf{X}_{L,i}^{(n)} = \frac{1}{N} W_{N,N+G}^{(L)} W_{N,N+G}^{\dagger} \mathbf{X}_i^{(n)}, \quad i = 0, 1, \cdots, M, \tag{3.31}$$

where $\mathbf{X}_i^{(n)}$ and $\mathbf{x}_i^{(n)}$ denote the nth OFDM symbol transmitted from the ith antenna in the frequency and time domain respectively, and $\mathbf{X}_{L,i}^{(n)}$ is the corresponding upsampled spectrum by a factor of L. Furthermore, we assume that $\mathbf{X}_0^{(n)}, \cdots, \mathbf{X}_M^{(n)}$ are uncorrelated transmissions.

Similar to Section 3.2.1, we assume that the primary user occupies a bandwidth equivalent to B subcarriers among the total N subcarriers of the OFDM cognitive system.

Furthermore, let H_i, $i = 0, \cdots, M$, be diagonal matrices that denote the channel matrix containing the frequency response in the primary band of the channel between the ith secondary transmitter antenna and the primary receiver antenna and these are assumed to be known to the cognitive system. Thus, H_i, $i = 0, \cdots, M$, are diagonal $[(B-1)L+1] \times [(B-1)L+1]$ matrices.

3.3.2 The Phase Adjustment Technique for Multi-antenna OFDM Transmitter

For the multi-antenna cognitive transmitter case, to reduce interference to the primary user, the phase of each OFDM symbol is adjusted based on the symbols of the other

transmitter antennas.

According to the system model described in Section 3.3.1, the interference vector of the nth OFDM symbol due to the ith antenna at the secondary transmitter is

$$\mathbf{d}_{\mathbf{x}_i}^{(n)} = \frac{1}{N}\widetilde{W}_{N,N+G}^{(L)} W_{N,N+G}^{\dagger}\mathbf{X}_i^{(n)}, \quad i = 0, 1, \cdots, M. \tag{3.32}$$

In the multi-antenna case, since signals transmitted from different antennas undergo different channels, it is important to consider the effect of the channels and minimize the total received interference power at the location of the primary receiver. Otherwise, minimizing the interference before the effect of the channel does not necessarily help to reduce the interference to the primary user. This is in comparison to the single-antenna case, where a reduction in the spectrum before the channel always results in a reduction in the spectrum after the channel.

Here, the total interference at the primary receiver is the sum of the received interference spectrum due to each secondary transmitter antenna. Therefore, the interference vector at the primary receiver is

$$\mathbf{d}^{(n)} = \sum_{i=0}^{M} \mathbf{d}_{\mathbf{y}_i}^{(n)}, \tag{3.33}$$

where

$$\mathbf{d}_{\mathbf{y}_i}^{(n)} = H_i \mathbf{d}_{\mathbf{x}_i}^{(n)}, \quad i = 0, \cdots, M, \tag{3.34}$$

is the interference vector at the primary receiver due to the ith secondary transmitter antenna.

In the proposed phase rotation technique for the multiple-antenna cognitive case, in order to reduce the interference to the primary user, OFDM symbols transmitted from each antenna of the secondary transmitter are rotated based on the symbols of other antennas such that the total interference power at the primary receiver is minimized. Thus, the optimal rotation phase that minimizes the interference at the primary receiver is computed as

$$\boldsymbol{\theta}_{\mathsf{opt}} = \arg\min_{\boldsymbol{\theta}} \|\mathbf{d}_{\mathbf{y}_0}^{(n)} + e^{j\theta_1}\mathbf{d}_{\mathbf{y}_1}^{(n)} + \cdots + e^{j\theta_M}\mathbf{d}_{\mathbf{y}_M}^{(n)}\|^2, \tag{3.35}$$

where $\boldsymbol{\theta}_{\mathsf{opt}} = [\theta_1, \cdots, \theta_M]^T$ is the optimal rotation phase of the transmitter antennas. Similar to Section 3.2.2, the LS minimization expressed in (3.35) can be reformulated as an LS minimization with multiple equality constraints. Therefore, to the best of our knowledge, no analytical solution for this optimization problem is known in general that gives a closed form expression.

Algorithm 2: The Block Coordinate Descent Method for the Multiple-antenna Case

Result: A heuristic approximation $\boldsymbol{\theta}^\star$ to the solution of (3.35).
Compute $\mathbf{d}_{\mathbf{y}_0}^{(n)}, \mathbf{d}_{\mathbf{y}_1}^{(n)}, \cdots, \mathbf{d}_{\mathbf{y}_M}^{(n)}$ from (3.34) and (3.32);
Initialize $\boldsymbol{\theta}^0 = \mathbf{0}$
for $k = 1$ to Num-Iterations **do**
  for $i = 1$ to M **do**
    $\tilde{\mathbf{d}}^{(n,\bar{i})} = \mathbf{d}_{\mathbf{y}_0}^{(n)} + e^{j\theta_1^k}\mathbf{d}_{\mathbf{y}_1}^{(n)} + \cdots + e^{j\theta_{i-1}^k}\mathbf{d}_{\mathbf{y}_{i-1}}^{(n)} + e^{j\theta_{i+1}^{k-1}}\mathbf{d}_{\mathbf{y}_{i+1}}^{(n)} + \cdots + e^{j\theta_M^{k-1}}\mathbf{d}_{\mathbf{y}_M}^{(n)}$,
    $\theta_i^k = \pi - \arg\langle\tilde{\mathbf{d}}^{(n,\bar{i})}, \mathbf{d}_{\mathbf{y}_i}^{(n)}\rangle$.
$\boldsymbol{\theta}^\star = \boldsymbol{\theta}^{\text{Num-Iterations}}$.

Algorithm 3: The Greedy Technique for the Multiple-antenna Case

Result: A heuristic approximation $\boldsymbol{\theta}^\star$ to the solution of (3.35).
Compute $\mathbf{d}_{\mathbf{y}_0}^{(n)}, \mathbf{d}_{\mathbf{y}_1}^{(n)}, \cdots, \mathbf{d}_{\mathbf{y}_M}^{(n)}$ from (3.34) and (3.32);
for $i = 1$ to M **do**
  $\tilde{\mathbf{d}}^{(n)} = \mathbf{d}_{\mathbf{y}_0}^{(n)} + e^{j\theta_1^\star}\mathbf{d}_{\mathbf{y}_1}^{(n)} + \cdots + e^{j\theta_{i-1}^\star}\mathbf{d}_{\mathbf{y}_{i-1}}^{(n)} + \mathbf{d}_{\mathbf{y}_{i+1}}^{(n)} + \cdots + \mathbf{d}_{\mathbf{y}_M}^{(n)}$,
  $\theta_i^\star = \pi - \arg\langle\tilde{\mathbf{d}}^{(n)}, \mathbf{d}_{\mathbf{y}_i}^{(n)}\rangle$.

However, for the special case of $M = 1$, i.e. two transmitter antennas, (3.35) specializes as

$$\theta_{\mathsf{opt}} = \arg\min_{\theta_1} \|\mathbf{d}_{\mathbf{y}_0}^{(n)} + e^{j\theta_1}\mathbf{d}_{\mathbf{y}_1}^{(n)}\|^2, \tag{3.36}$$

and, according to Theorem 1, θ_{opt} is calculated as

$$\theta_{\mathsf{opt}} = \pi - \arg\langle\mathbf{d}_{\mathbf{y}_0}^{(n)}, \mathbf{d}_{\mathbf{y}_1}^{(n)}\rangle. \tag{3.37}$$

Therefore, similar to Section 3.2.2, the proposed technique has low complexity in this case.

Since the minimization problem defined in (3.35) has the same structure as (3.9), the three techniques proposed in Section 3.2.2 can be used here to solve (3.35) in the general case of $M > 1$. Here we summarize these techniques in Algorithm 2, 3, and 4.

Moreover, similar to Section 3.2.2, the proposed technique does not need explicit side information to be sent along with the data, since it can be absorbed as a part of channel effect in the form of a common phase error.

In the following section, the improvement in interference reduction achieved by the phase adjustment technique is analytically investigated for the case of $M = 1$, i.e. two

Algorithm 4: The Opportunistic Co-phase Technique for the Multiple-antenna Case

Result: A heuristic approximation $\boldsymbol{\theta}^\star$ to the solution of (3.35).
Compute $\mathbf{d}_{\mathbf{y}_0}^{(n)}, \mathbf{d}_{\mathbf{y}_1}^{(n)}, \cdots, \mathbf{d}_{\mathbf{y}_M}^{(n)}$ from (3.34) and (3.32);
for $k = 1$ to P **do**
  for $l = 1$ to M **do**
    Generate random $\theta_l^k \sim U[0, 2\pi)$
  $\mathbf{d}^k = \mathbf{d}_{\mathbf{y}_0}^{(n)} + e^{j\theta_1^k}\mathbf{d}_{\mathbf{y}_1}^{(n)} + \cdots + e^{j\theta_M^k}\mathbf{d}_{\mathbf{y}_M}^{(n)}$
$\hat{k} = \arg\min_{k=1,\cdots,P} \|\mathbf{d}^k\|^2$,
$\boldsymbol{\theta}^\star = \boldsymbol{\theta}^{\hat{k}}$

antennas, since only for this case an analytical solution is known. Evaluation of other cases using the proposed techniques are presented in Section 3.4.2.

3.3.3 Performance Analysis

The performance of the proposed phase rotation technique is analyzed in this section. Note that the analysis here is different than of the single-antenna case as now the interference vectors have the same statistics, i.e. the corresponding covariance matrices can be simultaneously diagonalized. This allows for a stronger analysis of the performance of the proposed method for the multi-antenna case. For analytical tractability, it is assumed that the secondary transmitter employs two antennas and the channels between the secondary transmitter antennas and the primary receiver are flat fading channels, i.e.,

$$H_i = h_i I, \quad i = 0, 1, \tag{3.38}$$

where h_i is the Rayleigh flat fading gain which we model by a zero-mean unit-variance complex Gaussian random variable, and I is the identity matrix. This assumption would be valid when the delay spread of the channel is small, specifically when there exists a line of sight between the transmitter and the receiver. Frequency selective fading channels are investigated numerically in the next section, where it is found that the performance of the proposed scheme is in line with the analytical predictions for flat fading channels.

In order to analyze the performance of the proposed technique in interference reduction, we use the improvement factor defined in (3.19) for the multiple-antenna scenario, i.e.,

$$\xi \triangleq \frac{\mathbb{E}\{\|\mathbf{d}_{\mathbf{y}_0}^{(n)} + \mathbf{d}_{\mathbf{y}_1}^{(n)}\|^2\}}{\mathbb{E}\{\min_\theta \|\mathbf{d}_{\mathbf{y}_0}^{(n)} + e^{j\theta}\mathbf{d}_{\mathbf{y}_1}^{(n)}\|^2\}}. \tag{3.39}$$

In the multi-antenna case, similar to the single-antenna case, OFDM interference vectors at the secondary transmitter side can be approximated as *correlated Gaussian* vectors according to the central limit theorem. However, in this case, covariance matrices of the interference vectors $\mathbf{d}_{\mathbf{x}_0}^{(n)}$ and $\mathbf{d}_{\mathbf{x}_1}^{(n)}$ are the same and expressed as

$$R_{\mathbf{x}_i} = \widetilde{W}_{N,N+G}^{(L)} \mathbb{E}\{\mathbf{x}_i^{(n)} \mathbf{x}_i^{(n)\dagger}\} \widetilde{W}_{N,N+G}^{(L)\dagger}, \quad i = 0, 1. \tag{3.40}$$

Therefore, the received interference vectors at the primary receiver are also approximated as correlated Gaussian vectors with covariance matrices

$$R_{\mathbf{y}_i} = \mathbb{E}\{\mathbf{d}_{\mathbf{y}_i}^{(n)} \mathbf{d}_{\mathbf{y}_i}^{(n)\dagger}\} = |h_i|^2 R_{\mathbf{x}_i}, \quad i = 0, 1. \tag{3.41}$$

The following theorem gives an approximation of the improvement factor of OFDM interference vectors $\mathbf{d}_{\mathbf{y}_0}^{(n)}$ and $\mathbf{d}_{\mathbf{y}_1}^{(n)}$. We use this approximation to obtain the improvement of the proposed technique in interference reduction to the primary user in Theorem 4.

***Theorem* 3** *Assume that $R_{\mathbf{y}_0}$ (and $R_{\mathbf{y}_1}$) have $l < K$ dominant eigenvalues, i.e.,*

$$\lambda_1 \geq \ldots \geq \lambda_l \gg \lambda_{l+1} \geq \ldots \lambda_K, \tag{3.42}$$

where λ_i, $i = 1, \ldots, K$, are eigenvalues of $R_{\mathbf{y}_0}$ (and $R_{\mathbf{y}_1}$), and $K = (B-1)L + 1$ is the length of the interference vectors $\boldsymbol{d}_{\boldsymbol{y}_0}^{(n)}$ and $\boldsymbol{d}_{\boldsymbol{y}_1}^{(n)}$. Then,

$$\frac{\mathbb{E}\{\|\boldsymbol{d}_{\boldsymbol{y}_0}^{(n)} + \boldsymbol{d}_{\boldsymbol{y}_1}^{(n)}\|^2\}}{\mathbb{E}\{\min_\theta \|\boldsymbol{d}_{\boldsymbol{y}_0}^{(n)} + e^{j\theta} \boldsymbol{d}_{\boldsymbol{y}_1}^{(n)}\|^2\}} \approx \frac{\mathbb{E}\{\|\tilde{\boldsymbol{d}}_{\boldsymbol{y}_0}^{(n)} + \tilde{\boldsymbol{d}}_{\boldsymbol{y}_1}^{(n)}\|^2\}}{\mathbb{E}\{\min_\theta \|\tilde{\boldsymbol{d}}_{\boldsymbol{y}_0}^{(n)} + e^{j\theta} \tilde{\boldsymbol{d}}_{\boldsymbol{y}_1}^{(n)}\|^2\}}, \tag{3.43}$$

where

$$\tilde{\boldsymbol{d}}_{\boldsymbol{y}_j}^{(n)} = [\tilde{d}_{j1}, \tilde{d}_{j2}, \ldots, \tilde{d}_{jl}]^T, \quad j = 0, 1, \tag{3.44}$$

and $\tilde{d}_{0i} \sim \mathcal{CN}(0, \lambda_i)$, $\tilde{d}_{1i} \sim \mathcal{CN}(0, \frac{|h_1|^2}{|h_0|^2}\lambda_i)$, $i = 1, \ldots l$, are independent complex Gaussian random variables. The approximation in (3.43) becomes equality when $\frac{\lambda_{l+1}}{\lambda_l} \longrightarrow 0$. ■

Proof: See Appendix 3.A.3. □

According to Theorem 3, the improvement factor of the OFDM interference vectors $\mathbf{d}_{\mathbf{y}_0}^{(n)}$ and $\mathbf{d}_{\mathbf{y}_1}^{(n)}$ can be approximated as the improvement factor of complex Gaussian vectors

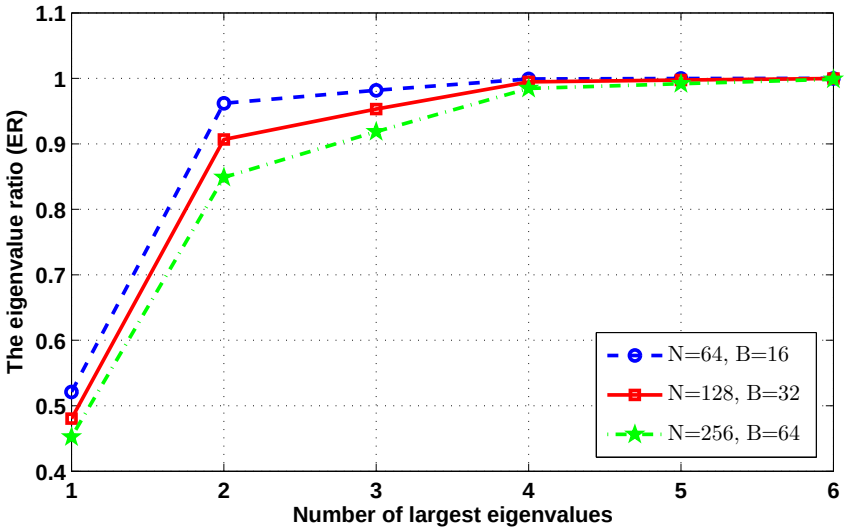

Figure 3.4: The eigenvalue ratio (ER).

of length l with *independent* entries, where l here is the number of dominant eigenvalues of the covariance matrices $R_{\mathbf{y}_0}$ and $R_{\mathbf{y}_1}$.

Now, in order to investigate the number of dominant eigenvalues of $R_{\mathbf{y}_i}, i = 0, 1$, we define the *eigenvalue ratio (ER)* as

$$\mathrm{ER}(l) = \frac{\sum_{i=1}^{l} \lambda_i}{\sum_{i=1}^{K} \lambda_i}. \tag{3.45}$$

According to (3.29), the covariance matrices do not depend on the data symbols and the ER can be calculated separately. Indeed, the covariance matrices depend statistically only on the configuration of detected primary user spectrum. Hence, we run numerical simulations for different spectral opportunity configurations to investigate the behavior of the ER as a function of l. The result is shown in Fig. 3.4 where B is the number of deactivated subcarriers due to the detected primary user bandwidth. It is observed from Fig. 3.4 that for all configurations,

$$\lambda_1 \approx \lambda_2 \gg \lambda_3 \geq \ldots \geq \lambda_K, \tag{3.46}$$

since $\mathrm{ER}(2) \geq 0.85$ (and in some configurations $\mathrm{ER}(2) \geq 0.95$). In other words, it can be concluded that $R_{\mathbf{y}_0}$ and $R_{\mathbf{y}_1}$ have $l = 2$ almost equal dominant eigenvalues. This is intuitively true, because, due to the diminishing tail of active subcarriers, most of the

interference is produced by sidelobes of the nearest subcarriers to the primary band, namely one subcarrier on each side of the primary band.

Therefore, according to Theorem 3, the improvement factor of the interference vectors $\mathbf{d}_{\mathbf{y}_0}^{(n)}$ and $\mathbf{d}_{\mathbf{y}_1}^{(n)}$ is approximated as the improvement factor of two i.i.d. complex Gaussian vectors of length 2 defined as

$$\tilde{d}_{0i} \sim \mathcal{CN}(0, \lambda_1), \quad i = 1, 2, \tag{3.47}$$

$$\tilde{d}_{1i} \sim \mathcal{CN}(0, \frac{|h_1|^2}{|h_0|^2}\lambda_1), \quad i = 1, 2. \tag{3.48}$$

In Theorem 4, we calculate the improvement factor of i.i.d. complex Gaussian vectors.

***Theorem* 4** *Let $\tilde{\boldsymbol{d}}_{\boldsymbol{y}_0}^{(n)}$ and $\tilde{\boldsymbol{d}}_{\boldsymbol{y}_1}^{(n)}$ be two zero-mean i.i.d. complex Gaussian random vectors of length l with entries $\tilde{d}_{0i} \sim \mathcal{CN}(0, \lambda_1)$ and $\tilde{d}_{1i} \sim \mathcal{CN}(0, \frac{|h_1|^2}{|h_0|^2}\lambda_1)$, $i = 1, \ldots, l$. Then,*

$$\frac{\mathbb{E}\{\|\tilde{\boldsymbol{d}}_{\boldsymbol{y}_0}^{(n)} + \tilde{\boldsymbol{d}}_{\boldsymbol{y}_1}^{(n)}\|^2\}}{\mathbb{E}\{\min_\theta \|\tilde{\boldsymbol{d}}_{\boldsymbol{y}_0}^{(n)} + e^{j\theta}\tilde{\boldsymbol{d}}_{\boldsymbol{y}_1}^{(n)}\|^2\}} = \frac{l[1 + \frac{|h_1|^2}{|h_0|^2}]}{l[1 + \frac{|h_1|^2}{|h_0|^2}] - \sqrt{\pi}\frac{|h_1|}{|h_0|}\frac{\Gamma(l+\frac{1}{2})}{\Gamma(l)}}, \tag{3.49}$$

where Γ denotes the Gamma function. ■

Proof: See Appendix 3.A.4. □

According to Theorem 4, the improvement factor of $\tilde{\mathbf{d}}_{\mathbf{y}_0}^{(n)}$ and $\tilde{\mathbf{d}}_{\mathbf{y}_1}^{(n)}$ depends on the length of the corresponding vectors l and the ratio of the channel gains h_0 and h_1. Now, considering (3.46) together with Theorem 3 and Theorem 4, the improvement factor of the OFDM interference vectors $\mathbf{d}_{\mathbf{y}_0}^{(n)}$ and $\mathbf{d}_{\mathbf{y}_1}^{(n)}$ will be

$$\begin{aligned}\frac{\mathbb{E}\{\|\mathbf{d}_{\mathbf{y}_0}^{(n)} + \mathbf{d}_{\mathbf{y}_1}^{(n)}\|^2\}}{\mathbb{E}\{\min_\theta \|\mathbf{d}_{\mathbf{y}_0}^{(n)} + e^{j\theta}\mathbf{d}_{\mathbf{y}_1}^{(n)}\|^2\}} &\approx \frac{2(1 + \frac{|h_1|^2}{|h_0|^2})}{2(1 + \frac{|h_1|^2}{|h_0|^2}) - \sqrt{\pi}\frac{|h_1|}{|h_0|}\frac{\Gamma(2.5)}{\Gamma(2)}} \\ &\cong \frac{1 + \frac{|h_1|^2}{|h_0|^2}}{1 + \frac{|h_1|^2}{|h_0|^2} - 1.1781 \times \frac{|h_1|}{|h_0|}}\end{aligned} \tag{3.50}$$

which depends on the ratio of channel fading gains h_1 and h_2.

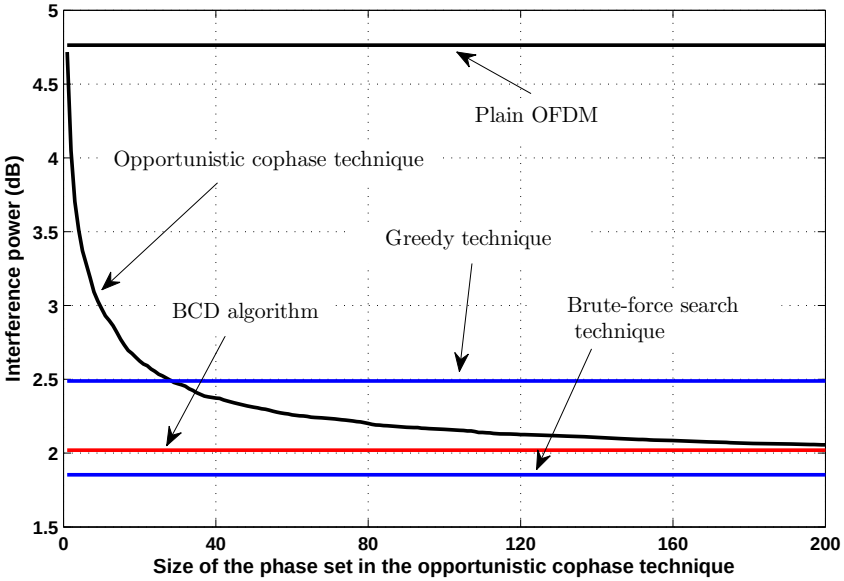

Figure 3.5: Comparison of the proposed techniques for finding the optimal adjustment phases in the single-antenna case where $m = 3$.

3.4 Simulation Results

In this section, the performance of the proposed phase rotation technique for single-antenna and multi-antenna OFDM cognitive transmitters is investigated using numerical simulations. In simulations, for both single-antenna and multi-antenna cases, the cognitive systems employ OFDM signaling with $N = 256$ subcarriers and the spectrum is upsampled by a factor of $L = 8$. A number of subcarriers corresponding to the primary user bandwidth are deactivated and the remaining are BPSK-modulated.

3.4.1 Single-antenna OFDM Cognitive Transmitter

Fig. 3.5 shows the performance of the three proposed techniques in Section 3.2.2 for $m = 3$. Here the primary user bandwidth is assumed to be spread over $B = 16$ consecutive subcarriers from subcarrier 97 to 112. Also, for the BCD method we have run the simulations for 4 iterations. As can be observed from the figure, the block coordinate descent method

Table 3.1: The improvement factor and upper bound for 1-sided and 2-sided OFDM signals

	1-sided OFDM	2-sided OFDM
ξ (dB)	2.1	1.9
Upper bound (dB)	2.7	2.4

has the best performance and reduces the interference by almost 3 dB on average. Moreover, the gap between the performance obtained using the BCD algorithm and the optimal performance of brute-force algorithm is negligible.

In order to show the performance of the proposed methods in reducing the spectrum at the primary band, the spectrum of the transmitted OFDM symbols is depicted in Fig. 3.6 where the spectrum of the plain OFDM signal is compared to the phase adjusted OFDM for $m = 3$.

The upper bound derived in Section 3.2.3 for the case of $m = 1$ is also evaluated numerically under two different primary activity configurations. In the first configuration, the primary user band is spread over 16 subcarriers that are located from subcarrier 121 to 136. We call this configuration 2-sided OFDM. In the second configuration, the primary user's band is located at one end of the total OFDM signal bandwidth on the last 8 subcarriers. We call this configuration 1-sided OFDM. It can also be considered as out-of-band (OOB) radiation mitigation for current OFDM systems. Table 3.1 shows the improvement factors of the proposed technique for these OFDM configurations obtained from numerical simulations and the corresponding theoretical upper bounds. As can be seen from Table 3.1, the upper bounds are relatively tight.

3.4.2 Multi-antenna OFDM Cognitive Transmitter

In the multi-antenna case, we first use numerical simulations to evaluate the analysis derived in Section 3.3.3 for the case of $M = 1$, i.e. two secondary transmitter antennas. Here the channels are Rayleigh fading, i.e., $|h_i|$ and $\angle h_i$ are independent and have Rayleigh and uniform distributions, respectively. In Fig. 3.7, the solid line shows the behavior of (3.50) vs. $\frac{|h_1|}{|h_0|}$. Computer simulations are used to find the interference reduction obtained by the proposed technique for different realizations of the channel gains h_0 and h_1. The numerical results are shown in Fig. 3.7 as dots. In the simulations, the primary bandwidth is assumed to be spread over $B = 32$ consecutive subcarriers. As can be seen in Fig. 3.7, the numerical results approximately agree with the analytical results for the improvement

Table 3.2: Improvement of the proposed technique for different channel models.

channel model	RMS delay spread (μs)	improvement (dB)
flat fading	0	3.23
SUI-1	0.111	3.12
SUI-3	0.264	2.84
SUI-4	1.257	2.62

of the proposed phase adjustment technique. The slight difference between the analytical and numerical results is attributed to the Gaussian assumption of the interference vectors, which is an approximation.

Fig. 3.8 illustrates the power spectral density of the received OFDM signals transmitted from 4 secondary antennas, i.e. $M = 3$, at the primary receiver. Here the primary user band is spread over 16 subcarriers from subcarrier 97 to 112. The performance of the BCD algorithm with 4 iterations and the greedy technique is shown in the figure. It can be seen from Fig. 3.8 that the proposed BCD algorithm for finding the optimal rotation phases decreases the interference to the primary user by up to 6 dB.

Finally, Fig. 3.9 gives a comparison of the performance of the proposed techniques for calculating the optimal rotation phases in Section 3.3.2 for the case of $M = 3$, i.e., 4 transmitter antennas. Here again 4 iterations are used in the BCD algorithm. Similar to the single-antenna case, the BCD algorithm outperforms the other techniques and yields close to optimal performance.

Frequency selective fading channels– The performance of the proposed phase rotation technique is also investigated under frequency selective channels using numerical simulations for a cognitive system with 3 transmit antennas. In frequency selective fading channels, each subcarrier in the OFDM symbols undergoes different fading. In other words, $H_i,\ i = 0, 1, 2$, are diagonal matrices whose diagonal entries are not necessarily equal. In computer simulations, $H_i,\ i = 0, 1, 2$, are modeled by the SUI-4 channel model [38] which is a tapped-delay-line model with 3 taps, and is suitable for MIMO broadband wireless applications. Moreover, the transmitter antennas are assumed to be sufficiently spatially separated. Therefore, the channels are generated independently. Here the primary user occupies a bandwidth of 16 subcarriers. The power spectral density of the received OFDM signal at the primary receiver is depicted in Fig. 3.10, which shows an improvement of approximately 6 dB in sidelobe reduction using the BCD algorithm for finding the adjustment phases.

Furthermore, the performance of the proposed phase adjustment technique for a 2-antenna secondary transmitter using different frequency selective channel models with different delay spreads is investigated. For each channel model, the median improvement over 2000 realizations of the channels is computed. The results are shown in Table 3.2. It is observed from Table 3.2 that for channels with different delay spreads, the improvements are in approximate agreement with 3.23 dB for flat fading channels. However, as the delay spread is reduced, the performance improvement is better predicted by that of the flat fading results.

3.5 Conclusion

A new technique to reduce the interference to the primary users in single-antenna and multi-antenna transmitter OFDM cognitive radios has been presented. In the single-antenna case, the proposed phase-adjustment technique rotates all subcarriers of m consecutive OFDM symbols based on the prior OFDM symbols, such that the entire interference is minimized. In the multi-antenna case, transmitted symbols of one antenna are rotated in the complex space such that the interference to the primary receiver is minimized. The technique does not suffer from existing drawbacks such as loss in useful data rate, increase in BER, and high complexity. Moreover, the performance of the technique is evaluated analytically for both single-antenna and multi-antenna OFDM cognitive systems and verified by computer simulations.

3.A Appendices

3.A.1 Proof of Theorem 1

We can expand the right hand side of (3.9) as

$$\begin{aligned}
&\arg\min_{\theta} \|\mathbf{d}^{(n)} + e^{j\theta}\mathbf{d}^{(n+1)}\|^2 \\
&= \arg\min_{\theta}\{\|\mathbf{d}^{(n)}\|^2 + \|\mathbf{d}^{(n+1)}\|^2 + \langle \mathbf{d}^{(n)}, \mathbf{d}^{(n+1)}\rangle e^{j\theta} \\
&\quad + \langle \mathbf{d}^{(n)}, \mathbf{d}^{(n+1)}\rangle e^{-j\theta}\} \\
&= \arg\min_{\theta}(2\Re\{\langle \mathbf{d}^{(n)}, \mathbf{d}^{(n+1)}\rangle e^{j\theta}\}). \qquad (3.51)
\end{aligned}$$

The argument in (3.51) is minimized when $\arg(\langle \mathbf{d}^{(n)}, \mathbf{d}^{(n+1)}\rangle e^{j\theta}) = \pi$. Hence,

$$\theta = \pi - \arg\langle \mathbf{d}^{(n)}, \mathbf{d}^{(n+1)}\rangle \qquad (3.52)$$

3.A.2 Proof of Theorem 2

The numerator of the right hand side of (3.19) is expanded as

$$\begin{aligned}
\mathbb{E}\{\|\mathbf{d}^{(n)} + \mathbf{d}^{(n+1)}\|^2\} &= \mathbb{E}\{\|\mathbf{d}^{(n)}\|^2\} + \mathbb{E}\{\|\mathbf{d}^{(n+1)}\|^2\} \qquad (3.53) \\
&= 2\ \mathbb{T}r(R_n) \qquad (3.54)
\end{aligned}$$

where (3.53) follows from the fact that $\mathbf{d}^{(n)}$ and $\mathbf{d}^{(n+1)}$ are zero-mean and independent. Similarly, we can expand the denominator of the right hand side of (3.19) as

$$\begin{aligned}
&\mathbb{E}\{\min_{\theta} \|\mathbf{d}^{(n)} + e^{j\theta}\mathbf{d}^{(n+1)}\|^2\} \\
&= \mathbb{E}\{\|\mathbf{d}^{(n)}\|^2 + \|\mathbf{d}^{(n+1)}\|^2 + \min_{\theta}[2\Re(e^{j\theta}\mathbf{d}^{(n)\dagger}\ \mathbf{d}^{(n+1)})]\} \\
&= \mathbb{E}\{\|\mathbf{d}^{(n)}\|^2\} + \mathbb{E}\{\|\mathbf{d}^{(n+1)}\|^2\} - 2\mathbb{E}|\mathbf{d}^{(n)\dagger}\ \mathbf{d}^{(n+1)}|, \qquad (3.55)
\end{aligned}$$

where (3.55) follows by choosing a proper θ to minimize $\Re(e^{j\theta}\mathbf{d}^{(n)\dagger}\ \mathbf{d}^{(n+1)})$. Now, $\mathbb{E}|\mathbf{d}^{(n)\dagger}\ \mathbf{d}^{(n+1)}|$ can be upperbounded as

$$\begin{aligned}
[\mathbb{E}|\mathbf{d}^{(n)\dagger}\ \mathbf{d}^{(n+1)}|]^2 &\leq \mathbb{E}|\mathbf{d}^{(n)\dagger}\ \mathbf{d}^{(n+1)}|^2 \\
&= \mathbb{E}|\mathbf{a}^\dagger U^\dagger \widetilde{D}_1 U\mathbf{b}|^2 \\
&= \mathbb{E}\{\mathbb{T}r(\mathbf{a}^\dagger U^\dagger \widetilde{D}_1 U\mathbf{b}\mathbf{b}^\dagger U^\dagger \widetilde{D}_1^\dagger U\mathbf{a})\} \\
&= \mathbb{E}\{\mathbb{T}r(U\mathbf{a}\mathbf{a}^\dagger U^\dagger \widetilde{D}_1 U\mathbf{b}\mathbf{b}^\dagger U^\dagger \widetilde{D}_1^\dagger)\} \\
&= \mathbb{T}r(U\Sigma U^\dagger \widetilde{D}_1 U\Sigma U^\dagger \widetilde{D}_1^\dagger) \\
&= \mathbb{T}r(R_n R_{n+1}). \qquad (3.56)
\end{aligned}$$

Therefore, by applying (3.56) to (3.55), the upper bound is proved.

3.A.3 Proof of Theorem 3

The covariance matrices $R_{\mathbf{y}_1}$ and $R_{\mathbf{y}_2}$ are diagonalized as

$$Q^\dagger R_{\mathbf{y}_0} Q = \mathrm{diag}(\{\lambda_i\}_{i=1}^K), \qquad (3.57)$$

$$Q^\dagger R_{\mathbf{y}_1} Q = \mathrm{diag}(\{\frac{|h_1|^2}{|h_0|^2}\lambda_i\}_{i=1}^K), \qquad (3.58)$$

where $Q = [\mathbf{q}_1\ \mathbf{q}_2\ \ldots\ \mathbf{q}_K]$ is the eigenvector matrix of $R_{\mathbf{y}_1}$ and $R_{\mathbf{y}_2}$, and is unitary. Thus, $\mathbf{d}_{\mathbf{y}_0}^{(n)}$ and $\mathbf{d}_{\mathbf{y}_1}^{(n)}$ can be expressed as

$$\mathbf{d}_{\mathbf{y}_j}^{(n)} = \sum_{i=1}^K \tilde{d}_{ji}\ \mathbf{q}_i, \quad j = 0, 1, \qquad (3.59)$$

where $\tilde{d}_{0i}$ and $\tilde{d}_{1i}$ are independent Gaussian random variables with $\tilde{d}_{0i} \sim \mathcal{CN}(0, \lambda_i)$, $\tilde{d}_{1i} \sim \mathcal{CN}(0, \frac{|h_1|^2}{|h_0|^2}\lambda_i), i = 1, \ldots K$. Thus, the numerator on the left hand side of (3.43) can be

written as

$$\begin{aligned}\mathbb{E}\{\|\mathbf{d}_{\mathbf{y}_0}^{(n)}+\mathbf{d}_{\mathbf{y}_1}^{(n)}\|^2\} &= \mathbb{E}\{\|\sum_{i=1}^{K}\tilde{d}_{0i}\,\mathbf{q}_i+\sum_{i=1}^{K}\tilde{d}_{1i}\,\mathbf{q}_i\|^2\}\\ &= \sum_{i=1}^{K}\lambda_i+\sum_{i=1}^{K}\frac{|h_1|^2}{|h_0|^2}\lambda_i\\ &\approx \mathbb{E}\{\sum_{i=1}^{l}(|\tilde{d}_{0i}|^2+|\tilde{d}_{1i}|^2)\}\\ &= \mathbb{E}\{\|\tilde{\mathbf{d}}_{\mathbf{y}_0}^{(n)}+\tilde{\mathbf{d}}_{\mathbf{y}_1}^{(n)}\|^2\}. \end{aligned} \tag{3.60}$$

Similarly, the denominator on the left hand side of (3.43) is expanded as

$$\begin{aligned}&\mathbb{E}\{\min_{\theta}\|\mathbf{d}_{\mathbf{y}_0}^{(n)}+e^{j\theta}\mathbf{d}_{\mathbf{y}_1}^{(n)}\|^2\}\\ &= \mathbb{E}\{\min_{\theta}\|\sum_{i=1}^{K}\tilde{d}_{0i}\,\mathbf{q}_i+e^{j\theta}\sum_{i=1}^{K}\tilde{d}_{1i}\,\mathbf{q}_i\|^2\}\\ &= \mathbb{E}\{\sum_{i=1}^{K}(|\tilde{d}_{0i}|^2+|\tilde{d}_{1i}|^2)+\min_{\theta}\sum_{i=1}^{K}(e^{j\theta}\tilde{d}_{0i}^{*}\tilde{d}_{1i}+e^{-j\theta}\tilde{d}_{0i}\tilde{d}_{1i}^{*})\}\\ &= \mathbb{E}\{\sum_{i=1}^{K}(|\tilde{d}_{0i}|^2+|\tilde{d}_{1i}|^2)+2\min_{\theta}[\Re(\sum_{i=1}^{K}e^{j\theta}\tilde{d}_{0i}^{*}\tilde{d}_{1i})]\}\\ &\approx \mathbb{E}\{\sum_{i=1}^{l}(|\tilde{d}_{0i}|^2+|\tilde{d}_{1i}|^2)-2|\sum_{i=1}^{l}\tilde{d}_{0i}^{*}\tilde{d}_{1i}|\}\\ &= \mathbb{E}\{\min_{\theta}\|\tilde{\mathbf{d}}_{\mathbf{y}_0}^{(n)}+e^{j\theta}\tilde{\mathbf{d}}_{\mathbf{y}_1}^{(n)}\|^2\}, \end{aligned} \tag{3.61}$$

and the proof is complete.

3.A.4 Proof of Theorem 4

The numerator of the left hand side of (3.49) is expanded as

$$\mathbb{E}\{\|\tilde{\mathbf{d}}_{\mathbf{y}_0}^{(n)}+\tilde{\mathbf{d}}_{\mathbf{y}_1}^{(n)}\|^2\} = \mathbb{E}\{\|\tilde{\mathbf{d}}_{\mathbf{y}_0}^{(n)}\|^2\}+\mathbb{E}\{\|\tilde{\mathbf{d}}_{\mathbf{y}_1}^{(n)}\|^2\} \tag{3.62}$$

$$= l\lambda_1+l\frac{|h_1|^2}{|h_0|^2}\lambda_1, \tag{3.63}$$

where (3.62) follows from the fact that $\tilde{\mathbf{d}}_{\mathbf{y}_1}^{(n)}$ and $\tilde{\mathbf{d}}_{\mathbf{y}_2}^{(n)}$ are zero-mean and independent.

Similarly, we expand the denominator as

$$\begin{aligned}
&\mathbb{E}\{\min_{\theta} \|\tilde{\mathbf{d}}_{\mathbf{y}_0}^{(n)} + e^{j\theta}\tilde{\mathbf{d}}_{\mathbf{y}_1}^{(n)}\|^2\} \\
&= \mathbb{E}\{\min_{\theta}[\|\tilde{\mathbf{d}}_{\mathbf{y}_0}^{(n)}\|^2 + \|\tilde{\mathbf{d}}_{\mathbf{y}_1}^{(n)}\|^2 + e^{j\theta}\tilde{\mathbf{d}}_{\mathbf{y}_0}^{(n)\dagger}\tilde{\mathbf{d}}_{\mathbf{y}_1}^{(n)} + e^{-j\theta}\tilde{\mathbf{d}}_{\mathbf{y}_1}^{(n)\dagger}\tilde{\mathbf{d}}_{\mathbf{y}_0}^{(n)}]\} \\
&= \mathbb{E}\{\|\tilde{\mathbf{d}}_{\mathbf{y}_0}^{(n)}\|^2 + \|\tilde{\mathbf{d}}_{\mathbf{y}_1}^{(n)}\|^2 + \min_{\theta}[2\Re\{e^{j\theta}\tilde{\mathbf{d}}_{\mathbf{y}_0}^{(n)\dagger}\tilde{\mathbf{d}}_{\mathbf{y}_1}^{(n)}\}]\} \qquad (3.64) \\
&= \mathbb{E}\{\|\tilde{\mathbf{d}}_{\mathbf{y}_0}^{(n)}\|^2\} + \mathbb{E}\{\|\tilde{\mathbf{d}}_{\mathbf{y}_1}^{(n)}\|^2\} - 2\mathbb{E}\{|\tilde{\mathbf{d}}_{\mathbf{y}_0}^{(n)\dagger}\tilde{\mathbf{d}}_{\mathbf{y}_1}^{(n)}|\}, \qquad (3.65)
\end{aligned}$$

where (3.65) follows by choosing θ to minimize the argument inside (3.64).

Due to rotational symmetry of $\tilde{\mathbf{d}}_{\mathbf{y}_0}^{(n)}$ and $\tilde{\mathbf{d}}_{\mathbf{y}_1}^{(n)}$, without loss of generality, we may assume that the vector $\tilde{\mathbf{d}}_{\mathbf{y}_0}^{(n)}$ is along the first coordinate $\boldsymbol{e}_1$ of the l-dimensional complex space, i.e., $\tilde{\mathbf{d}}_{\mathbf{y}_0}^{(n)} = \|\tilde{\mathbf{d}}_{\mathbf{y}_0}^{(n)}\|\boldsymbol{e}_1$. Therefore, (3.65) can be written as

$$\begin{aligned}
&\mathbb{E}\{\|\tilde{\mathbf{d}}_{\mathbf{y}_0}^{(n)}\|^2\} + \mathbb{E}\{\|\tilde{\mathbf{d}}_{\mathbf{y}_1}^{(n)}\|^2\} - 2\mathbb{E}\{\|\tilde{\mathbf{d}}_{\mathbf{y}_0}^{(n)}\|\,|\boldsymbol{e}_1^{\dagger}\tilde{\mathbf{d}}_{\mathbf{y}_1}^{(n)}|\} \\
&= l\lambda_1 + l\frac{|h_1|^2}{|h_0|^2}\lambda_1 - 2\mathbb{E}\{\|\tilde{\mathbf{d}}_{\mathbf{y}_0}^{(n)}\|\}\mathbb{E}\{|\tilde{d}_{11}|\} \qquad (3.66) \\
&= l\lambda_1 + l\frac{|h_1|^2}{|h_0|^2}\lambda_1 - \left(\sqrt{2\lambda_1}\frac{\Gamma(\frac{2l+1}{2})}{\Gamma(l)}\right)\frac{|h_1|}{|h_0|}\sqrt{\lambda_1}\sqrt{\frac{\pi}{2}} \qquad (3.67) \\
&= l\lambda_1 + l\frac{|h_1|^2}{|h_0|^2}\lambda_1 - \sqrt{\pi}\sqrt{\lambda_1}\frac{|h_1|}{|h_0|}\sqrt{\lambda_1}\frac{\Gamma(l+\frac{1}{2})}{\Gamma(l)} \qquad (3.68)
\end{aligned}$$

where $\tilde{d}_{11}$ is the first coordinate of $\tilde{\mathbf{d}}_{\mathbf{y}_1}^{(n)}$ and (3.66) follows from independence of $\tilde{\mathbf{d}}_{\mathbf{y}_0}^{(n)}$ and $\tilde{\mathbf{d}}_{\mathbf{y}_1}^{(n)}$. Also, since $\tilde{\mathbf{d}}_{\mathbf{y}_0}^{(n)}$ and $\tilde{\mathbf{d}}_{\mathbf{y}_1}^{(n)}$ are i.i.d. complex Gaussian vectors, $\|\tilde{\mathbf{d}}_{\mathbf{y}_0}^{(n)}\|/\sqrt{\lambda_1}$ is a chi-distributed and $|\tilde{d}_{11}|$ is a Rayleigh random variable. Hence, (3.67) follows, and the proof is complete.

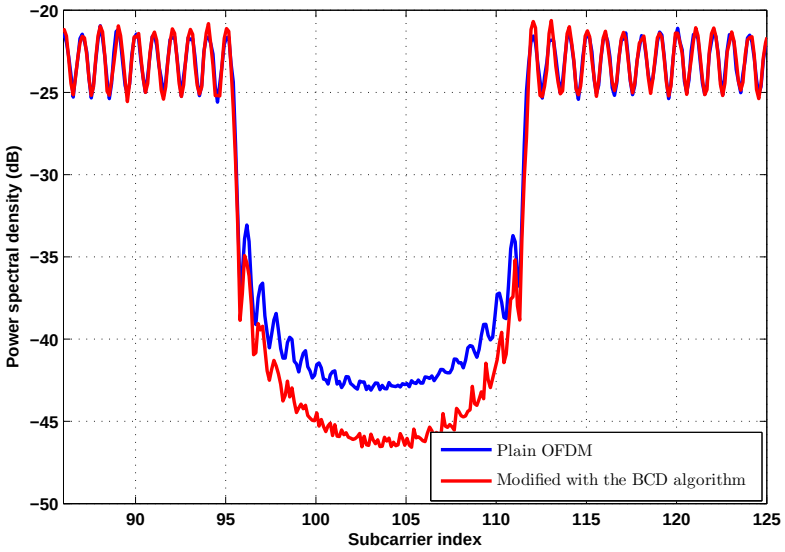

(a)

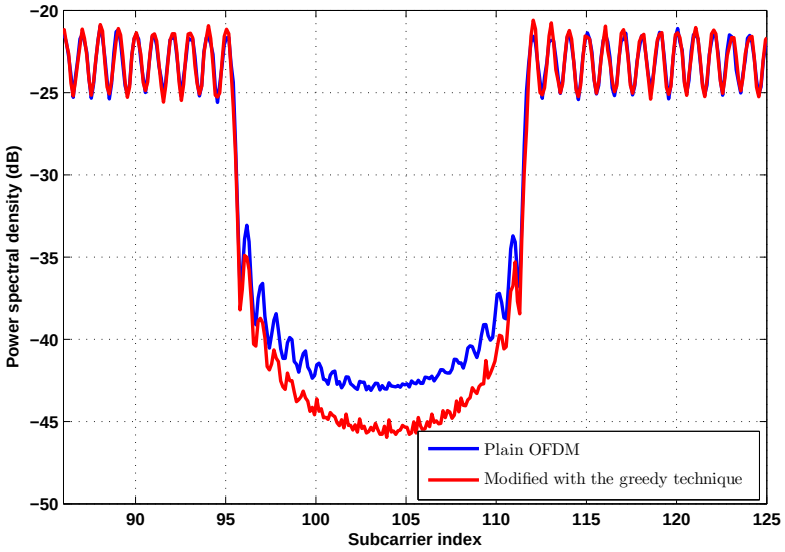

(b)

Figure 3.6: Power spectrum of the phase adjusted OFDM signal transmitted from a single-antenna cognitive transmitter where $m = 3$; (a): optimal phases are found using the BCD algorithm, (b): optimal phases are found using the greedy technique.

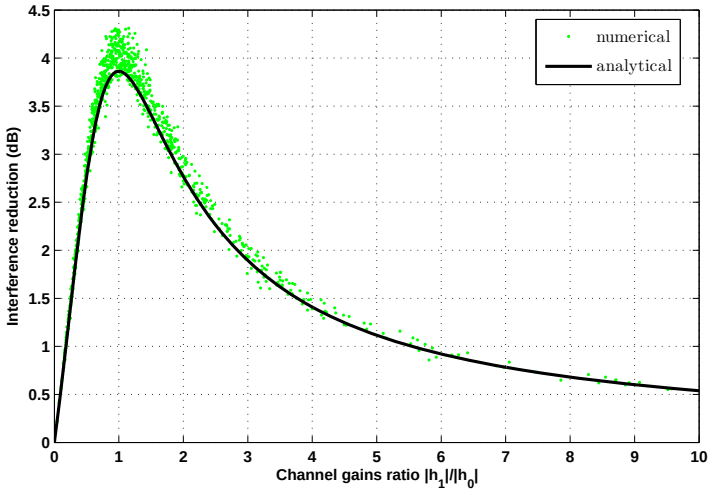

Figure 3.7: Improvement of the proposed technique in interference reduction for different channel gains ratios $\frac{|h_1|}{|h_0|}$ for the multi-antenna case with two transmitter antennas.

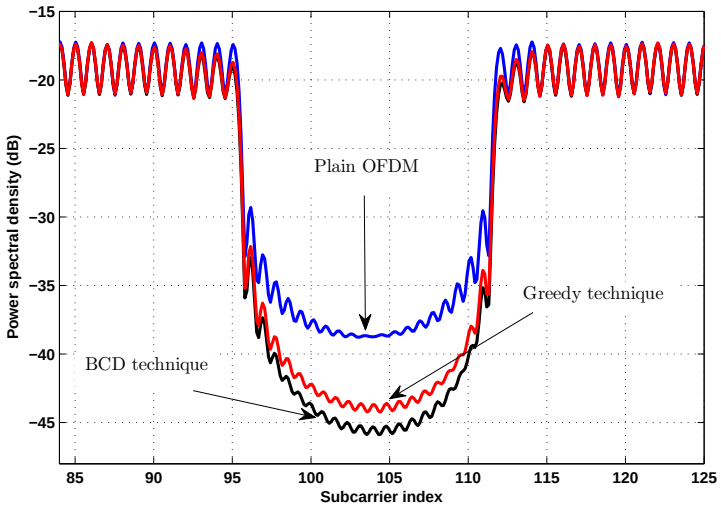

Figure 3.8: Power spectrum of the phase adjusted OFDM signal transmitted from a 4-antenna cognitive transmitter using the BCD and the greedy technique.

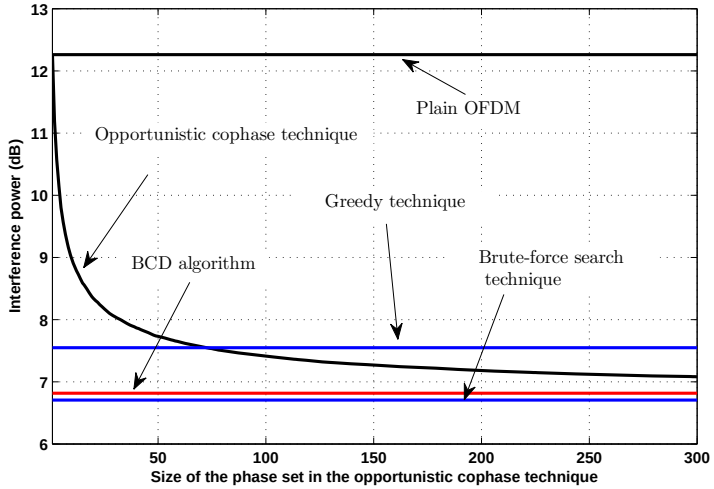

Figure 3.9: Comparison of the proposed techniques for finding the optimal adjustment phases in the multiple-antenna case with four transmit antennas.

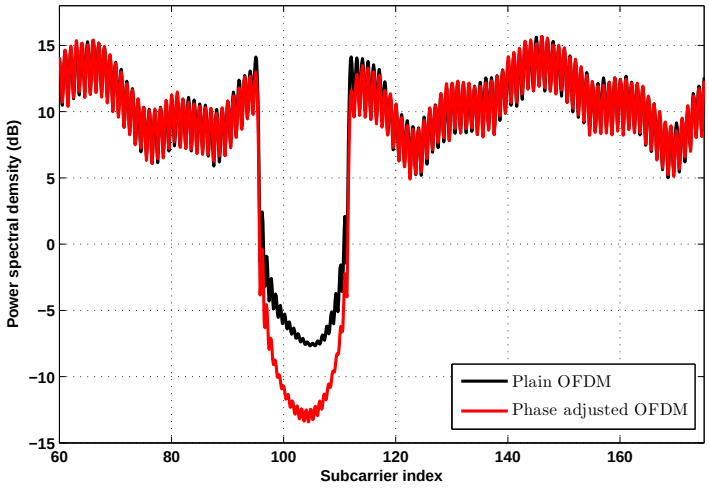

Figure 3.10: Spectrum of the received OFDM signals transmitted from three antennas with frequency selective fading channels. Adjustment phases are calculated using the BCD algorithm.

Chapter 4

Jitter-Robust Spectral Shaping in OFDM

4.1 Introduction

In this chapter, the impact of timing jitter on the spectrum of a transmission OFDM signal is investigated. Timing jitter in OFDM results in non-ideal sampling and pulse-shaped transmission and thus, is an important limiting factor for practical OFDM systems.

Due to sensitivity of OFDM to time and frequency synchronization errors, timing jitter can lead to a performance degradation of OFDM systems in terms of bit-error-rate (BER) by introducing inter-carrier-interference (ICI). This effect has been extensively investigated in several works for both single-carrier and multi-carrier systems. In [44], the error-rate performance of uncoded and trellis-coded discrete multitone (DMT) systems is analyzed in the presence of timing jitter. In [45], a model for analysis of jitter is presented where the error due to the timing jitter is treated as additive noise. Then, analytical expressions for the power spectral density (PSD) of the noise are derived for both coded and uncoded OFDM systems. The impact of jitter on introducing inter-carrier interference (ICI) is addressed in [46] and a lower bound on the variance of the interference between different subcarriers is derived. In [47], however, a more detailed analysis on ICI due to timing jitter is presented and lower and upper bounds on the ICI power are established for colored (correlated) and white (independent) jitter in ultra-wide band (UWB) OFDM systems.

The results presented in this chapter have been submitted to *IEEE Transactions on Wireless Communications* in December 2013.

Furthermore, in [48], it is shown how oversampling can help to mitigate the ICI due to timing jitter.

However, sampling jitter has also a significant effect on the spectrum of the transmission signal, and, to the best of our knowledge, this effect has not been considered in the literature. In particular, this effect can degrade the performance of sidelobe suppression techniques and introduce high out-of-band interference. This is because the proposed sidelobe suppression techniques in OFDM are based on the assumption of exact time and frequency synchronization.

In this chapter, we consider the effect of timing jitter on the performance of sidelobe suppression techniques in OFDM. In particular, the active interference cancellation (AIC) technique [18, 49] is studied as the base sidelobe suppression technique, as it is known to be one of the most effective out-of-band radiation reduction techniques in OFDM. However, the analysis in this chapter is general and can be applied to many other techniques in this area.

In the remainder of this chapter, in Section 4.2, we first derive exact expressions for the transmitted OFDM signal spectrum in presence of timing jitter and then, using a first order Maclaurin series expansion, the spectrum is further evaluated. The results of Section 4.2 are used in Section 4.3.1 where the performance degradation to the AIC technique due to timing jitter is investigated and numerical results are presented. Finally, in Section 4.4, using a minimax approach, we propose a novel scheme that protects the AIC against the worst-case random jitter. Throughout the simulations in this chapter, the timing jitter is assumed to be independent in different sampling times, i.e., the timing jitter is the so-called *white jitter*.

4.2 System Model

Fig. 4.1 presents the block diagram of a baseband OFDM transmitter that we consider in this chapter. The input data bits are first mapped to some complex constellation points such as 4-QAM. Then, the stream of complex symbols $\{X_i\}$ is divided into N sub-streams in the serial to parallel block creating the data vector $\mathbf{X} = [X_0, X_1, \cdots, X_{N-1}]^T$, where N is the total number of available subchannels and $[\cdot]^T$ denotes the transpose operator.

In order to modulate the N OFDM subcarriers, an N-point inverse fast Fourier transform (IFFT) is taken from X resulting in the time-domain vector $\mathbf{x} = [x_0, x_1, \cdots, x_{N-1}]^T$

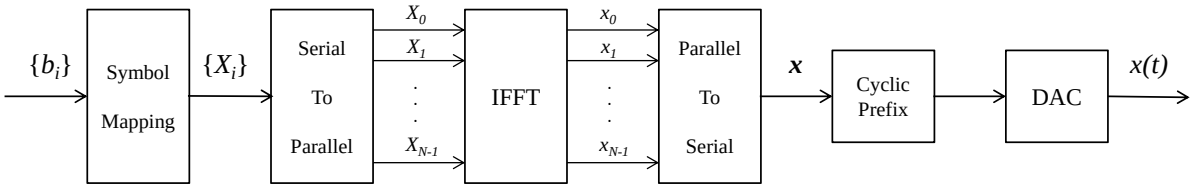

Figure 4.1: Simplified block diagram of a typical OFDM transmitter.

with

$$x_n = \sum_{k=0}^{N-1} X_k \, e^{j2\pi kn/N}, \quad n = 0, \cdots, N-1. \tag{4.1}$$

After adding the cyclic prefix to $\mathbf{x}$ in order to eliminate the intersymbol interference (ISI), the ideal continuous-time impulse train $s_\delta(t)$ is generated from $\mathbf{x}$ as

$$s_\delta(t) = \sum_{n=-G}^{N-1} x_n \, \delta(t - nT_s), \quad -T_G \leq t < T, \tag{4.2}$$

where G is the size of the cyclic prefix and T_s is the sampling interval in the time-domain. Also, $T_G = GT_s$ and $T = NT_s$ denote the length of the cyclic prefix and duration of the OFDM symbol in the time-domain, respectively. Moreover, $\delta(t)$ is the Dirac delta function.

The signal $s_\delta(t)$ is then fed into a low-pass pulse shaping filter $h(t)$ in the DAC block in order to generate the baseband transmission signal $s(t)$ which is expressed as

$$s(t) = s_\delta(t) * h(t) \tag{4.3}$$

$$= [\sum_{n=-G}^{N-1} x_n \, \delta(t - nT_s)] * h(t) \tag{4.4}$$

$$= \sum_{n=-G}^{N-1} x_n \, h(t - nT_s), \quad -T_G \leq t < T. \tag{4.5}$$

Ideally, the filter $h(t)$ is a normalized rectangular low-pass filter which is expressed in the time-domain as

$$h(t) = \frac{1}{T_s}\text{sinc}(t/T_s) = \frac{\sin(\pi t/T_s)}{\pi t}. \tag{4.6}$$

Equations (4.2)-(4.5) are derived based on the assumption of perfect timing synchronization, i.e., no offset or timing jitter. However, in practical systems, the sampling clocks have deviations from the ideal sampling times nT_s. In other words, the actual time-domain baseband signal with timing jitter will be

$$\hat{s}(t) = \sum_{n=-G}^{N-1} x_n \, h(t - nT_s + \varepsilon_n), \quad -T_G \leq t < T, \tag{4.7}$$

where ε_n denotes the timing jitter of the nth sample x_n.

Timing jitter in general affects the OFDM system performance metrics such as the bit-error-rate (BER) and the signal spectrum. The latter, which is the focus of this work, can be evaluated by taking the Fourier transform of the signal with jitter $\hat{s}(t)$,

$$\begin{aligned} S(f) &= \mathcal{F}\{\hat{s}(t)\} && (4.8)\\ &= H(f) \sum_{n=-G}^{N-1} x_n \, e^{-j2\pi f(nT_s - \varepsilon_n)} && (4.9) \end{aligned}$$

in which

$$\begin{aligned} H(f) &= \mathcal{F}\{h(t)\} \\ &= \text{rect}(T_s f), \end{aligned} \tag{4.10}$$

is the ideal normalized rectangular pulse shaping filter in the frequency-domain.

In this chapter, in order to be able to evaluate the effect of timing jitter on the spectrum of OFDM signal analytically, we consider the upsampled spectrum of $\hat{s}(t)$. Thus, we have

$$\begin{aligned} S_l &= S(f)|_{f=\frac{l\Delta f}{L}} \\ &= H\left(\frac{l\Delta f}{L}\right) \sum_{n=-G}^{N-1} x_n \, e^{-j2\pi \frac{l\Delta f}{L}(nT_s - \varepsilon_n)}, \end{aligned} \tag{4.11}$$

for $l = 0, \cdots, NL-1$, where $\Delta f = \frac{1}{T}$ is the subcarrier spacing and L is the upsampling factor. Furthermore,

$$H\left(\frac{l\Delta f}{L}\right) = 1, \quad \text{for } \; l = 0, \cdots, NL-1. \tag{4.12}$$

Therefore, we have

$$S_l = \sum_{n=-G}^{N-1} x_n \; e^{-j2\pi \frac{l}{L}(\frac{n}{N} - \frac{\varepsilon_n}{T})} \tag{4.13}$$

$$= \sum_{n=-G}^{N-1} x_n \; e^{-j2\pi \frac{ln}{LN}} e^{j2\pi \frac{l}{L}\frac{\varepsilon_n}{T}}. \tag{4.14}$$

Now, reasonably assuming that $\frac{\varepsilon_n}{T} \ll 1$, and using the first order Maclaurin series expansion of the exponential function, S_l can be approximated as

$$\begin{aligned} S_l &\approx \sum_{n=-G}^{N-1} x_n \; e^{-j2\pi \frac{ln}{LN}} \left(1 + j2\pi \frac{l}{L}\frac{\varepsilon_n}{T}\right) \\ &= \sum_{n=-G}^{N-1} \sum_{k=0}^{N-1} X_k \; e^{j2\pi kn/N} \; e^{-j2\pi \frac{ln}{LN}} + \sum_{n=-G}^{N-1} \sum_{k=0}^{N-1} j2\pi \frac{l}{L}\frac{\varepsilon_n}{T} \; X_k \; e^{j2\pi kn/N} \; e^{-j2\pi \frac{ln}{LN}}, \end{aligned} \tag{4.15}$$

for $l = 0, \cdots, NL-1$. In (4.15), the second term appears due to the timing jitter and affects the signal spectrum. It is worth noting that in case of no timing jitter, i.e. $\varepsilon_n = 0$, and $L = 1$, if the cyclic prefix is removed before taking the Fourier transform, we recover $S_l = X_l$, the original subcarrier values in the frequency-domain.

From (4.15), the upsampled spectrum of the OFDM signal in presence of timing jitter can be expressed in the form of

$$\boldsymbol{S}(\mathbf{X}, \boldsymbol{\varepsilon}) = \mathbf{a}(\mathbf{X}) + B(\mathbf{X}) \; \boldsymbol{\varepsilon}, \tag{4.16}$$

where $\boldsymbol{S} = [S_l]_{NL\times 1}$ is the upsampled signal spectrum, $\mathbf{a} = [a_l]_{NL\times 1}$ and $B = [b_{l,n}]_{NL\times(N+G)}$ are defined as

$$a_l \triangleq \sum_{n=-G}^{N-1} \sum_{k=0}^{N-1} X_k \; e^{j2\pi \frac{n}{N}(k - \frac{l}{L})}, \tag{4.17}$$

$$b_{l,n} \triangleq \sum_{k=0}^{N-1} j2\pi \frac{l}{LT} \; X_k \; e^{j2\pi \frac{n}{N}(k - \frac{l}{L})}, \tag{4.18}$$

and $\boldsymbol{\varepsilon} = [\varepsilon_n]_{(N+G)\times 1}$ is the timing jitter vector. Clearly, from (4.17) and (4.18), the dependence of $\mathbf{a}$ and B on $\mathbf{X}$ is linear.

4.3 Effect of Timing Jitter on Spectral Shaping Techniques

In OFDM spectral shaping, the objective is to sculpt the spectrum of the transmission signal such that the corresponding standard spectral requirements are satisfied. Standard requirements typically refer to the maximum emitted power in both in-band and out-of-band frequency regions.

Out-of-band radiation power is an inherent challenge to OFDM systems as it can interfere with the adjacent frequency bands. The problem is more acute in cognitive radio applications where adjacent primary users should be carefully protected from the secondary users' interference.

Many of the proposed out-of-band radiation reduction techniques in OFDM sacrifice a part of the available resources such as bandwidth (e.g. AIC [18, 49] and N-continuous OFDM [22]) or time (e.g. adaptive symbol transition (AST) [19]) in order to achieve the desired spectral characteristics. In this work, the AIC technique is chosen as the base method of spectral shaping as it has shown remarkable performance in sidelobe suppression and has attracted a great interest. However, the formulation of the problem in this section and the next section is general and can be applied to many other sidelobe suppression techniques.

4.3.1 The AIC technique and jitter effect

In the AIC technique, a subset of active subcarriers are reserved to be modulated in such a way as to reduce the out-of-band power emission. In other words, the complex weights of the reserved AIC tones are calculated such that their sidelobes cancel (mitigate) those of data subcarriers in some desired part of the bandwidth, which is referred to as the *victim band*. The principle of the AIC technique is depicted in Fig. 2.1, where the reserved tones –also called cancellation carriers– are located adjacent to the victim band.

Let $\boldsymbol{\mu}$ and $\mathbf{X}_d$ denote the set of reserved AIC tones and data subcarriers respectively, i.e., the vector $\mathbf{X}$ is a combination of $\boldsymbol{\mu}$ and $\mathbf{X}_d$. Also, let $\boldsymbol{I}$ denote the upsampled spectrum in the victim band containing the effect of both data subcarriers $\mathbf{X}_d$ and reserved tones $\boldsymbol{\mu}$, i.e., $\boldsymbol{I} = \boldsymbol{I}(\boldsymbol{\mu}, \mathbf{X}_d)$. Thus, in an ideal system without timing jitter, according to the system model defined in Section 3.3, we have $\boldsymbol{I} = \tilde{\mathbf{a}}(\boldsymbol{\mu}, \mathbf{X}_d)$, where $\tilde{\mathbf{a}}(\boldsymbol{\mu}, \mathbf{X}_d)$ is a subvector of $\mathbf{a}(\boldsymbol{\mu}, \mathbf{X}_d)$ given in (4.16), containing only the elements associated with the victim band.

Therefore, in the AIC technique, the optimal complex weights for the reserved tones are calculated as

$$\boldsymbol{\mu}_{\text{opt.}} = \arg\min_{\boldsymbol{\mu}\in\Omega} \|\tilde{\mathbf{a}}(\boldsymbol{\mu}, \mathbf{X}_d)\|^2, \tag{4.19}$$

where $\|\tilde{\mathbf{a}}(\boldsymbol{\mu}, \mathbf{X}_d)\|^2$ represents the emission power in the victim band and $\Omega = \{\boldsymbol{\mu} \in \mathbb{C}^{|\boldsymbol{\mu}|} : \|\boldsymbol{\mu}\|^2 \leq p\}$, in which $|\boldsymbol{\mu}|$ is the number of AIC subcarriers and p is the power constraint. According to [49], a proper choice for the power constraint is

$$p = |\boldsymbol{\mu}| \, \frac{E_s}{N}, \tag{4.20}$$

where E_s is the energy of the OFDM symbol before applying the technique. A semi-analytical solution to (4.19) is provided in [49].

However, as shown in Section 4.2, in a practical OFDM system with timing jitter $\boldsymbol{\varepsilon}$, the actual interference vector, which is denoted by $\boldsymbol{I}_J$, is expressed as

$$\boldsymbol{I}_J = \tilde{\mathbf{a}}(\boldsymbol{\mu}, \mathbf{X}_d) + \widetilde{B}(\boldsymbol{\mu}, \mathbf{X}_d)\, \boldsymbol{\varepsilon}, \tag{4.21}$$

in which $\widetilde{B}(\boldsymbol{\mu}, \mathbf{X}_d)$ is a submatrix of $B(\boldsymbol{\mu}, \mathbf{X}_d)$ containing only the rows associated with the victim band.

The second term in (4.21) represents the effect of the jitter to the spectrum in the victim band and is not considered in finding the optimal reserved tones weights in the traditional AIC technique. Accordingly, the performance of the AIC method is significantly degraded in the presence of timing jitter.

4.3.2 Numerical results

In the numerical evaluations throughout this chapter, timing jitter is assumed to be independent at different samples and is modeled as a wide-sense stationary (WSS) Gaussian process with zero-mean and variance σ_ε^2 [45]. Moreover, according to [50] and [51], the deviation of the timing jitter σ_ε is typically $3 - 8\%$ of the sampling interval T_s of the symbol.

Here, we investigate the performance degradation of the AIC technique in a jittery OFDM system using numerical simulations. In the simulations, there are a total of $N = 128$ subcarriers from which 32 subcarriers are deactivated in the victim band and are located in the middle of the band from subcarrier 50 to 81. This configuration can represent a cognitive system where the bandwidth of the primary licensed user coincides with the

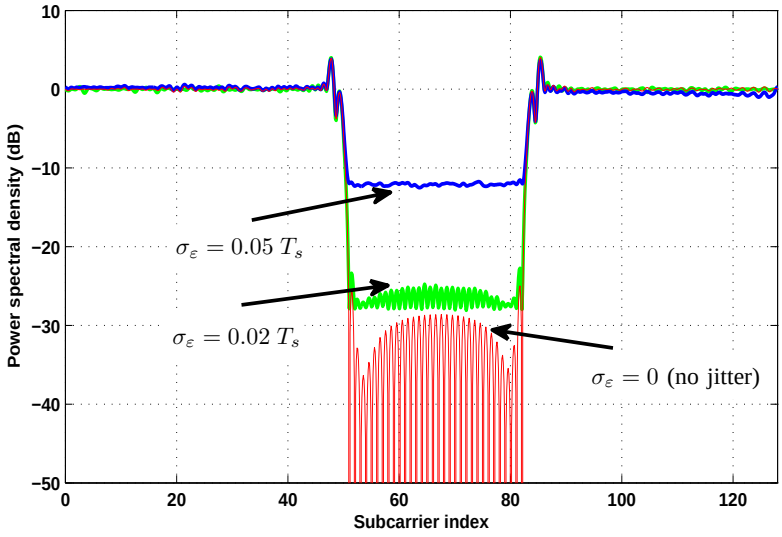

Figure 4.2: Impact of the timing jitter on the performance of the AIC technique.

victim band. Furthermore, $|\boldsymbol{\mu}| = 6$ subcarriers (3 on each side of the victim band) are reserved as the AIC tones and the rest of the subcarriers are data tones that are modulated using BPSK symbols. Moreover, a cyclic prefix of length $N/4 = 32$ is appended to the signal in the time-domain.

In order to reduce interference in the victim band, the AIC tones are calculated using (4.19) without taking the jitter into account. The jitter is then added to the signal. Fig. 4.2 illustrates the resulting spectrum of the OFDM signal for the ideal case, i.e., no timing jitter, as well as the practical case, i.e., with random timing jitter. Here, the spectrum is calculated using (4.14). Two samples of jittery spectrums with jitter deviations of 2% and 5% are plotted in the figure, and, as can be seen, even a timing jitter of 5% of the sampling interval T_s degrades the performance of the AIC technique by about 18 dB in such a scenario.

In Fig. 4.3, on the other hand, the amount of performance degradation to the AIC technique due to jitter with respect to the timing jitter deviation is shown. It is observed from this figure that for a reasonable amount of timing jitter, an increase in interference of up to about 30 dB can be introduced compared to the case with no timing jitter.

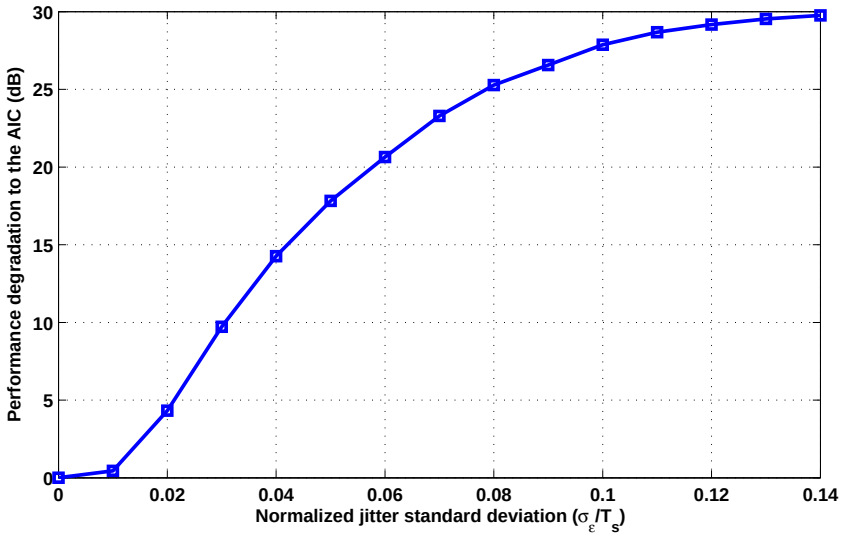

Figure 4.3: Performance degradation to the AIC technique due to timing jitter for different jitter levels.

4.4 Jitter-robust AIC

4.4.1 Problem formulation

As noted, in the conventional AIC technique, the sampling clocks are assumed to be perfectly synchronized. However, this is not the case in practical systems and, as shown in Section 4.3.1, even a deviation of as small as 2% from the ideal sampling time can introduce an interference of as high as 5 dB. This performance degradation is due to ignoring the term $\widetilde{B}\boldsymbol{\varepsilon}$ in (4.21) in the AIC optimization expressed in (4.19).

In this section, the objective is to propose a solution that makes the AIC technique robust against timing jitter. To this end, in order to find the optimal weights for the AIC tones, the jitter effect must also be considered in the optimization. In other words, the optimal AIC tones should be calculated in such a way as to minimize the *actual interference* power including the effect of timing jitter. Therefore, (4.19) could be re-formulated as

$$\boldsymbol{\mu}_{\text{opt.}} = \underset{\boldsymbol{\mu}\in\Omega}{\arg\min} \, \|\tilde{\mathbf{a}}(\boldsymbol{\mu}, \mathbf{X}_d) + \widetilde{B}(\boldsymbol{\mu}, \mathbf{X}_d)\, \boldsymbol{\varepsilon}\|^2. \tag{4.22}$$

However, since the jitter vector $\boldsymbol{\varepsilon}$ is random and not known a-priori, the optimization (4.22) is ill-posed and the problem cannot be solved in the same way as (4.19) is solved in [49]. As a solution, we propose a *minimax* approach where the optimal AIC tones are found such that the worst-case interference power is minimized. That is, in our proposed minimax scheme, the optimal AIC subcarriers minimize the maximum possible interference power created due to the random jitter, i.e.,

$$\boldsymbol{\mu}_{\text{opt.}} = \arg\min_{\boldsymbol{\mu}\in\Omega}(\max_{\boldsymbol{\varepsilon}\in\Delta} \|\tilde{\mathbf{a}}(\boldsymbol{\mu}, \mathbf{X}_d) + \widetilde{B}(\boldsymbol{\mu}, \mathbf{X}_d)\, \boldsymbol{\varepsilon}\|^2), \tag{4.23}$$

where $\Delta = \{\boldsymbol{\varepsilon} \in \mathbb{R}^{(N+G)} : \|\boldsymbol{\varepsilon}\|^2 \leq q\}$ in which q denotes the maximum power of the jitter vector.

4.4.2 Problem solution

In solving the minimax problem (4.23), our objective is to find a vector $\boldsymbol{\mu}^\star \in \Omega$ such that

$$\max_{\boldsymbol{\varepsilon}\in\Delta} \|\tilde{\mathbf{a}}(\boldsymbol{\mu}^\star, \mathbf{X}_d) + \widetilde{B}(\boldsymbol{\mu}^\star, \mathbf{X}_d)\, \boldsymbol{\varepsilon}\|^2 = \min_{\boldsymbol{\mu}\in\Omega} \max_{\boldsymbol{\varepsilon}\in\Delta} \|\tilde{\mathbf{a}}(\boldsymbol{\mu}, \mathbf{X}_d) + \widetilde{B}(\boldsymbol{\mu}, \mathbf{X}_d)\, \boldsymbol{\varepsilon}\|^2. \tag{4.24}$$

We first consider the function

$$\Phi(\boldsymbol{\mu}) = \max_{\boldsymbol{\varepsilon}\in\Delta} \|\tilde{\mathbf{a}}(\boldsymbol{\mu}, \mathbf{X}_d) + \widetilde{B}(\boldsymbol{\mu}, \mathbf{X}_d)\, \boldsymbol{\varepsilon}\|^2. \tag{4.25}$$

Note that for a fixed $\boldsymbol{\mu}$, since the set Δ is closed and bounded, the maximum in (4.25) exists and is finite. Now, for ease of notation, writing the cost function in (4.25) as $\|\tilde{\mathbf{a}} + \widetilde{B}\, \boldsymbol{\varepsilon}\|^2$, we have

$$\begin{aligned} \|\tilde{\mathbf{a}} + \widetilde{B}\, \boldsymbol{\varepsilon}\|^2 =& \tilde{\mathbf{a}}^\dagger\tilde{\mathbf{a}} + \tilde{\mathbf{a}}^\dagger\widetilde{B}\boldsymbol{\varepsilon} + \boldsymbol{\varepsilon}^\dagger\widetilde{B}^\dagger\tilde{\mathbf{a}} + \boldsymbol{\varepsilon}^\dagger\widetilde{B}^\dagger\widetilde{B}\boldsymbol{\varepsilon} \\ =& \tilde{\mathbf{a}}^\dagger\tilde{\mathbf{a}} + 2\,\mathbb{R}\{\boldsymbol{\varepsilon}^\dagger\widetilde{B}^\dagger\tilde{\mathbf{a}}\} + \boldsymbol{\varepsilon}^\dagger\widetilde{B}^\dagger\widetilde{B}\boldsymbol{\varepsilon}, \end{aligned} \tag{4.26}$$

where $\tilde{\mathbf{a}}^\dagger$ denotes the conjugate transpose of $\tilde{\mathbf{a}}$. Now, we claim that

$$\boldsymbol{\varepsilon}^\dagger\widetilde{B}^\dagger\widetilde{B}\boldsymbol{\varepsilon} = \boldsymbol{\varepsilon}^T\mathbb{R}\{\widetilde{B}^\dagger\widetilde{B}\}\boldsymbol{\varepsilon}. \tag{4.27}$$

This is because the jitter vector $\boldsymbol{\varepsilon}$ is real and thus $\boldsymbol{\varepsilon}^\dagger = \boldsymbol{\varepsilon}^T$. Also, $\widetilde{B}^\dagger\widetilde{B}$ is Hermitian, thereby

$$\begin{aligned} \widetilde{B}^\dagger\widetilde{B} &= H_r + jH_i \\ &= (H_r + jH_i)^\dagger \\ &= H_r^T - jH_i^T, \end{aligned} \tag{4.28}$$

where H_r and H_i denote the real and imaginary parts of $\widetilde{B}^\dagger \widetilde{B}$ respectively. Thus,

$$\boldsymbol{\varepsilon}^T (H_r + jH_i)\, \boldsymbol{\varepsilon} = \boldsymbol{\varepsilon}^T (H_r^T - jH_i^T)\, \boldsymbol{\varepsilon}, \tag{4.29}$$

and hence,

$$\boldsymbol{\varepsilon}^T H_r \boldsymbol{\varepsilon} + j\boldsymbol{\varepsilon}^T H_i \boldsymbol{\varepsilon} = \boldsymbol{\varepsilon}^T H_r^T \boldsymbol{\varepsilon} - j\boldsymbol{\varepsilon}^T H_i^T \boldsymbol{\varepsilon}. \tag{4.30}$$

Since all the terms in (4.30) are real scalars,

$$\boldsymbol{\varepsilon}^T H_i \boldsymbol{\varepsilon} = -\boldsymbol{\varepsilon}^T H_i^T \boldsymbol{\varepsilon}, \tag{4.31}$$

yet,

$$\begin{aligned} \boldsymbol{\varepsilon}^T H_i \boldsymbol{\varepsilon} &= (\boldsymbol{\varepsilon}^T H_i \boldsymbol{\varepsilon})^T \\ &= \boldsymbol{\varepsilon}^T H_i^T \boldsymbol{\varepsilon}, \end{aligned} \tag{4.32}$$

and therefore, $\boldsymbol{\varepsilon}^T H_i \boldsymbol{\varepsilon} = 0$. Using (4.27), equation (4.26) can be then further expressed as

$$\begin{aligned} \|\tilde{\mathbf{a}} + \widetilde{B}\, \boldsymbol{\varepsilon}\|^2 =& \tilde{\mathbf{a}}^\dagger \tilde{\mathbf{a}} + 2\boldsymbol{\varepsilon}^T \mathbb{R}\{\widetilde{B}^\dagger \tilde{\mathbf{a}}\} + \boldsymbol{\varepsilon}^T \mathbb{R}\{\widetilde{B}^\dagger \widetilde{B}\}\, \boldsymbol{\varepsilon} \\ =& c_0 + 2\, \boldsymbol{\varepsilon}^T \mathbf{c} + \boldsymbol{\varepsilon}^T A\, \boldsymbol{\varepsilon}, \end{aligned} \tag{4.33}$$

where in (4.33), $c_0 \triangleq \tilde{\mathbf{a}}^\dagger \tilde{\mathbf{a}}$, $\mathbf{c} \triangleq \mathbb{R}\{\widetilde{B}^\dagger \tilde{\mathbf{a}}\}$, and $A \triangleq \mathbb{R}\{\widetilde{B}^\dagger \widetilde{B}\}$.

Now, since $\widetilde{B}^\dagger \widetilde{B}$ is Hermitian, A is symmetric and can be diagonalized as $A = UDU^{-1}$, where

$$D = \mathrm{diag}(d_0, \cdots, d_{N+G-1}) \tag{4.34}$$

with $d_0 \leq d_1 \leq \cdots \leq d_{N+G-1}$ and $U^{-1} = U^T$. Note that the matrix A is a positive-semidefinite matrix because

$$\boldsymbol{v}^\dagger A \boldsymbol{v} = \|\widetilde{B}\boldsymbol{v}\|^2 \geq 0, \tag{4.35}$$

for any arbitrary vector $\boldsymbol{v} \in \mathbb{C}^{(N+G)}$. Accordingly, $d_i \geq 0$. Thus, we have

$$\begin{aligned} \|\tilde{\mathbf{a}} + \widetilde{B}\, \boldsymbol{\varepsilon}\|^2 =& c_0 + 2\, \boldsymbol{\varepsilon}^T \mathbf{c} + \boldsymbol{\varepsilon}^T U D U^T \boldsymbol{\varepsilon} \\ =& c_0 + 2\, \mathbf{y}^T \boldsymbol{\gamma} + \mathbf{y}^T D\, \mathbf{y}, \end{aligned} \tag{4.36}$$

where in (4.36),

$$\mathbf{y} = [y_0, \cdots, y_{N+G-1}]^T \triangleq U^T \boldsymbol{\varepsilon}, \tag{4.37}$$

$$\boldsymbol{\gamma} = [\gamma_0, \cdots, \gamma_{N+G-1}]^T \triangleq U^T \mathbf{c}. \tag{4.38}$$

Therefore,

$$\begin{aligned}\Phi(\boldsymbol{\mu}) &= \max_{\boldsymbol{\varepsilon}\in\Delta} \|\tilde{\mathbf{a}} + \widetilde{B}\,\boldsymbol{\varepsilon}\|^2 \\ &= \max_{\mathbf{y}\in\Delta} (c_0 + 2\,\mathbf{y}^T\boldsymbol{\gamma} + \mathbf{y}^T D\,\mathbf{y}) \qquad (4.39) \\ &= \max_{\mathbf{y}\in\Delta} \left(c_0 + 2\sum_{i=0}^{N+G-1} y_i\gamma_i + \sum_{i=0}^{N+G-1} d_i\,y_i^2 \right). \qquad (4.40)\end{aligned}$$

In (4.39) and (4.40), the constraint $\boldsymbol{\varepsilon} \in \Delta$ is replaced by $\mathbf{y} \in \Delta$ since U is orthogonal and thus, $\|\boldsymbol{\varepsilon}\|^2 = \|\mathbf{y}\|^2$.

Now, because $d_i \geq 0$, the first and the third terms in (4.40) are non-negative. By choosing y_i to have the same sign as γ_i, the second term becomes non-negative as well. Thus, in order to maximize the cost function in (4.40), the y_i should be chosen to have the same sign as the corresponding γ_i. Then, clearly any $\mathbf{y}$ such that $\|\mathbf{y}\|^2 < q$ is not a solution since scaling $\mathbf{y}$ until $\|\mathbf{y}\|^2 = q$ results in a larger objective value. Accordingly, the inequality constraint $\|\mathbf{y}\|^2 \leq q$ can be replaced by $\|\mathbf{y}\|^2 = q$ and we have

$$\begin{aligned}\Phi(\boldsymbol{\mu}) = &\max \left(c_0 + 2\sum_{i=0}^{N+G-1} y_i\gamma_i + \sum_{i=0}^{N+G-1} d_i\,y_i^2 \right), \qquad (4.41) \\ &\text{s.t.} \quad \|\mathbf{y}\|^2 = q.\end{aligned}$$

To solve (4.41), by using the method of Lagrange multipliers, we define the Lagrangian

$$\mathcal{L}(\mathbf{y},\lambda) \triangleq c_0 + 2\sum_{i=0}^{N+G-1} y_i\gamma_i + \sum_{i=0}^{N+G-1} d_i y_i^2 + \lambda(\|\mathbf{y}\|^2 - q). \qquad (4.42)$$

Taking derivative of the Lagrangian $\mathcal{L}(\mathbf{y},\lambda)$ with respect to y_i and setting $\frac{\partial \mathcal{L}}{\partial y_i} = 0$, we have

$$y_i = \frac{-\gamma_i}{\lambda + d_i}. \qquad (4.43)$$

Now, by imposing the power constraint $\sum_{i=0}^{N+G-1} y_i^2 = q$ to (4.43), the equation

$$f(\lambda) = \left(\sum_{i=0}^{N+G-1} \frac{\gamma_i^2}{(\lambda + d_i)^2} \right) - q = 0 \qquad (4.44)$$

is formed. Equation (4.44) has at least two and at most $2(N+G)$ solutions for λ. Since y_i in (4.43) should have the same sign as γ_i, we must have $\lambda < -d_i$ for all $i \in \{0, \cdots, N+G-1\}$, and thus

$$\lambda < -\max(d_i) = -d_{N+G-1}, \tag{4.45}$$

since the d_i are assumed ordered in increasing manner. Therefore, we need only consider the roots of $f(\lambda)$ in $(-\infty, -d_{N+G-1})$. To this end, we note that $f(\lambda)$ is monotonic on this interval and hence, has a unique root on this interval. Also, we can bound the root by finding a $\lambda' < -d_{N+G-1}$ such that

$$\sum_{i=0}^{N+G-1} \frac{\gamma_i^2}{(\lambda' + d_i)^2} < q. \tag{4.46}$$

Clearly, any λ' that satisfies

$$\frac{\gamma_i^2}{(\lambda' + d_i)^2} < \frac{q}{N+G}, \tag{4.47}$$

for all $i \in \{0, \cdots, N+G-1\}$, also satisfies (4.46). Following (4.47), we have

$$\lambda' < -d_i - |\gamma_i| \sqrt{\frac{N+G}{q}}, \tag{4.48}$$

for all $i \in \{0, \cdots, N+G-1\}$, and thus

$$\lambda' < -d_{N+G-1} - \max_i |\gamma_i| \sqrt{\frac{N+G}{q}}. \tag{4.49}$$

Therefore, we know that the desired root of $f(\lambda)$, denoted by $\lambda^\star$, is in $(-d_{N+G-1} - \max_i |\gamma_i| \sqrt{\frac{N+G}{q}}, -d_{N+G-1})$ and hence, it can be found in a simple manner by using a bisection method. By evaluating (4.43) with $\lambda = \lambda^\star$, we find

$$\mathbf{y}^\star = [y_0^\star, \cdots, y_{N+G-1}^\star], \tag{4.50}$$

where

$$y_i^\star = \frac{-\gamma_i}{\lambda^\star + d_i}, \quad i = 0, \cdots, N+G-1. \tag{4.51}$$

Then, the solution to (4.25) will be

$$\Phi(\boldsymbol{\mu}) = \|\tilde{\mathbf{a}}(\boldsymbol{\mu}, \mathbf{X}_d) + \widetilde{B}(\boldsymbol{\mu}, \mathbf{X}_d)\, \boldsymbol{\varepsilon}^\star\|^2, \tag{4.52}$$

where $\boldsymbol{\varepsilon}^\star = U\mathbf{y}^\star$.

Therefore, the problem (4.23) is reduced to

$$\boldsymbol{\mu}_{\text{opt.}} = \arg\min_{\boldsymbol{\mu}\in\Omega}(\|\tilde{\mathbf{a}}(\boldsymbol{\mu}, \mathbf{X}_d) + \widetilde{B}(\boldsymbol{\mu}, \mathbf{X}_d)\ \boldsymbol{\varepsilon}^\star\|^2). \tag{4.53}$$

In order to solve (4.53), we first note that for any fixed given $\boldsymbol{\varepsilon}^\star$, since $\tilde{\mathbf{a}}(\boldsymbol{\mu}, \mathbf{X}_d)$ and $\widetilde{B}(\boldsymbol{\mu}, \mathbf{X}_d)$ are linear in $\boldsymbol{\mu}$, the function $\Phi(\boldsymbol{\mu}) = \|\tilde{\mathbf{a}}(\boldsymbol{\mu}, \mathbf{X}_d) + \widetilde{B}(\boldsymbol{\mu}, \mathbf{X}_d)\boldsymbol{\varepsilon}^\star\|^2$ is a non-negative quadratic form in terms of $\boldsymbol{\mu}$ and hence is convex in $\boldsymbol{\mu}$. Therefore, the problem of finding

$$\boldsymbol{\mu}_{\text{opt.}} = \arg\min_{\boldsymbol{\mu}\in\Omega} \Phi(\boldsymbol{\mu}), \tag{4.54}$$

falls in the category of *convex minimization* problems for which there exist efficient and fast numerical estimators that can be used such as the method of coordinatedwise descent, the method of steepest descent (gradient descent), or the methods of successive approximations [52]. In this thesis, we use the MATLAB built-in function `fmincon` that employs the interior-point algorithm, which is based on the gradient descent method, to find the optimal solution.

4.5 Numerical Results

In this section, we evaluate the performance of the proposed jitter-robust scheme using computer simulations. In simulations, the total number of OFDM subcarriers in each symbol is set to $N = 256$. Similar to Section 4.3.2, we consider the application of OFDM in a cognitive radio system. In our considered configuration, there is a primary user occupying a part of spectrum in the middle of bandwidth of the OFDM system. Therefore, the subcarriers that coincide with the primary user band are switched off. To further suppress interference to the primary user, as in the AIC technique, a few subcarriers on each side of the primary user band are allocated to be the AIC tones. The rest of subcarriers are modulated by BPSK random data symbols with a normalized power such that the ith element $X_{d,i}$ of $\mathbf{X}_d$ has power $|X_{d,i}|^2 = 1$.

4.5.1 Power spectral density

In Fig. 4.4, the power spectral density of an OFDM signal in presence of timing jitter is depicted in two different cases. In the first case, the conventional AIC technique is applied

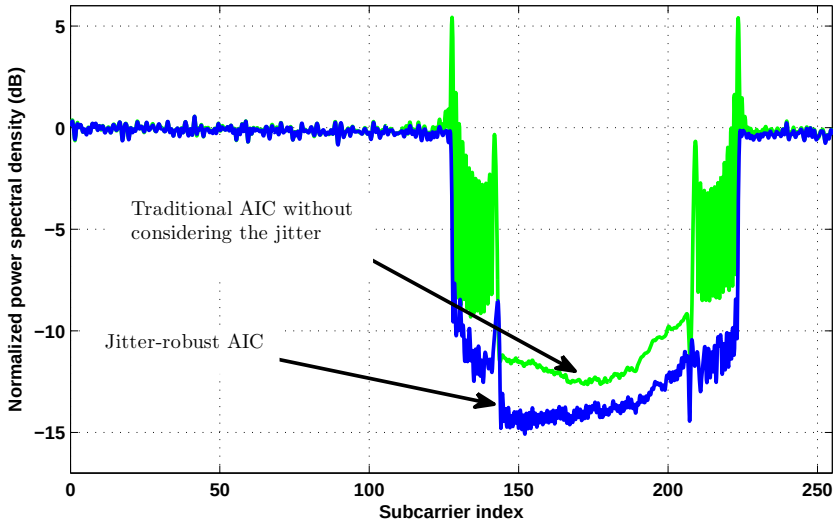

Figure 4.4: Power spectral density of the OFDM signal in presence of timing jitter using the jitter-robust technique compared to the case when the jitter is ignored in the AIC technique; $N = 256$, primary user bandwidth $= 64$ subcarriers, $\sigma_\varepsilon = 0.1T_s$.

to the signal without considering the jitter, i.e., the AIC tones are calculated using (4.19). Then, the worst-case jitter as computed by (4.52) is added to the signal. In the second case, the proposed jitter-robust AIC scheme is applied to the signal, i.e., the cancellation tones are calculated using (4.23), and the signal is then distorted by the corresponding worst case timing jitter. In both cases, 16 AIC tones are employed at each side of the primary band. The spectrum is estimated using a simple rectangular pulse shaping window and an upsampling factor of $L = 8$. Moreover, the timing jitter deviation is set to $\sigma_\varepsilon = 0.1T_s$, i.e., the maximum power of the jitter vector is $q = N\sigma_\varepsilon^2$.

As can be seen from Fig. 4.4, the proposed robust scheme is able to reduce the spectrum in the victim band by about $3 - 4$ dB in this scenario.

Another observation form Fig. 4.4 is that in the proposed jitter-robust scheme, the cancellation tones on the two sides of the primary band consume much less power compared to the ones in the traditional AIC technique. In particular, as can be seen in the figure, there is a considerable power overshoot on the spectrum of the signal optimized by the traditional AIC technique, whereas, in the jitter-robust technique, the spectrum has no overshoot. In other words, compared to the traditional AIC, the proposed technique not

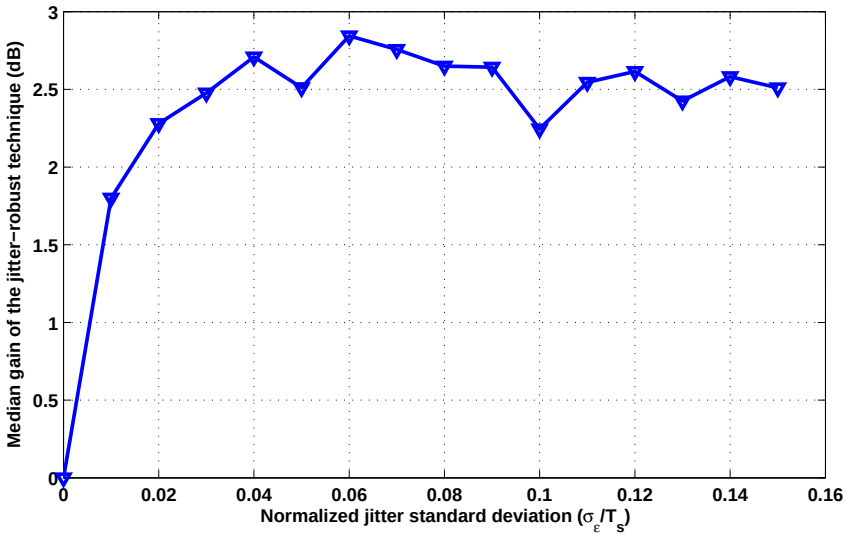

Figure 4.5: Median performance improvement achieved by the proposed jitter-robust technique compared to the traditional AIC technique in presence of random timing jitter.

only reduces the *out-of-band* radiation power of the OFDM subcarriers, but also prevents creating *in-band* harmful power emission, known as spectral overshoot. This is reasonable as in the traditional AIC, the cancellation tones are calculated based the assumption of exact synchronization, i.e., no jitter, and therefore, as much power as allowed is consumed to cancel as much interference as possible. However, the random phase shifts introduced to the subcarriers due to the jitter can lead to constructive superposition of subcarriers' spectrums and thus creating large out-of-band radiation as well as significant in-band overshoot. Whereas in the jitter-robust technique, in order to protect the technique against random jitter, much less power is allocated to the cancellation tones resulting in less or no overshoot.

4.5.2 Performance gain

We define the gain of the proposed scheme as the amount of interference power reduction, in dB, that is achieved by using the robust AIC technique, compared to the conventional AIC technique for the same jitter deviation. The interference power is also defined as the squared-norm of the interference vector I_J expressed in (4.21).

Using the above definitions, the median gain performance of the proposed scheme is shown in Fig. 4.5 for various normalized jitter standard deviations σ_ε/T_s. It is worth noting that the improvement seen in Fig. 4.4 is in close agreement with the results shown in this figure and shows 2.5 to 3 dB improvement in sidelobe reduction over a wide range of jitter levels.

4.6 Conclusion

In this chapter we considered the impact of timing jitter on spectral shaping techniques in OFDM. Focusing on active interference cancellation (AIC) as the core technique of spectral shaping, we first evaluated the effect of timing jitter on the performance of the technique analytically and through numerical simulations. Secondly, in order to design a jitter-robust AIC technique, a minimax approach was proposed and solved. Numerical results verify that in the worst-case scenario, the proposed robust scheme has almost 3 dB improvement compared to the non-robust traditional AIC technique. Furthermore, the proposed robust scheme is shown in simulations to remove the spectral overshoot created in the non-robust technique.

Chapter 5

Conclusion and Future Work

5.1 Summary of achievements and conclusion

There are two main challenges in the physical layer of cognitive radios to be addressed: spectrum sensing and appropriate signaling scheme. From the signaling scheme point-of-view, some candidate techniques have been proposed in the literature such as filter bank multi-tone modulation, single-carrier frequency division multiple access (SC-FDMA), and multi-carrier modulation. Due to its spectral efficiency and flexibility in dynamic spectrum usage, OFDM has become popular among researchers in cognitive radio applications. However, OFDM suffers from a number of shortcomings, e.g. high PAPR, sensitivity to synchronization errors, and large out-of-band radiation. In particular, out-of-band radiation, which is a result of high sidelobes of OFDM subcarriers, is more problematic in cognitive radio applications since it results in power leakage to the neighboring spectrum bands, which causes interference to either primary users or other secondary users. Thus, sidelobe suppression in OFDM is of great interest in the literature. In this research, we have considered the problem of interference reduction in OFDM-based cognitive radios. The main achievements of this thesis consist of three parts as elaborated in the subsequent sections.

5.1.1 Time-frequency trade-off study

Several techniques have been proposed in the literature for interference reduction in OFDM where some are performed in the time-domain and some in the frequency -domain. In the

first part of this thesis, we have studied the time-frequency trade-offs in sidelobe reduction techniques. To this end, we have proposed a new joint time-frequency scheme based on two recent and efficient sidelobe suppression techniques in OFDM, i.e., the AIC (a frequency-based technique) and AST (a time-based technique). The new scheme is proposed for both single-antenna and multiple-antenna OFDM-based cognitive systems and the effect of wireless channel is also considered to improve the performance of interference reduction. Moreover, the joint scheme enables us to investigate and study the trade-off between frequency-based and time-based interference minimization. In other words, the proposed method jointly minimizes the interference over subcarriers (frequency-domain) and symbol extension (time-domain). The main achievements of the new joint method are as follows:

1. We have studied the tradeoff between the AIC and AST methods to optimize the rate for a fixed interference reduction (or vice versa). It is shown that the tradeoff depends on the configuration of spectral opportunities; specifically, whether there is one large primary band, or multiple small primary bands.

2. Channel state information is used to better minimize interference to the primary user at the location of the primary user.

3. Based on the simulation results, we have shown that for a single wideband primary, the best trade-off is achieved by using only one sample extension and several cancellation carriers for a desired interference reduction level. The extension sample can be approximated as the simple average of the two end samples of the two consecutive OFDM symbols as the role of the extension is to smooth the transition between successive symbols. This approximation significantly reduces the complexity of the system.

4. For the multiple-antenna case, it has been shown that using channel state information, the secondary transmitter can design the sequences that are to be transmitted from its antennas in such a way that the interference at the primary receiver antenna is better minimized.

5.1.2 Phase adjustment technique

In order to reduce out-of-band radiation of OFDM subcarriers, in the second part of this thesis, a new technique have been proposed referred to as the phase adjustment technique. The technique is proposed for both single-antenna and multi-antenna secondary systems. In the single-antenna case, each OFDM symbol is rotated by a common phase based on

the previous symbols transmitted in previous time slots, such that the interference in a desired part of spectrum is minimized. In the multi-antenna case, each OFDM symbol is phase-rotated based on the symbols transmitted from other antennas at the same time in an attempt to minimize interference at the desired frequency band. The main achievements of this part of the thesis are:

1. The new phase adjustment technique has none of the main shortcomings of the previous techniques in this area, that is
   - It does not decrease useful data throughput.
   - It does not increase the bit-error-rate of the system.
   - It has very low complexity.
2. The performance of the proposed phase adjustment technique has been analytically investigated for some special cases and is shown to agree with numerical simulations.

5.1.3 Jitter-robust AIC

All the proposed sidelobe suppression techniques in OFDM are based on the assumption of exact time and frequency synchronization. However, in practical systems, sampling clocks have deviations form ideal sampling times resulting in timing jitter. In the third part of this thesis, it is shown that timing jitter can be a noticeable limiting factor to spectral shaping techniques in OFDM. In particular, it can degrade the performance of sidelobe reduction techniques significantly. Therefore, in order to develop a sidelobe suppression technique that is robust against random timing jitter, the effect of jitter is considered in the setting of the sidelobe reduction problem and a mathematical framework based on a minimax approach is established to solve the problem. The main achievements of this part of the thesis are as follows:

1. A mathematical model has been proposed for timing jitter and exact expressions have been derived for an OFDM signal spectrum in presence of timing jitter.
2. Considering the AIC technique as the base sidelobe suppression technique, the effect of timing jitter on the performance of the technique has been investigated and the amount of degradation to the technique's performance has been evaluated numerically.

3. A new jitter-robust scheme based on a minimax approach has been proposed that takes the random jitter effect into account for sidelobe suppression. The technique has been shown to outperform the traditional AIC technique where the jitter effect is ignored.

5.2 Future work

As mentioned in Chapter 1, cognitive radio is a new concept in the area of data communications and there are still several challenges that need to be addressed. From the physical layer perspective, which is the focus of this thesis, here we list future directions that can be pursued as a continuation to this research.

5.2.1 Timing jitter effect

As noted in Chapter 4, timing jitter is an important limiting factor in practical OFDM systems. This factor is more acute in high data rate systems where the time-domain pules width is very small and more accurate synchronization is required. Using the mathematical model for timing jitter developed in Chapter 4, the following problems can be considered:

- It can be interesting to study the effect of jitter on other techniques in the area of sidelobe reduction (or in general, spectral shaping) in OFDM. The main challenge here is to find an appropriate mathematical formulation of the problem in such a way as to include the jitter effect correctly.
- The effect of timing jitter on the BER performance of OFDM systems has been well-studied in the literature. We have also considered the jitter effect on the OFDM signal spectrum in this thesis. However, it can also be interesting to evaluate the impact of timing jitter on other areas of interest in OFDM such as PAPR reduction techniques. Here again the main challenge is to find a proper formulation that can employ the jitter model and can be solved at a reasonable complexity.

5.2.2 Other synchronization errors

As noted, a shortcoming to an OFDM systems is its high sensitivity to synchronization errors. In this work, we considered timing jitter as a time synchronization error at the

transmitter. However, other synchronization errors such as phase noise, frequency offset due to mismatch in local oscillators, and timing offset can also affect the performance of any OFDM system. Again, these effects on the BER performance have been considered in several works. However, to the best of our knowledge, the impact of the aforementioned errors on the OFDM signal spectrum and in particular on the performance of spectral shaping techniques has not been addressed yet and can be a possible and interesting future research. The key challenge here is to find a model for the considered synchronization error that can properly describe the characteristics of that random error, and can be employed in the setting of the problem of interest.

5.2.3 Other modulation techniques

In this thesis, our focus was on OFDM as the modulation technique for the cognitive system. However, as noted in Chapter 1, there are other modulation techniques that have been proposed to be used as the transmission technique in cognitive radios such as SC-FDMA and filter-bank multitone. In particular, according to [8], SC-FDMA can be employed in spectrum sharing systems. In that case, the time-domain signal has to be shaped such that the frequency-domain signal fits into the spectrum holes without causing interference to active primary users. Therefore, as a continuation to this thesis, the following problems can be of interest:

- The phase adjustment technique proposed in Chapter 3 can be applied to SC-FDMA systems as well.
- The performance of the techniques proposed for SC-FDMA systems are also degraded in presence of timing jitter. Therefore, considering the jitter effect in the problems involved in such systems is a possible future research work.

References

[1] *United States Frequency Allocation Chart.* [Online]. Available: http://www.ntia.doc.gov/osmhome/allochrt.html.

[2] S. Mishra, D. Cabric, C. Chang, D. Willkomm, B. van Schewick, S. Wolisz, and B. Brodersen, "A real time cognitive radio testbed for physical and link layer experiments," in *New Frontiers in Dynamic Spectrum Access Networks, 2005. DySPAN 2005. 2005 First IEEE International Symposium on*, pp. 562 –567, 8-11 2005.

[3] J. Mitola, *Cognitive Radio: An Integrated Agent Architecture for Software Defined Radio*. PhD thesis, Royal Institute of Technology, Sweden, Sweden, 2000.

[4] D. Cabric and R. Brodersen, "Physical layer design issues unique to cognitive radio systems," vol. 2, pp. 759 –763 Vol. 2, Sep. 2005.

[5] P. Amini, R. Kempter, R.-R. Chen, L. Lin, and B. Farhang-Boroujeny, "Filter bank multitone: A candidate for physical layer of cognitive radio," Sep. 2005.

[6] C. H. Yuen, P. Amini, and B. Farhang-Boroujeny, "Single carrier frequency division multiple access (SC-FDMA) for filter bank multicarrier communication systems," pp. 1 –5, Jun. 2010.

[7] T. Weiss and F. Jondral, "Spectrum pooling: an innovative strategy for the enhancement of spectrum efficiency," *Communications Magazine, IEEE*, vol. 42, pp. S8 – 14, Mar. 2004.

[8] B. Negash and H. Nikookar, "Wavelet-based multicarrier transmission over multipath wireless channels," *Electronics Letters*, vol. 36, pp. 1787 –1788, Oct. 2000.

[9] C. Van Bouwel, J. Potemans, S. Schepers, B. Nauwelaers, and A. Van de Capelle, "Wavelet packet based multicarrier modulation," pp. 131 –138, 2000.

[10] I. Budiarjo, H. Nikookar, and L. Ligthart, "Cognitive radio modulation techniques," *Signal Processing Magazine, IEEE*, vol. 25, pp. 24 –34, Nov. 2008.

[11] T. Weiss, J. Hillenbrand, A. Krohn, and F. Jondral, "Mutual interference in OFDM-based spectrum pooling systems," in *Vehicular Technology Conference, 2004. VTC 2004-Spring. 2004 IEEE 59th*, vol. 4, pp. 1873 – 1877, May 2004.

[12] P. Tan and N. Beaulieu, "Reduced ICI in OFDM systems using the "better than" raised-cosine pulse," *Communications Letters, IEEE*, vol. 8, pp. 135 – 137, Mar. 2004.

[13] A. Assalini and A. Tonello, "Improved Nyquist pulses," *Communications Letters, IEEE*, vol. 8, pp. 87 – 89, Feb. 2004.

[14] H. Nikookar and R. Prasad, "Waveshaping of multicarrier signal for data transmission over wireless channels," in *Universal Personal Communications Record, 1997. Conference Record., 1997 IEEE 6th International Conference on*, vol. 1, pp. 173 –177, Oct. 1997.

[15] I. Cosovic, S. Brandes, and M. Schnell, "Subcarrier weighting: a method for sidelobe suppression in OFDM systems," *Communications Letters, IEEE*, vol. 10, pp. 444 –446, June 2006.

[16] I. Cosovic and T. Mazzoni, "Suppression of sidelobes in OFDM systems by multiple-choice sequences," *European Transactions on Telecommunications*, vol. 17, pp. 623–630, June 2006.

[17] M. Naghsh and M. Omidi, "Reduction of out of band radiation using carrier-by-carrier partial response signalling in orthogonal frequency division multiplexing," *Communications, IET*, vol. 4, pp. 1433 –1442, Aug. 2010.

[18] H. Yamaguchi, "Active interference cancellation technique for MB-OFDM cognitive radio," in *Microwave Conference, 2004. 34th European*, vol. 2, pp. 1105 – 1108, Oct. 2004.

[19] H. Mahmoud and H. Arslan, "Sidelobe suppression in OFDM-based spectrum sharing systems using adaptive symbol transition," *Communications Letters, IEEE*, vol. 12, pp. 133 –135, Feb. 2008.

[20] S. Brandes, I. Cosovic, and M. Schnell, "Reduction of out-of-band radiation in OFDM based overlay systems," in *New Frontiers in Dynamic Spectrum Access Networks, 2005. DySPAN 2005. 2005 First IEEE International Symposium on*, pp. 662 –665, Nov. 2005.

[21] S. G. Huang and C. H. Hwang, "Improvement of Active Interference Cancellation: Avoidance Technique for OFDM Cognitive Radio," *Wireless Communications, IEEE Transactions on*, vol. 8, pp. 5928 –5937, December 2009.

[22] J. van de Beek and F. Berggren, "Out-of-Band Power Suppression in OFDM," *Communications Letters, IEEE*, vol. 12, no. 9, pp. 609–611, 2008.

[23] E. Teletar, "Capacity of multi-antenna gaussian channels," *Euro. Transactions on Telecommunication*, Nov. 1999.

[24] V. Tarokh, N. Seshadri, and A. Calderbank, "Space-time codes for high data rate wireless communication: performance criterion and code construction," *Information Theory, IEEE Transactions on*, vol. 44, pp. 744 –765, Mar. 1998.

[25] Y. Wang and J. Coon, "Active interference cancellation for systems with antenna selection," in *Communications, 2008. ICC '08. IEEE International Conference on*, pp. 3785 –3789, May 2008.

[26] F. Sarabchi and C. Nerguizian, "Interference cancellation technique for MIMO MB-OFDM UWB cognitive radio," in *Wireless and Mobile Communications (ICWMC), 2010 6th International Conference on*, pp. 472 –477, 2010.

[27] Q. Liang, Y. Xiao, X. He, and S. Li, "Iterative estimation and cancellation of N-continuous distortion for MIMO OFDM systems," in *Wireless Communications and Signal Processing (WCSP), 2010 International Conference on*, pp. 1 –4, oct. 2010.

[28] J. van de Beek and F. Berggren, "N-continuous OFDM," *Communications Letters, IEEE*, vol. 13, pp. 1 –3, January 2009.

[29] E. Alian, H. Saffar, and P. Mitran, "Cross-Band Interference Reduction Trade-Offs in SISO and MISO OFDM-Based Cognitive Radios," *Wireless Communications, IEEE Transactions on*, vol. 11, pp. 2436 –2445, July 2012.

[30] E. Alian and P. Mitran, "A Phase Adjustment Approach for Interference Reduction in OFDM-based Cognitive Radios," *Wireless Communications, IEEE Transactions on*, 2013.

[31] A. Ghasemi and E. S. Sousa, "Fundamental limits of spectrum-sharing in fading environments," *Wireless Communications, IEEE Transactions on*, vol. 6, pp. 649 –658, Feb. 2007.

[32] L. Musavian and S. Aissa, "Capacity and power allocation for spectrum-sharing communications in fading channels," *Wireless Communications, IEEE Transactions on*, vol. 8, pp. 148 –156, Jan. 2009.

[33] R. Zhang, S. Cui, and Y.-C. Liang, "On ergodic sum capacity of fading cognitive multiple-access and broadcast channels," *Information Theory, IEEE Transactions on*, vol. 55, pp. 5161 –5178, Nov. 2009.

[34] T. Yoo and A. Goldsmith, "On the optimality of multiantenna broadcast scheduling using zero-forcing beamforming," *Selected Areas in Communications, IEEE Journal on*, vol. 24, pp. 528 – 541, March 2006.

[35] S. Boyd and L. Vandenberghe, *Convex Optimization*. Cambridge University Press, 2010.

[36] M. Grant and S. Boyd, "CVX: Matlab software for disciplined convex programming, version 1.21." http://cvxr.com/cvx, Apr. 2011.

[37] M. Grant and S. Boyd, "Graph implementations for nonsmooth convex programs," in *Recent Advances in Learning and Control* (V. Blondel, S. Boyd, and H. Kimura, eds.), Lecture Notes in Control and Information Sciences, pp. 95–110, Springer-Verlag Limited, 2008. http://stanford.edu/~boyd/graph_dcp.html.

[38] *Channel Models for Fixed Wireless Applications (IEEE802.16.3c-01/29r4)*. IEEE P802.16, 2001.

[39] D. Petrovic, W. Rave, and G. Fettweis, "Common phase error due to phase noise in OFDM-estimation and suppression," in *Personal, Indoor and Mobile Radio Communications, 2004. PIMRC 2004. 15th IEEE International Symposium on*, vol. 3, pp. 1901 – 1905 Vol.3, 2004.

[40] G. Sridharan and T. J. Lim, "Blind estimation of common phase error in OFDM and OFDMA," in *GLOBECOM 2010, 2010 IEEE Global Telecommunications Conference*, pp. 1 –5, 2010.

[41] M. H. Hayes, *Statistical Digital Signal Processing and Modeling*. Wiley, 1996.

[42] D. Bertsekas, *Nonlinear programming*. Athena Scientific, 1999.

[43] M. Xia, W. Wen, and S. Kim, "Opportunistic cophasing transmission in MISO systems," *Communications, IEEE Transactions on*, vol. 57, no. 12, pp. 3764–3770, 2009.

[44] T. Zogakis and J. Cioffi, "The Effect of Timing Jitter on the Performance of a Discrete Multitone System," *Communications, IEEE Transactions on*, vol. 44, no. 7, pp. 799–808, 1996.

[45] L. Tomba and W. Krzymien, "A Model for the Analysis of Timing Jitter in OFDM Systems," in *Communications, 1998. ICC 98. Conference Record. 1998 IEEE International Conference on*, vol. 3, pp. 1227–1231 vol.3, 1998.

[46] K. N. Manoj and G. Thiagarajan, "The Effect of Sampling Jitter in OFDM Systems," in *Communications, 2003. ICC '03. IEEE International Conference on*, vol. 3, pp. 2061–2065 vol.3, 2003.

[47] U. Onunkwo, Y. Li, and A. Swami, "Effect of timing jitter on ofdm-based uwb systems," *Selected Areas in Communications, IEEE Journal on*, vol. 24, no. 4, pp. 787–793, 2006.

[48] L. Yang and J. Armstrong, "Oversampling to Reduce the Effect of Timing Jitter on High Speed OFDM Systems," *Communications Letters, IEEE*, vol. 14, no. 3, pp. 196–198, 2010.

[49] S. Brandes, I. Cosovic, and M. Schnell, "Sidelobe Suppression in OFDM Systems by Insertion of Cancellation Carriers," in *Vehicular Technology Conference, 2005. VTC-2005-Fall. 2005 IEEE 62nd*, vol. 1, pp. 152–156, 2005.

[50] P. B. Hor, C. Ko, and W. Zhi, "BER Performance of Pulsed UWB System in the Presence of Colored Timing Jitter," in *Ultra Wideband Systems, 2004. Joint with Conference on Ultrawideband Systems and Technologies. Joint UWBST IWUWBS. 2004 International Workshop on*, pp. 293–297, 2004.

[51] T.-T. Liu and C.-K. Wang, "A 14 GHz DLL Based Low-Jitter Multi-Phase Clock Generator for Low-Band Ultra-Wideband Application," in *Advanced System Integrated Circuits 2004. Proceedings of 2004 IEEE Asia-Pacific Conference on*, pp. 330–333, 2004.

[52] V. Demyanov and V. Malozemov, *Introduction to Minimax*. Dover books on advanced mathematics, Dover Publications, 1990.